Ingenieurfakultät Bau Geo Umwelt
Lehrstuhl für Wasserbau und Wasserwirtschaft

Impact of climate change on hydraulic regimes and salinity intrusion in the Mekong Delta. Case study of the Hau River

Duong Tran Anh

Vollständiger Abdruck der von der Ingenieurfakultät für Bau Geo Umwelt der Technischen Universität München zur Erlangung des akademischen Grades eines
Doktor-Ingenieurs (Dr.-Ing.)
genehmigten Dissertation.

Vorsitzender: Prof. Dr.-Ing. Markus Disse

Prüfer der Dissertation:

1. Prof. Dr.-Ing. Peter Rutschmann;
2. Prof. Dr. -Ing. Dr.h.c. mult. Franz Nestman;
3. Prof. Dr.-Ing. Wolfram Mauser;

Die Dissertation wurde am 01/08/2018 bei der Technischen Universität München eingereicht und durch die Ingenieurfakultät Bau Geo Umwelt am 08/01/2019 angenommen.

There are undeniably certain kinds of knowledge that must be of a general nature and, more importantly, a certain cultivation of the mind and character that nobody can afford to be without. People obviously cannot be good craftworkers, merchants, soldiers or businessmen unless, regardless of their occupation, they are good, upstanding and – according to their condition – well-informed human beings and citizens. If this basis is laid through schooling, vocational skills are easily acquired later on, and a person is always free to move from one occupation to another, as so often happens in life.

(Wilhelm von Humboldt, 1767-1835)

by Karl-Heinz Günther, in *Prospects*, Vol. 18, Issue 1,1988

Declaration

I hereby declare that except where specific reference is made to the work of others, the contents of this dissertation are original and have not been submitted in whole or in part for consideration for any other degree or qualification in this, or any other university. This dissertation is my own work and contains nothing which is the outcome of work done in collaboration with others, except as specified in the text and Acknowledgements. This dissertation contains fewer than 41,122 words including appendices, bibliography, footnotes, 36 tables and equations and has fewer than 58 figures.

Duong Tran Anh
August 2018

Acknowledgements

This PhD research is a turning-point in my life with many valuable academic experiences and the improved ability to surpass myself. The outcome of the research had the assistance and cooperation of many individuals and organizations.

I would like to offer my grateful thanks to all of them. Particularly, I would like to thank Cuomo Foundation and IPCC scholarship Board for offering me a prestigious international scholarship with which to conduct this study. My special thanks must first go to my supervisors, Prof. Dr. Peter Rutschmann, and Research Coordinator Dr.-Ing. Bui Minh Duc for their continuous assistance, guidance, supervision to support me during my research candidacy. Their invaluable support and advice was critical both in enhancing my understanding of the subject and in providing me additional perspective on the study.

I am indebted to all those who generously, honestly, bravely gave their time to help and engaged in this research as Dr. Hoang Phi Long, Dr. Mai Thai Son, Dr. Thannob Aribarg, Dr. Tue Vu, Dang Quang Thanh, Kieu Tung, Quan Nguyen, Tung Nguyen, Hieu Bui, Keivan Kaveh.... Without them, this research would not have been possible. Enormous thanks to all colleagues at Institute of Hydraulic and Water Resources Engineering - Technical University of Munich, Germany, for stimulating discussions and insights that have informed this thesis.

Most importantly, I would like to thank my family, my love, close friends for their forbearance, support and words of courage particularly during some difficult moments. Finally, I am thankful to my parents and for their unconditional love, great understanding for supporting me spiritually throughout writing this thesis and my life in general.

Munich, August 2018
Duong Tran Anh
Trananhduong1981@gmail.com

Abstract

Climate change is undeniable and devastating global warming is inevitable due to the inaction of the international community. The assessment of the effect of climate change on water resources is critical and necessary to evaluate adequately. The impact of climate change on the mesoscale of hydrological cycles in large or inter-basin watersheds has had negative results on the availability of water resources for agriculture, food and water security for the many regions in developing countries such as Africa, and South East Asia, especially the Mekong Delta.

Despite the importance of climate change, a lack of financial resources and observed data mean, there are few studies recent years that attempt to evaluate thoroughly the effect of climate change on hydraulic regimes and salinity intrusion at estuaries in Vietnamese Mekong Delta (VMD). Nevertheless, this region is highly vulnerable to climate change and climate-induced water problems. This study adds more current knowledge of these problems on VMD. Sea level rise and salinity intrusion in Mekong river estuaries has increased rapidly over the last ten years. This thesis contributes new and additional understanding of the effect of climate change on hydraulic regimes and salinity intrusion on the Hau River, Mekong Delta. This research used 1D-MIKE 11 and 2D-MIKE 21 hydrodynamic modelling and applied different statistical downscaling techniques to draw plausible consequences of climate change derived from five GCM outputs for precipitation in the Mekong Delta. Machine learning and deep learning for artificial intelligent systems were also employed to improve the skill of precipitation and runoff prediction. The novelty of this work is the combination of 1D model for the whole VMD and a 2D model for the Hau River estuary to simulate the salinity intrusion at the present and in the future. Furthermore, Artificial Neural Network (ANN) and Long Short Term Memory (LSTM) Recurrent neural network were also developed to enhance the precipitation prediction in different hydrological stations in VMD.

Keywords: Mekong Delta, MIKE11, MIKE21, ANN, LSTM

Zusammenfassung

Der Klimawandel und die globale Erwärmung sind unleugbar und aufgrund der Untätigkeit der internationalen Gemeinschaft unvermeidlich. Der Einfluss des Klimawandels in dem mesoskaligen Wasserkreislauf von großen Einzugsgebieten hat negative Auswirkungen auf die Wasserressourcenverfügbarkeit, z.B. für die Landwirtschaft, was die Wassersicherheit und die Lebensmittelsicherheit in viele Regionen der Welt beeinflusst, wie Entwicklungsländer in Afrika oder in Südostasien, und insbesondere das Mekong Delta. In den letzten Jahren gab es mehrere Arbeiten, die die Auswirkungen des Klimawandels auf die Wasserwirtschaft und das Salzeintragen in das Mündungsgebiet des vietnamesischen Mekong-Deltas (VMD) untersucht haben.

Die VDM-Region ist sehr anfällig für Klimawandelauswirkungen und klimabedingten Wasserproblemen. Diese Arbeit trägt dazu bei, ein neues, zusätzliches Verständnis der Klimawandelauswirkungen auf das Wasserhaushalt und das Salzeintragen des Hau Flusses im VMD zu schaffen. Der Meerwasserspiegelanstieg und das Salzeintragen in das Mündungsgebiet des VMD haben sich in den letzten Jahren rasant erhöht. Die hydrodynamische Modelle 1D-MIKE 11 und 2D- MIKE 21 sowie verschiedene Downscaling-Techniken wurden benutzt, um plausible Konsequenzen des Klimawandels, abgeleitet aus fünf GCM-Ausgaben für den Niederschlag im Mekong Delta, zu ziehen. Maschinelles Lernen und tiefes Lernen für künstliche intelligente Systeme wurde ebenso benutzt, um die Vorhersagfähigkeit für Niederschlag und Abfluss und das statische Downscaling zu verbessern. Die Neuheit dieser Arbeit besteht in der Kombination eines 1D-Modells für das ganze VMD und eines 2D-Modells für die Hau-Flussmündung für die Simulation des derzeitigen und zukünftigen Salzeintragens. Darüber hinaus, wurden ein Künstliches Neuronales Netz (ANN) und Langes Kurzzeitgedächtnis (LSTM) - Wiederkehrendes neuronales Netz entwickelt, um die Qualität des statistischen Downscaling und der Hervorsage des Niederschlags in verschiedenen meteorologischen und hydrologischen Stationen im VMD zu verbessern.

Schlüsselwörter: Mekong Delta, MIKE11, MIKE21, ANN, LSTM

Table of contents

List of figures

List of tables

Nomenclature

Subscripts

VMD	Vietnamese Mekong Delta

Acronyms / Abbreviations

ADB	Asia Development Bank
ANN	Artificial Neural Network
AR5	Fifth Assessment Report
CRU	Climatic Research Unit
DARD	Department of Agriculture and Rural Development
DM	Distribution mapping
DONRE	Department of Natural Resources and Environment
FAO	Food and Agriculture Organization of the United Nations
GCM	General Circulation Model
GDP	Gross Domestic Product
GHG	Green House Gases
GSO	General Statistics Office
IPCC	Intergovernmental Panel on Climate Change
LMBP	Levenberg-Marquardt Back-Propagation
LOCI	Local intensity scaling

LS	Linear scaling
LSTM	Long Short Term Memory
MARD	Ministry of Agriculture and Rural Development
MONRE	Ministry of Natural Resources and Environment
MRC	Mekong River Commission
RCP	Representative Concentration Pathways
SIWRP	South Institute of Water Resources Planning
SRHMC	Southern Regional Hydrometeorology Center
UNCED	United Nations Conference on Environment and Development
UNDP	United Nations Development Programme
UNEP	United Nations Environment Programme
UNFCC	United Nations Framework Convention on Climate Change
WG1AR5	Working Group I Fifth Assessment Report
WMO	World Meteorological Organization

Chapter 1

Introduction

1.1 Background

Vietnam is one of five countries that is seriously impacted by climate change. From the study of Ministry of Natural Resources and Environment, the climatic calculations over the past 50 year indicate the average temperature has increased 0.5 to 0.7°C and sea level rise 20 cm (MonRE, 2009). Climate change has made natural disasters including typhoon, floods and droughts more severe, especially since sea level rise will change on hydraulic regime and salt intrusion at estuaries will become increased. Most of developing countries depend on agriculture for their development; the effect of global warming on productive croplands will threaten the welfare of their population and the socio-economic development of the country. Agriculture is strongly dependent on water resources and climatic conditions. In the countries where technological buffering to droughts and floods is less advanced, and where the main physical factors affecting production (soil, terrain, climate) are less suited to farming, crop production is consequently extremely sensitive to large year-to-year weather fluctuation (Iizumi and Ramankutty, 2015).

Prospective water resources management is very challenging in the 21st century due to issues with water supply and utilization at the inter-basin level, both of which are exacerbated by climate change, as is the case with the Mekong Delta (Gupta, 2005) . These circumstances have a considerable effect on economic development and the livelihoods of people in riparian countries (Todd et al., 2011). The Mekong delta is considered to be the most complex basin in current times, as a number of countries manage the River simultaneously. So far, the lower Mekong delta is very likely to be the most vulnerable area affected, not only sea level rise and climate change but also by construction of a planned dams for upper basin (Hoanh et al., 2010; Kingston, Thompson, and Kite, 2011). Moreover, salinity intrusion in the low part

of delta in recent years has further aggravated the situation for integrated water resources management in Vietnamese Mekong Delta.

The VMD plays a crucial role in the economic development of Vietnam; it has contributed approximately twenty-seven percent of the country's GDP, supporting sixteen million inhabitants (nearly twenty-two percent of the total population), providing about fifty percent of the annual rice production (Dasgupta et al., 2009; Carew-Reid, 2008). However, Vietnam is one of five countries that could be seriously impacted by climate change and sea-level rise (Bernstein et al., 2007). Currently, the VMD is experiencing faster alteration due to population growth and infrastructure development (Varis, Kummu, and Salmivaara, 2012; Keskinen et al., 2010), which create substantial pressure on water resources utilization (Lebel, Garden, and Imamura, 2005; Piman, Lennaerts, and Southalack, 2013). Moreover, dam construction, operation and water diversion in upstream countries influence the changes to the hydraulic regime in the VMD (Vastila et al., 2010; Kingston, Thompson, and Kite, 2011). It is therefore necessary to evaluate and forecast the water resources in current and future conditions for long-term sustainable development in this river basin.

Salinity intrusion is a natural phenomenon occurring in the lands, estuaries, and aquifers adjacent to the sea. There is notable variability in estuaries depending on the differences in tides, river flows and topography (Dyer, 1997). There are many factors affecting salinity intrusion: discharge and river flow periods, topography, morphology, river bed slope, tides on the sea, wind velocity and direction, water temperature, the friction of the flow, and others (Pritchar, 1955; Cameron and Pritchard, 1963). One of the consequences of sea-level rise impact on estuaries is the change of salinity. Seasonal and inter-annual variations of salinity directly influence the physical, chemical, and biological processes of estuaries. Changes of salinity will result in changes of horizontal and vertical salinity gradients, which will alter the estuarine circulation (Hansen, 1965) and oxygen depletion (Kuo and Neilson, 1987; Boicourt, 1992).

The study of estuaries is very difficult because these water systems usually include complex geometries, hydrodynamics, and transport patterns. In fact, the interface between fresh and salt waters controlled by river discharges, tides and wind presents specific characteristics that affect the mixing properties of the estuarine water masses. There is a large variability in estuaries depending on the differences in the tides, river discharges and the way these factors interact with topography (Dyer, 1997). The salinity distribution within the estuary is commonly used for classification purposes (Cameron and Pritchard, 1963). However, the estuaries salinity structure can be modified by changes of river discharges regime caused by dam construction and bathymetric changes due to either sediment fluxes variation or

sand removals. These modifications can significantly impact established water uses like agricultural, domestic and industrial supply. The extent of salinity intrusion depends on the balance between fresh water discharges and salt water flow from the sea. This phenomenon can be reasonably predicted through to mathematical models supported by monitored data. These tools can be used to quantify how much fresh water is required to counterbalance salinity intrusion at the upstream water intakes.

1.2 Objectives of the research

The main objective of this research is to investigate the impact of upstream discharge, precipitation in the whole Mekong delta and sea level rise by climate change on salinity intrusion on the Hau River, Vietnam. To achieve this, the research has the specific objectives to pursue:

1. To forecast the amount of future rainfall in the study area under climate change conditions with different scenarios from 5 GCMs[1] outputs using LSTM, ANN;
2. To develop a new model of Artificial Neural Network (ANN) and Recurrent neural network – Long short term memory (LSTM) for predicting rainfall and runoff;
3. To apply 1D-MIKE 11 to simulate the total volume of rainfall at the VMD and the effect of discharge from Kratie station as the sources and sinks in MIKE 21 input;
4. To apply 2D-MIKE 21 model to simulate hydraulic regime and salinity intrusion in the Hau river under different scenarios;
5. To simulate fresh and salt water balance based on sea level rise and upstream water level scenarios;

1.3 Scope of the work

The proposed study is conducted at Vietnamese Mekong delta, Vietnam. For this level, all required data collected from the secondary sources include water level, discharge, rainfall, salinity concentration, cross section of river, bathymetry, wind condition, tidal regime, hydraulic works... Water resources plans, strategies, policies of Mekong River Committee in operation and sharing water resources... are also collected.

[1] General Circulation Models

- Data collection on rainfall, evaporation, water level, discharge as secondary data from meteorological and rain gauge stations and Tan Chau, Chau Doc, Can Tho hydro-meteorological stations on Mekong River, Vietnam;
- Data collection on salinity concentration at Tran De, Dai Ngai, My Thanh stations and tidal magnitude at My Thanh and offshore boundary is obtained from global tidal model.
- Data collection on water availability, water supply and dam constructions, hydropower plants and discharge at some stations along Mekong River;
- Elevation and digital map, cross section, bathymetry of Hau estuaries and offshore area are collected to apply MIKE 21 model;
- The Representative Concentration Pathway (RCP) scenarios including RCP4.5 and RCP 8.5 are selected and downloaded five GCM outputs for future periods of 2035-2065 based on the reference periods of 1978 to 2001;
- Base on observed water levels and simulated data to calibrate and validate the MIKE 11 and MIKE 21 models;
- Apply MIKE 21 model to simulate salinity intrusion and salt and fresh water balance on estuaries with different scenarios of sea level rise and discharges;
- Develop Artificial Neural network (ANN) and Recurrent neural network – Long Short term memory (LSTM) model to improve the capacity of statistically downscaling and prediction for rainfall – runoff in Vietnamese Mekong delta.

1.4 Outline of the thesis

In **Chapter 2**, the fundamental literature review of hydrodynamic models and downscaling techniques are briefly reviewed in preparation for their application in Chapters 4, and 5. The first part of this chapter introduces MIKE 11 and MIKE 21 model. The second part of this chapter consists of a definition and explanation of climate change and general circulation models. The last part of this chapter provides the basics of the downscaling technique and bias correction applied in this study which are also described in terms of mathematical meaning and applications.

Chapter 3 described the concept and application of ANN, SANN and LSTM that are applied this study. The structure of three models and mathematical expression will be explain in this part.

Chapter 4 contains the main part of this research which provides the methodology and study area which explains in detail how to obtain the objectives of study and also describes the tools and models applyed in this study. The research framework is presented to clearly define all tasks and sub-objectives using different tools.

Chapter 5 focuses on the model application with five sub-parts including application of ANN, SANN and LSTM for rainfall and rainfall – runoff prediction. This chapter also shows the development of the new model of machine learning using ANN, SANN and LSTM for hydrological simulation. Deep learning of Long Short Term Memory (LSTM) is also employed to train the model for rainfall prediction and rainfall – runoff relationship prediction.

The hydrodynamic model for simulating hydraulic regimes on Mekong delta is the most central objective of this research. 1D-MIKE 11 and 2D-MIKE 21 models and their application for the whole Mekong Delta from Kratie to estuaries and the smaller domain from Can Tho to the offshore area for 2D model for simulating salinity intrusion and hydraulic regime which is given in this part. The results and discussion are are used to make a comprehensive examination on climate change and upstream effect to lower Mekong Delta.

Chapter 6 makes some conclusions and recommendations of further research.

Chapter 2

Hydrodynamic modelling, climate change and downscaling technique

2.1 1D-MIKE 11 model

The MIKE 11 model system is a commercial software package developed by the Danish Hydraulic Institute. The system has four editor interfaces including a river network, cross sections, boundary conditions, simulation and designing with various modules including Hydrodynamic (HD), Advection Dispersion (AD), Water Quality (WQ), runoff and rainfall (NAM), non-cohesive sediment transport, and flood forecasting (DHI, 2007).

The MIKE 11-HD is a model for one dimensional unsteady flow computation and can be applied to looped networks and quasi-two dimensional flow simulation on floodplains. The model has been designed to perform detailed modelling of rivers, including special treatment of floodplains, road overtopping, culverts, gate openings and weirs. It is capable of using the 1D Saint-Venant equations. The solution of the continuity and momentum equations is based on an implicit finite difference scheme. Boundary types include water level (h), flow discharge (Q) and Q/h relation (Fig. 2.1). The water level must be specified at either the upstream or the downstream boundary of the model. The flow discharge can be applied to either the upstream or the downstream boundary condition, and can also be applied to the side tributary flow (lateral inflow). The lateral inflow is used to describe runoff. The Q/h relation can only be applied to the downstream boundary. MIKE 11 is a modelling package for the simulation of surface runoff, flow, sediment transport, and water quality in rivers, channels, estuaries, and floodplains. The most commonly applied hydrodynamic (HD) model is a flood management tool simulating the unsteady flows in complex rivers and channel systems. It has been successfully applied in different river basins around the world. The main

governing equations are known as Saint-Venant equations (Shooshtari, 2008) as follows.

$$\frac{\partial Q}{\partial x} + \frac{\partial A}{\partial t} = q \tag{2.1}$$

$$\frac{\partial Q}{\partial t} + \frac{\partial}{\partial x}\left(\alpha \frac{Q^2}{A}\right) + gA\frac{\partial h}{\partial x} + \frac{gQ|Q|}{ARC^2} = 0 \tag{2.2}$$

Where: Q - discharge, $m^3 s^{-1}$; A - flow area, m^2; q - lateral flow, $m^2 s^{-1}$; h - depth above datum, m;C - Chezy resistance coefficient, $m^{1/2} s^{-1}$; R - hydraulic radius, m; α- momentum distribution coefficient.

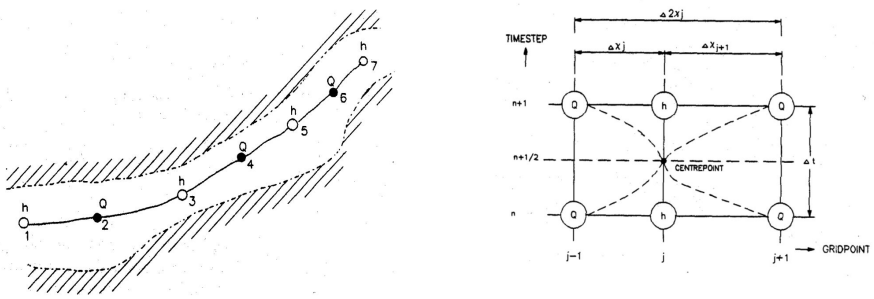

Fig. 2.1 The solution of scheme of MIKE 11 model

2.2 2D-MIKE 21 model

The MIKE 21 is a dynamic modeling system used within coastal and estuarine environments. The MIKE 21 comprises several modules: the Hydrodynamic Module, Advection – Dispersion module, Spectral Wave Module, Transport Module, etc. The mutual interaction between salinity concentration and currents can be simulated using dynamic coupling between the Hydrodynamic Module and Transport Module. (Fig. 2.2) shows the mechanism of the two modules running with inputs, outputs and interaction for hydrodynamic and transport modules applied in this study.

MIKE 21 model has been developed based the two-dimensional shallow water equations with several governing equations such as Reynolds-averaged Navier–Stokes equations involving the assumption of Boussinesq and of hydrostatic pressure as well as the convection diffusion equation. Integrating the horizontal momentum equations and the continuity

equation over depth the following two-dimensional shallow water equations are obtained:

$$\frac{\partial h}{\partial t}+\frac{\partial h\bar{u}}{\partial x}+\frac{\partial h\bar{v}}{\partial y}=hS \tag{2.3}$$

$$\frac{\partial h\bar{u}}{\partial t}+\frac{\partial h\bar{u}^2}{\partial x}+\frac{\partial h\overline{uv}}{\partial y}=f\bar{v}h-gh\frac{\partial \eta}{\partial x}-\frac{h}{\rho_o}\frac{\partial p_a}{\partial x}-\frac{gh^2}{2\rho_o}\frac{\partial \rho}{\partial x}+\frac{\tau_{sx}}{\rho_o}-\frac{\tau_{bx}}{\rho_o} \tag{2.4}$$

$$-\frac{1}{\rho_o}\left(\frac{\partial S_{xx}}{\partial x}+\frac{\partial S_{xy}}{\partial y}\right)+\frac{\partial}{\partial x}\left(hT_{xx}\right)+\frac{\partial}{\partial y}\left(hT_{xy}\right)+hu_sS \tag{2.5}$$

$$\frac{\partial h\bar{v}}{\partial t}+\frac{\partial h\overline{uv}}{\partial x}+\frac{\partial h\bar{v}^2}{\partial y}=-f\bar{u}h-gh\frac{\partial \eta}{\partial y}-\frac{h}{\rho_o}\frac{\partial p_a}{\partial y}-\frac{gh^2}{2\rho_o}\frac{\partial \rho}{\partial y}+\frac{\tau_{sx}}{\rho_o}-\frac{\tau_{by}}{\rho_o} \tag{2.6}$$

$$-\frac{1}{\rho_o}\left(\frac{\partial S_{yx}}{\partial x}+\frac{\partial S_{yy}}{\partial y}\right)+\frac{\partial}{\partial x}\left(hT_{xy}\right)+\frac{\partial}{\partial y}\left(hT_{yy}\right)+hv_sS \tag{2.7}$$

Where: $h\bar{u}=\int_{-d}^{\eta}udz \quad h\bar{v}=\int_{-d}^{\eta}vdz$

$$T_{xx}=2A\frac{\partial \bar{u}}{\partial x} \quad T_{xy}=A\left(\frac{\partial \bar{u}}{\partial y}+\frac{\partial \bar{v}}{\partial x}\right) \quad T_{yy}=2A\frac{\partial \bar{v}}{\partial y} \tag{2.8}$$

And the depth average transport equation for salt:

$$\frac{\partial h\bar{s}}{\partial t}+\frac{\partial h\overline{us}}{\partial x}+\frac{\partial h\overline{vs}}{\partial y}=hF_s+hs_sS \tag{2.9}$$

Where: Fs is the horizontal diffusion term, s is salinity concentration.

$$F_s=\left[\frac{\partial}{\partial x}\left(D_h\frac{\partial s}{\partial x}\right)+\frac{\partial}{\partial y}\left(D_h\frac{\partial s}{\partial y}\right)\right] \tag{2.10}$$

$D_h=\frac{A}{\sigma_T}$ $\sigma_T$is the Prandlt number, A is the horizontal eddy viscosity.

Where:

t is the time; x, yz are the Cartesian co-ordinates; η is the surface elevation; $d$is the still water depth; $h=\eta+d$ is the total water depth; u, v are the depth average velocity components in the x, y direction; f =2Ωsinφ is the Coriolis parameter; $g$is the gravitational acceleration; ρ is the density of water; S_{xx}, S_{xy}, S_{yx} and S_{yy} are components of the radiation stress tensor; p_a is the atmospheric pressure; ρ_o is the reference density of water. S is the magnitude of the discharge due to point sources; (u_s, v_s) is the velocity by which the water is discharged into the ambient water; s is the depth average salinity concentration.

MIKE 21 FM is based on a flexible mesh approach. The spatial discretization of the primitive equation is performed using a cell – centered finite volume method. The spatial

domain is discretized by subdivision of the continuum into non-overlapping cell. The mesh is divided by triangles or quadrilateral elements.

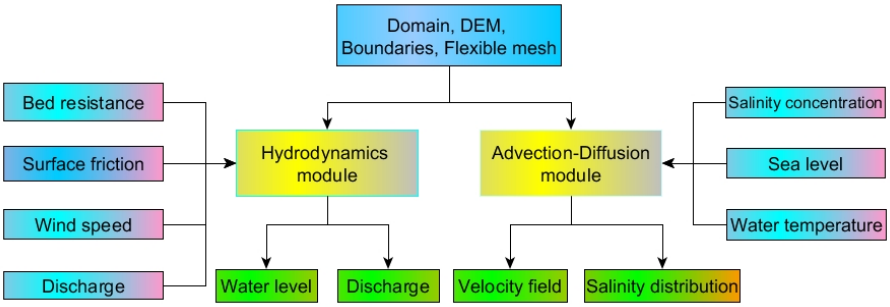

Fig. 2.2 The scheme of MIKE 21 HD and TR simulations (developed from (Manson, 2012))

2.3 Climate Change and General Circulation Models

2.3.1 Climate change

Climate change is widely recognized as the most urgent issue facing planet Earth and has been involved in Summit G7 or G20 agendas. The Intergovernmental Panel on Climate Change (Bernstein et al., 2007) defined the term of "climate change" as "*A change in the state of the climate that can be identified (e.g. using statistical tests) by changes in the mean and/or the variability of its properties, and that persists for an extended period, typically decades or longer. It refers to any change in climate over time, whether due to natural variability or as a result of human activity*".

The United Nations Framework Convention on Climate Change defines climate change as "*change of climate which is attributed directly or indirectly to human activity that alters the composition of the global atmosphere and which is in addition to natural climate variability observed over comparable time periods*" (Turner, 2013).

The global climate change is referred to long term changes of climate and weather pattern. The consequences of climate change are attributed to both anthropogenic activities and natural fluctuations over time. The main reason for global warming is the significant rise of greenhouse gas emission such as carbon dioxide from fossil fuel burning and deforestation, natural gas leakage, methane from agriculture, and ozone in the lower atmosphere from the products of vehicle exhausts, all off which are widely agreed upon by scientist community (Bernstein et al., 2007).

According to IPCC's Fifth Assessment Report (AR5), new evidence of climate change based on many independent scientific analyses from the observations of the climate system, paleoclimate archives, theoretical studies of climate processes and simulations using climate models. We described briefly the main finding of AR5 in term of temperature changes, precipitation alterations and sea level rise as following:

"Warming of the climate system is unequivocal, and since the 1950s, many of the observed changes are unprecedented over decades to millennia. The atmosphere and ocean have warmed, the amounts of snow and ice have diminished, sea level has risen, and the concentrations of greenhouse gases have increased" (Stocker et al., 2013).

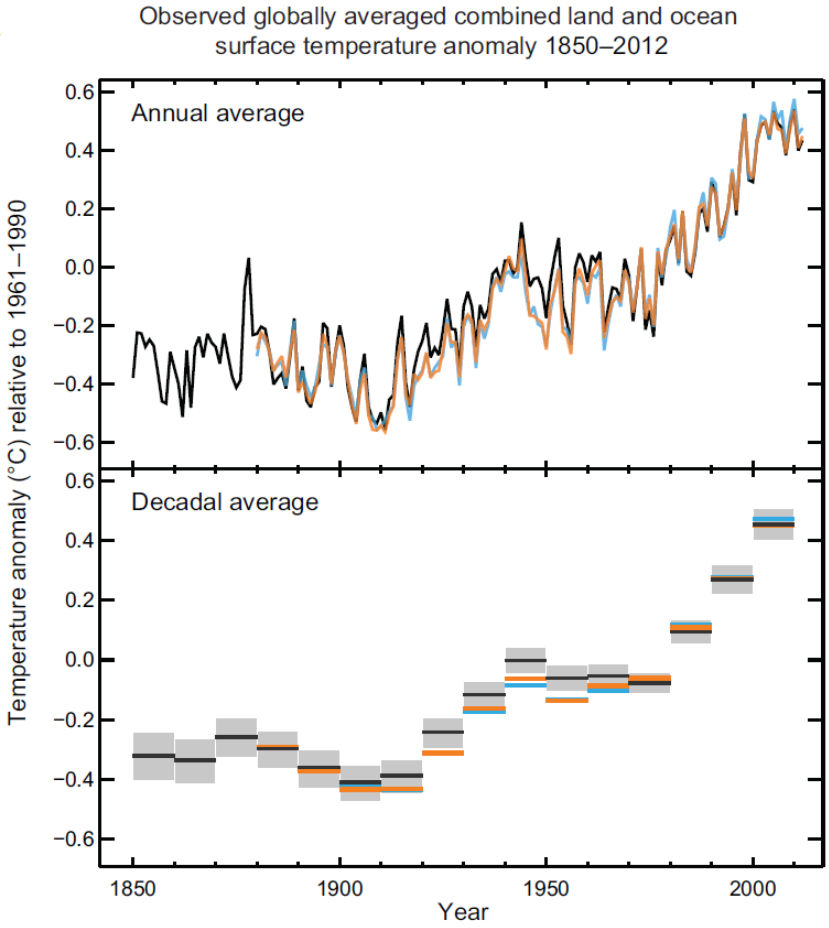

Fig. 2.3 Observed global mean combined land and ocean surface temperature anomalies, from 1850 to 2012 from three data sets. Top panel: annual mean values. Bottom panel: decadal mean values including the estimate of uncertainty for one dataset (black) (Stocker et al., 2013)

"Ocean warming dominates the increase in energy stored in the climate system, accounting for more than 90% of the energy accumulated between 1971 and 2010 (high confidence). It is virtually certain that the upper ocean (0−700 m) warmed from 1971 to 2010 (see Fig. 2.3), and it likely warmed between the 1870s and 1971" (Stocker et al., 2013).

"The rate of sea level rise since the mid-19th century has been larger than the mean rate during the previous two millennia (high confidence). Over the period 1901 to 2010, global mean sea level rose by 0.19 [0.17 to 0.21] m" (Stocker et al., 2013).

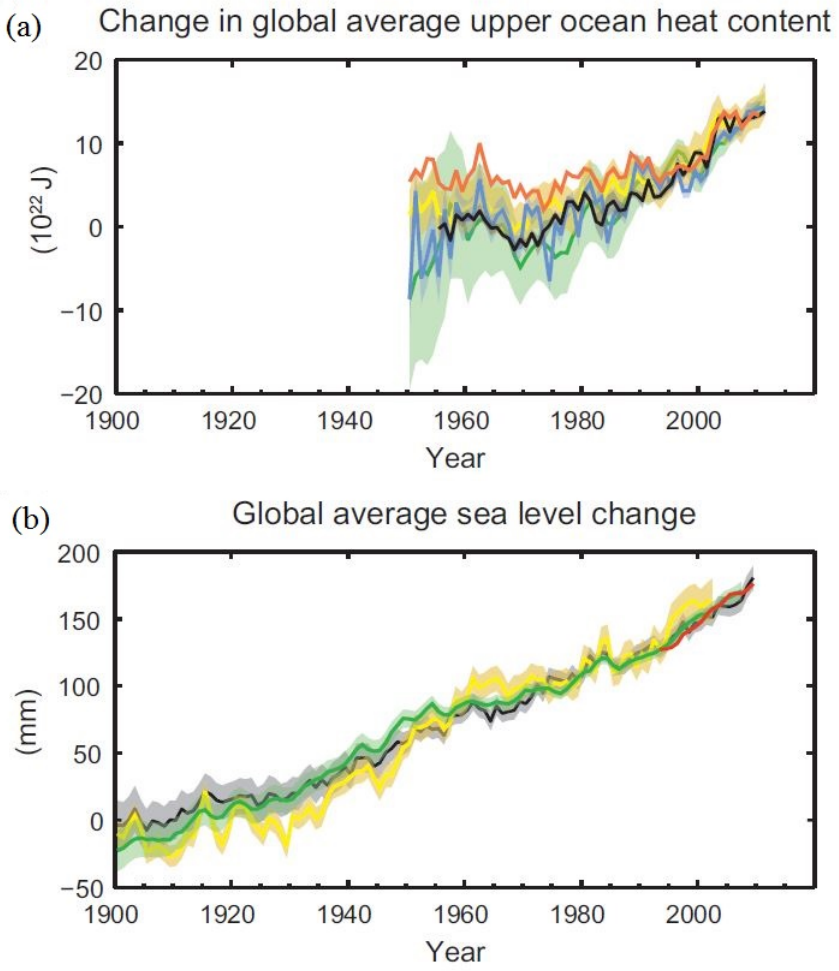

Fig. 2.4 (a) change in global mean upper ocean (0–700 m) heat content aligned to 2006−2010, and relative to the mean of all datasets for 1970; (b) global mean sea level relative to the 1900–1905 mean of the longest running dataset, and with all datasets aligned to have the same value in 1993, the first year of satellite altimetry data

"Human influence has been detected in warming of the atmosphere and the ocean, in changes in the global water cycle, in reductions in snow and ice, in global mean sea level

rise, and in changes in some climate extremes. This evidence for human influence has grown since AR4. It is extremely likely that human influence has been the dominant cause of the observed warming since the mid-20th century".

"Global surface temperature change for the end of the 21st century is likely to exceed 1.5°C relative to 1850 to 1900 for all RCP scenarios except RCP2.6. It is likely to exceed 2°C for RCP6.0 and RCP8.5, and more likely than not to exceed 2°C for RCP4.5. Warming will continue beyond 2100 under all RCP scenarios except RCP2.6. Warming will continue to exhibit interannual-to-decadal variability and will not be regionally uniform" (Stocker et al., 2013)

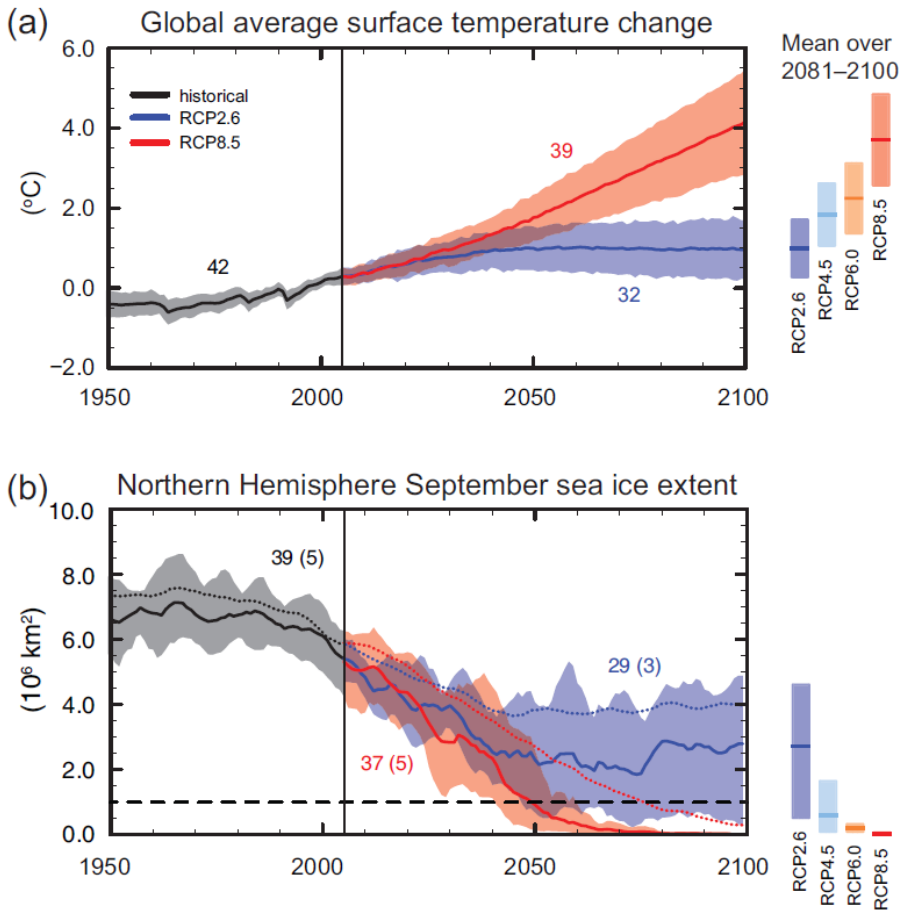

Fig. 2.5 CMIP5 multi-model simulated time series from 1950 to 2100 for (a) change in global annual mean surface temperature relative to 1986–2005, (b) Northern Hemisphere sea ice extent (5-year running mean)

Global mean sea level will continue to rise during the 21st century (see Fig. 2.6). Under all RCP scenarios, the rate of sea level rise will very likely exceed that observed during 1971

to 2010 due to increased ocean warming and increased loss of mass from glaciers and ice sheets.

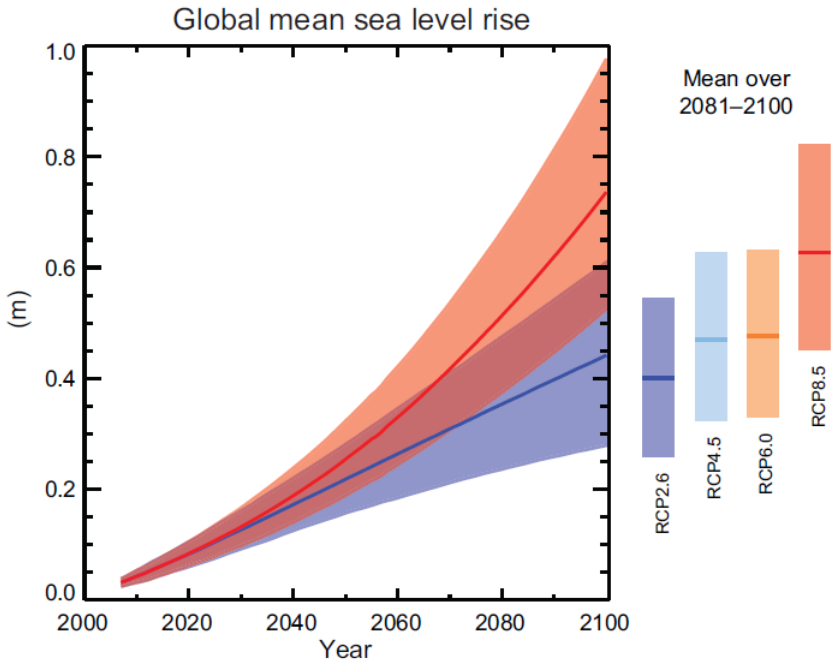

Fig. 2.6 Projections of global mean sea level rise over the 21st century relative to 1986–2005 from the combination of the CMIP5 ensemble with process-based models, for RCP2.6 and RCP8.5

2.3.2 General Circulation Models

Numerical models (General Circulation Models or GCMs), representing physical processes in the atmosphere, ocean, cryosphere and land surface, are the most advanced tools currently available for simulating the response of the global climate system to increasing greenhouse gas concentrations (Houghton et al., 2001) and use different equations based on the basic laws of physics, fluid motion and chemistry (see Fig. 2.7). GCMs depict the climate using a three dimensional grid over the globe, typically having a horizontal resolution of between 250 km and 600 km, 10 to 20 vertical layers in the atmosphere and sometimes as many as 30 layers in the oceans. Their resolution is thus quite coarse relative to the scale of exposure units in most impact assessments. Moreover, many physical processes, such as those related to clouds, also occur at smaller scales and cannot be properly modelled. The most powerful tools available with which to assess future climate are coupled climate models, which include

three-dimensional representations of the atmosphere, ocean, cryosphere and land surface (Gates et al., 1996).

In 2008, IPCC promoted to make a new set of coordinated climate model experiments so-called the fifth phase of the Coupled Model Inter-comparison Project (CMIP5). CMIP5 will notably provide a multi-model context for 1) assessing the mechanisms responsible for model differences in poorly understood feedbacks associated with the carbon cycle and with clouds, 2) examining climate predictability and exploring the ability of models to predict climate on decadal time scales, and, more generally, 3) determining why similarly forced models produce a range of responses. (https://pcmdi.llnl.gov/mips/cmip5/).
CMIP5 is meant to provide a framework for coordinated climate change experiments for the next five years and thus includes simulations for assessment in the AR5 as well as others that extend beyond the AR5. There are basically 20 GCM groups from around the world for impact assessments. The list of GCM models are available for impact assessment is presented in Table 2.1.

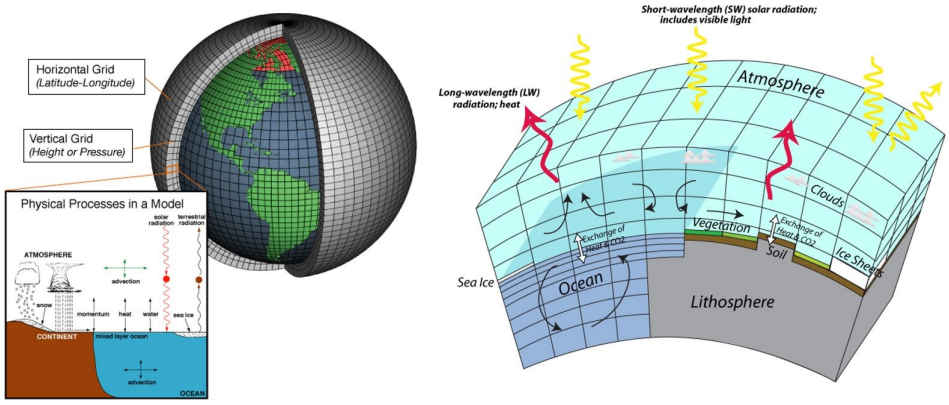

Fig. 2.7 Schematic for General Circulation Models
(Source: McGuffie and Henderson-Sellers, 2005; D. Bice, 2009)

Table 2.1 The list of available GCM models for climate change impact assessment

CMIP5 Model ID	Institute and Country of Origin	Ocean horz. resolution (°lat x °lon)	Atm. horz. resolution (°lat x °lon)	Atm. Eq. resolution Latitude (Km)	Longitude (Km)
ACCESS-1.0	CSIRO-BOM, Australia	1.0×1.0	1.9×1.2	210	130

ACCESS-1.3	CSIRO-BOM, Australia	1.0×1.0	1.9×1.2	210	130
BCC-CSM1-1	BCC, CMA, China	1.0×1.0	2.8×2.8	310	310
BCC-CSM1-1-M	BCC, CMA, China	1.0×1.0	1.1×1.1	120	120
BNU-ESM	BNU, China	0.9×1.0	2.8×2.8	310	310
CanCM4	CCCMA, Canada	1.4×0.9	2.8×2.8	310	310
CanESM2	CCCMA, Canada	1.4×0.9	2.8×2.8	310	310
CCSM4	NCAR, USA	1.1×0.6	1.2×0.9	130	100
CESM1-BGC	NSF-DOE-NCAR, USA	1.1×0.6	1.2×0.9	130	100
CESM1-CAM5	NSF-DOE-NCAR, USA	1.1×0.6	1.2×0.9	130	100
CESM1-FASTCHEM	NSF-DOE-NCAR, USA	1.1×0.6	1.2×0.9	130	100
CESM1-WACCM	NSF-DOE-NCAR, USA	1.1×0.6	2.5×1.9	275	210
CMCC-CESM	CMCC, Italy	2.0×1.9	3.7×3.7	410	410
CMCC-CM	CMCC, Italy	2.0×1.9	0.7×0.7	78	78
CMCC-CMS	CMCC, Italy	2.0×2.0	1.9×1.9	210	210
CNRM-CM5	CNRM-CERFACS, France	1.0×0.8	1.4×1.4	155	155
CNRM-CM5-2	CNRM-CERFACS, France	1.0×0.8	1.4×1.4	155	155
CSIRO-Mk3-6-0	CSIRO-QCCCE, Australia	1.9×0.9	1.9×1.9	210	210
EC-EARTH	EC-EARTH, Europe	1.0×0.8	1.1×1.1	120	120
FIO-ESM	FIO, SOA, China	1.1×0.6	2.8×2.8	310	310

GFDL-CM2p1	NOAA, GFDL, USA	1.0×1.0	2.5×2.0	275	220
GFDL-CM3	NOAA, GFDL, USA	1.0×1.0	2.5×2.0	275	220
GFDL-ESM2G	NOAA, GFDL, USA	1.0×1.0	2.5×2.0	275	220
GFDL-ESM2M	NOAA, GFDL, USA	1.0×1.0	2.5×2.0	275	220
GISS-E2-H	NASA/GISS, NY, USA	2.5×2.0	2.5×2.0	275	220
GISS-E2-H-CC	NASA/GISS, NY, USA	1.0×1.0	1.0×1.0	110	110
GISS-E2-R	NASA/GISS, NY, USA	2.5×2.0	2.5×2.0	275	220
GISS-E2-R-CC	NASA/GISS, NY, USA	1.0×1.0	1.0×1.0	110	110
HadCM3	MOHC, UK	1.2×1.2	3.7×2.5	410	280
HadGEM2-AO	NIMR-KMA, Korea	1.0×1.0	1.9×1.2	210	130
HadGEM2-CC	MOHC, UK	1.0×1.0	1.9×1.2	210	130
HadGEM2-ES	MOHC, UK	1.0×1.0	1.9×1.2	210	130
INMCM4	INM, Russia	0.8×0.4	2.0×1.5	220	165
IPSL-CM5A-LR	IPSL, France	2.0×1.9	3.7×1.9	410	210
IPSL-CM5A-MR	IPSL, France	1.6×1.4	2.5×1.3	275	145
IPSL-CM5B-LR	IPSL, France	2.0×1.9	3.7×1.9	410	210
MIROC4h	JAMSTEC, Japan	0.3×0.2	0.56×0.56	60	60
MIROC5	JAMSTEC, Japan	1.6×1.4	1.4×1.4	155	155
MIROC-ESM	JAMSTEC, Japan	1.4×0.9	2.8×2.8	310	310

MIROC-ESM-CHEM	JAMSTEC, Japan	1.4×0.9	2.8×2.8	310	310
MPI-ESM-LR	MPI-N, Germany	1.5×1.5	1.9×1.9	210	210
MPI-ESM-MR	MPI-N, Germany	0.4×0.4	1.9×1.9	210	210
MPI-ESM-P	MPI-N, Germany	1.5×1.5	1.9×1.9	210	210
MRI-CGCM3	MRI, Japan	1.0×0.5	1.1×1.1	120	120
MRI-ESM1	MRI, Japan	1.0×0.5	1.1×1.1	120	120
NorESM1-M	NCC, Norway	1.1×0.6	2.5×1.9	275	210
NorESM1-ME	NCC, Norway	1.1×0.6	2.5×1.9	275	210

Source: https://www.climatechangeinaustralia.gov.au/en/climate-projections

2.4 Downscaling techniques

Downscaling is the procedure that takes information known at large scales to make predictions at local scales weather and climate. Other definition in climate change study stated that downscaling is the process by which coarse-resolution GCM outputs are translated into finer resolution climate information, so that they better account for regional climatic influences, such as local topography (Flint and Flint, 2012). Figure 2.8 described the concept of spatial downscaling from different GCM models to local scale needed in impact models. The two main approaches to downscaling climate information are dynamical and statistical, both implemented to obtain a finer spatial resolution: The dynamical methods, which create a higher-resolution climate model by embedding this model into GCM, and the statistical methods, which establish empirical relationships between GCM-resolution climate variables and local climate. Each method has advantages and disadvantages as described in Table 2.2.

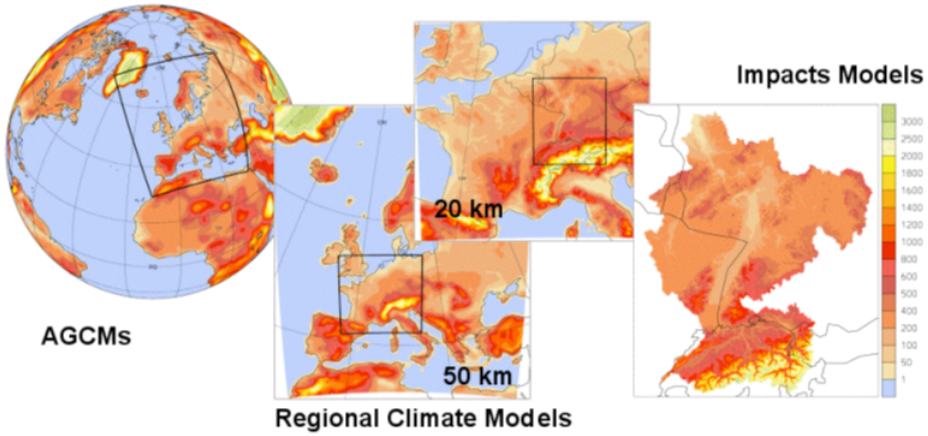

Fig. 2.8 The concept of spatial downscaling from GCMs to local scale

Dynamical downscaling

Dynamical downscaling refers to the Regional Climate Models (RCMs). The large-scale and lateral boundary conditions of GCMs are applied to produce higher resolution outputs with 0.5^o latitude and longitude spacing. Therefore, these models can reproduce more detail regional climate characteristics like orographic precipitation (Frei et al., 2003), extreme climate events (Fowler et al., 2005; Frei et al., 2006) and regional scale climate anomalies. However, models strongly influenced on biases inherited from the driving GCM and the presence and strength of regional scale forcing such as orography, land-sea contrast and vegetation cover as well.

In addition, variance of internal parameterizations also creates significantly uncertainty. Therefore, in climate change studies, the application of model ensembles with at least two to three GCM models should be employed for satisfactory results. Haylock et al., 2006 compared two dynamical downscaling models regarding to their ability to downscale seven seasonal indices of heavy precipitation for two station networks in northwest and southeast England. Almost dynamic models are expensive in computation, are very time-intensive and require super computer. The time window for which climate change projections are made is limited to about 30 years from 1961–1990 and 2070–2100. This means that it is difficult to assess climate change impacts for other periods.

Table 2.2 Advantages and disadvantages of statistic and dynamic methods (Fowler and Kilsby, 2007

	Statistical downscaling	**Dynamical downscaling**
Advantages	•Comparatively cheap and computationally efficient; •Can provide point-scale climatic variables from GCM-scale output; •Can be used to derive variables not available from RCMs; •Easily transferable to other regions; •Based on standard and accepted statistical procedures; •Able to directly incorporate observations into method;	•Produces responses based on physically consistent processes; •Produces finer resolution information from GCM-scale output that can resolve; atmospheric processes on a smaller scale;
Disadvantages	•Require long and reliable observed historical data series for calibration •Dependent upon choice of predictors •Non-stationarity in the predictor-predictand relationship •Climate system feedbacks not included •Dependent on GCM boundary forcing; affected by biases in underlying GCM; •Domain size, climatic region and season affects downscaling skill;	•Computationally intensive; •Limited number of scenario ensembles available; •Strongly dependent on GCM boundary forcing.

RCMs always produce small but non-negligible uncertainty by effect of GCM output. Some researches pointed out that the RCM's uncertainty is less than that from the emissions scenarios for temperature prediction, but bigger for precipitation predictions. However, the largest source of uncertainty derives from the structure and physics of the formulation of the driving GCM (Fowler et al., 2007).

Déqué et al., 2005 examined the uncertainty obtaining from ten RCMs applied to eight regions with the same emissions scenario. The research determined many factors that cause uncertainty such as spatial domain, region, and season, boundary forcing i.e. selection of GCM and particularly for temperature. There are numerous assessments of the RCMs' capacity for simulating climate variables, particularly in water resources and hydrological impact studies. Leung et al., 2004 stated that dynamical downscaling delivered a detailed picture of climate change and its potential impacts, and a better simulation than by GCMs because of orographic forcing and rainfall pattern effects. These models may improve the simulation of meso-scale precipitation processes(Schmidli, Frei, and Vidale, 2006)with longer duration, and higher spatial resolution. The assembled RCM simulations are necessary to overall assessment of climate change effects. The simulation of RCMs are more accurate due to higher spatial and temporal resolution especially for extreme events (Frei et al., 2006). RCMs should be applied for different geographical features in various regions to find its strengths and weaknesses (Wang et al., 2004). These researches have increased quantity of RMCs application in climate change impact studies (Bergström et al., 2001; Wood et al., 2004; Zhu et al., 2004; Graham et al., 2007).

Statistical downscaling (SD)

The purpose of downscaling techniques is to convert the climatic features of GCMs output to small regions or point scale with a finer resolution. Statistical downscaling is most popular in climate change studies. The simplest method is change factors (CFs), also called the 'perturbation method' (Arnell, 1992; Chiew et al., 1995; Arnell and Reynard, 1996; Prudhomme, Reynard, and Crooks, 2002). This method was only used for sensitivity studies, and quick analysis of multiple climate change scenarios (Wilby, Wedgbrow, and Fox, 2004). To reduce the uncertainty of the GCM outputs, it is recommended to use an ensemble of simulations, rather than one single GCM's result (Mitchell and Hulme, 1999). This method has some assumptions including: (i) GCMs have a constant bias through time; (ii) CFs only scale the mean, maximum and minimum of climatic variables but neglect changes in variability and the spatial pattern of climate will remain constant (Diaz-Nieto and Wilby, 2005). Although the statistical characteristics of the historical record did not change (Wood,

Lettenmaier, and Palmer, 1997), this method was widely applied in hydrology (Xu, 1999) because of its simplicity and applicability.

There are three complex statistical downscaling methods as following: a) Regression models, b) Weather typing schemes, c) Weather generators (WGs). The aim of these methods is to determine the best correlation between large-scale atmospheric variables (predictors) and local or regional climate variables (predictands) expressed as a stochastic and/or deterministic function. There are 26 predictor variables applied for downscaling that describe large-scale circulation such as sea-level pressure, humidity, and geopotential heights, etc. (Widmann and Bretherton, 2000; Salathé, 2005).

Some key assumptions (Wilby et al., 2004) in statistical downscaling techniques include: (1) predictor variables should be adequately reproduced by the GCM at the same spatial scales used to condition the downscaled responses (Osborn and Hulme, 1998). (2) The relationship between the predictors and predictands remains valid for periods outside of the base period. (3) The predictor set sufficiently incorporates the future climate change 'signal' (Hewitson, 1999). (4) The predictors used for determining future local climate should not lie outside the range of the climatology used to calibrate the SD model.

The selection of predictor variables is very important because this process significantly affects to downscaled results (Wilby and Wigley, 2000). Some predictors may not play a dominant role under present climate condition when applying a downscaling model, but these predictors may become critical in the future (Wilby, Hassan, and Hanaki, 1998). For example, radiative variables are of large to local temperature under a 2×CO2 scenario rather than circulation changes (Schubert, 1998) but atmospheric predictors can considerably contribute to better simulation results for local precipitation (Wilby, Hassan, and Hanaki, 1998). Until now, there is much discussion on how to select predictor variables in the downscaling process. When applying statistical downscaling, the most important requirement is long observation and available resources (Cavazos and Hewitson, 2005). Almost GCMs were designed for general circulation of which no predictor represents evaporation and moisture. Hence it does not seems to be sufficient for precipitation simulation because precipitation mechanisms are based on thermodynamics and vapor content. Therefore, humidity has recently been used to downscale precipitation (Wilby and Wigley, 1997; Murphy, 2000; Beckmann and Adri Buishand, 2002; Cavazos and Hewitson, 2005) assessed 29 NCEP reanalysis variables by applying an artificial neural network downscaling method in 15 locations. Geopotential heights and specific humidity predictors had good correlation with predictands in all locations and seasons.

Statistical methods are simpler than dynamical methods. However, disadvantages of statistical methods are underestimated result and poorly simulated extreme events. Three approaches frequently applied to downscale climate variables are: variable inflation, expanded downscaling and randomization. Variable inflation increases variability by multiplying by a suitable factor (Kilsby et al., 1998) proposed another approach namely randomization where additional variability is added in the form of white noise, of which produced good results examined by Kyselỳ, 2002). Bürger Bürger, 1996 developed the expanded downscaling approach, a variant of canonical correlation analysis (CCA). A comparison of the three methods revealed that the variable inflation approach did not produce acceptable spatial correlations, whereas the randomization approach had well performing simulations but was unable to model changes in variability. In contrast, expanded downscaling is sensitive to the selection of statistical process used during its application (Fowler and Kilsby, 2007).

Regression models are a conceptually simple means of representing linear or nonlinear relationships between predictands and a set of predictor variables. Multiple regression models are constructed based on grid cell values of atmospheric variables as predictors for surface temperature and precipitation (Murphy, 1999; Hellström and Chen, 2003; Schoof, Pryor, and Robeson, 2007; Raje and Mujumdar, 2011). Nowadays, there are numerous innovations in downscaling techniques including principal components (Kidson and Thompson, 1998; Hanssen-Bauer et al., 2003); Artificial neutral network is nonlinear regression (Zorita and Storch, 1997, Luk, Ball, and Sharma, 2000); Canonical Correlation Analysis (Karl et al., 1990; Wigley et al., 1990; Storch, Zorita, and Cubasch, 1993; Busuioc, Chen, and Hellström, 2001); Singular value decomposition (Huth, 1999; Storch and Zwiers, 1999); Analog method (Seguí et al., 2010; Wetterhall, Halldin, and Xu, 2005; Frias et al., 2006); Conditional random field (Raje and Mujumdar, 2009); K-nearest neighbor (Gangopadhyay, Clark, and Rajagopalan, 2005); Support vector machine (Smola and Schölkopf, 2004; Tripathi, Srinivas, and Nanjundiah, 2006; Anandhi et al., 2008).

Weather typing schemes: Weather typing or classification methods gather days into a limited number of distinct weather types based on their synoptic similarity. Typically, weather classes are defined by applying cluster analysis (Kidson, 2000; Hewitson and Crane, 2002; Fowler et al., 2005) or fuzzy rules (Bárdossy, Stehlík, and Caspary, 2002; Bardossy, Bogardi, and Matyasovszky, 2005) to atmospheric pressure fields or using subjective circulation classification schemes (Bardossy and Caspary, 1990; Jones, Hulme, and Briffa, 1993). In both cases, the 'nearest neighbor' method is applied to group the similarities of weather patterns. Classification-based methods are unable to capture the continuous characteristics of wet and dry spells at site level (Wilby, 1994; Anandhi et al., 2011). New approaches

have been developed as multi–site and multi–variate series (Bardossy and Van Mierlo, 2000; Palutikof et al., 2002; Jeong et al., 2012; Jeong et al., 2013). One other approach is to classify spatial rainfall occurrence patterns using hidden Markov models (Hughes and Guttorp, 1994; Hughes, Guttorp, and Charles, 1999; Mehrotra and Sharma, 2005; Greene, Robertson, and Kirshner, 2008, Ailliot, Thompson, and Thomson, 2009; Frost et al., 2011). This model constitutes a double stochastic process, including a fundamental stochastic process that is translated into another stochastic process that delivers the sequence of observations (Rabiner and Juang, 1986).

Weather generators are models that modify the statistical characteristics of a local climate variable (Wilks and Wilby, 1999). These models are based on daily precipitation with two-state, first-order Markov chains: precipitation amounts on wet days using a gamma distribution (Wilks, 1992) and secondary variables such as temperatures, humidity, and solar radiation are modeled conditional on precipitation occurrence (Wilby et al., 2004; Burton et al., 2008). The main advantage of WGs is that they can precisely simulate ensembles of observed climate variables and can be broadly applied, particularly for risk analysis scenarios and hydrologic impact assessment. The autocorrelation process can improve WGs in term of distribution of wet and dry spell length and extreme events, both based on the probability of precipitation on current and previous circulation pattern (Wilby, Dawson, and Barrow, 2002). The major disadvantage is that the parameters of precipitation are adjusted arbitrarily for future climate change, and to the unforeseen effects that these changes may have on secondary variables such as temperature, and humidity (Wilby, Wedgbrow, and Fox, 2004; Kilsby et al., 2007) the simulation of WGs tends to underestimate inter-annual variability (Semenov and Stratonovitch, 2010). In addition, WGs cannot be applied automatically for all climatic features because of different characteristics of local climate relationships (Fowler et al., 2007).

2.5 Bias correction

We define a bias as the systematic difference between a modelled property of the climate system and the corresponding real property. Such properties could be mean temperature variance or a 100-year return value. The term “systematic” refers to all differences that are not due to sampling uncertainty. Biases are typically assumed to be time-independent, but in principle may vary in time. Some authors define a bias as the time independent error component of a model.

As bias correction we consider all methods that calibrate an empirical transfer function between simulated and observed distributional parameters, and apply this transfer function to output simulated by the considered model. Bias correction according to this definition is a mere post-processing steps (Maraun et al., 2017).

The first obvious aim of a bias correction is adjusting selected simulated statistics such as means, variances or wet-day probabilities to match observations during a present-day calibration period. But several decisions need to be drawn, and the different possibilities may imply different specific assumptions to be fulfilled:

"– should a bias correction method be applied that preserves or alters the climate change signal? A trend preserving bias correction is justified under the assumption that the model bias is time invariant; a non-trend preserving method may sensibly be used if it can be assumed that this method captures the time invariance of the bias, i.e. that it corrects the simulated change.

– is downscaling to higher resolution or even point scales intended? In such a case, one has to assume that the downscaling captures the required local variations at the time scales of interest, as well as the response to climate change.

– which aspects of the climate distribution should be corrected? Most bias correction methods adjust marginal aspects only. Should also spatial, temporal and multivariate aspects be explicitly adjusted? In all cases, the underlying assumption is that the climate change signal of the considered aspects, after bias correction, is plausibly represented". (Maraun, 2016)

There are several bias correction methods for precipitation, each of which has advantages and disadvantages. In climate change studies, the combination of different methods of bias correction can reduce the errors and uncertainty. This part will briefly introduce five popular method for precipitation bias correction including linear scaling (LS), local intensity scaling (LOCI) and distribution mapping (DM), power transformation and delta-change. A list of all variables and indices used is presented in Tables 2.3.

Table 2.3 Definition of symbols and sub/superscript used in equation

Symbols	Details	Symbols	Details
α	Shape parameter of Gamma distribution	$*$	Shape parameter of Gamma distribution
β	Scale parameter of Gamma distribution	$'$	Scale parameter of Gamma distribution
d	Daily	γ	Gamma Distribution
F	Cumulative distribution function (CDF)	m	Within monthly interval
F^{-1}	Inverse of CDF	obs	Observed
μ	Mean	ref	RCM simulated 1980 – 2011
P	Precipitation	fut	RCM simulated 2012 - 2039
s	Scaling factor	th	Threshold

a Linear scaling (LS)

Linear Scaling (Lenderink, Buishand, and Deursen, 2007) operates with monthly correction values based on the differences between observed and RCM simulated values during the reference period. Corrected RCM simulations monthly mean values will perfectly agree with that of the observations. The adjusted daily precipitation for reference and future period is obtained using Eqs. (2.11) and (2.12).

$$P'_{ref}(d) = P_{ref}(d) \times \left(\frac{\mu_m(P_{obs}(d))}{\mu_m(P_{ref}(d))} \right) \tag{2.11}$$

$$P'_{fut}(d) = P_{fut}(d) \times \left(\frac{\mu_m(P_{obs}(d))}{\mu_m(P_{ref}(d))} \right) \tag{2.12}$$

b Local intensity scaling (LOCI)

The wet-day frequency and intensity corrected by the LOCI method presented by Schmidli, Frei, and Vidale, 2006 takes the linear scaling one step further and adjusts the mean as well as both wet-day frequencies and intensities separately in three steps:

(1) A precipitation threshold (P_{th}) is determined from the RCM simulated precipitation days such that the threshold exceeding matches the number of observed days with precipitation lager than 0 mm. Then the number of precipitation events for both reference and future periods are corrected by applying the precipitation threshold:

$$P^*_{ref}(d) = \begin{cases} 0, \text{ if } P_{ref}(d) < P_{th} \\ P_{ref}(d), \text{ otherwise} \end{cases} \tag{2.13}$$

$$P^*_{fut}(d) = \begin{cases} 0, \text{ if } P_{fut}(d) < P_{th} \\ P_{fut}(d), \text{ otherwise} \end{cases} \tag{2.14}$$

This step, all days with precipitation less than the threshold are redefined to dry days with 0 mm.

(2) Second step, a linear scaling factor is estimated based on the long-term monthly mean wet-day intensities. Taking only wet days of the observed days with precipitation larger than 0 mm and the RCM simulated days with precipitation larger than the precipitation threshold (P_{th}). The intensity scaling factor (s) is calculated by Eq. [2.15].

$$s = \frac{\mu_m\left(P_{obs}(d) \,|P_{obs}(d) > 0 \text{ mm}\right)}{\mu_m\left(P_{ref}(d) \,|P_{ref}(d) > P_{th}\right) - P_{th}} \tag{2.15}$$

(3) Finally, the RCM-simulated precipitation of reference and future periods are corrected as follows:

$$P'_{ref}(d) = P^*_{ref}(d) \times s \tag{2.16}$$

$$P'_{fut}(d) = P^*_{fut}(d) \times s \tag{2.17}$$

c Distribution mapping (DM)

The DM method (Teutschbein and Seibert, 2012) corrects the distribution shape of the daily precipitation based on cumulative distribution functions (CDFs) constructed for both the observed and the RCM simulated (1980-2010) for all days within a certain month. Thereafter, the value of RCM simulated precipitation of day d within month m was generated from the empirical cumulative distribution function (ECDFs) of the RCM simulations together with its corresponding cumulative probability. Then, the value of precipitation of same cumulative probability was located on the ECDFs of observations. Finally, the daily precipitation for reference and future periods are obtained by Eq. (2.18) and (2.19) in terms of the Gamma CDF (F_γ) and its inverse

(F_γ^{-1}).

$$P'_{ref}(d) = F_\gamma^{-1}\left(F_\gamma\left(P_{ref}(d)\,|\alpha_{ref,m},\beta_{ref,m}\right)|\alpha_{obs,m},\beta_{obs,m}\right) \tag{2.18}$$

$$P'_{fut}(d) = F_\gamma^{-1}\left(F_\gamma\left(P_{fut}(d)\,|\alpha_{ref,m},\beta_{ref,m}\right)|\alpha_{obs,m},\beta_{obs,m}\right) \tag{2.19}$$

The Gamma distribution with shape parameter α and scale parameter β is often assumed to be suitable for distribution of precipitation events:

$$f_\gamma(x|\,\alpha,\beta) = x^{\alpha-1}.\frac{1}{\beta^\alpha\Gamma(\alpha)}.e^{\frac{-x}{\beta}} \quad x \geq 0;\alpha,\beta > 0 \tag{2.20}$$

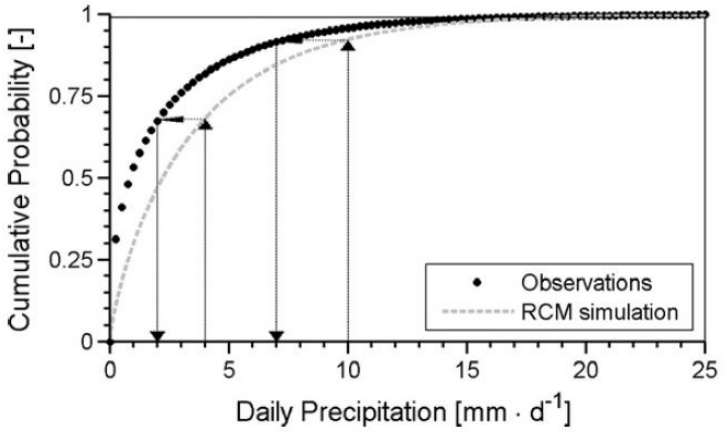

Fig. 2.9 Exemplary procedure of the distribution mapping (Teutschbein and Seibert, 2012)

d Power transformation of precipitation

While linear scaling account for a bias in the mean, it does not allow differences in the variance to be corrected. Therefore, a non-linear correction in an exponential form a.P^b (Leander and Buishand, 2007) can be used to specifically adjust the variance statistics of a precipitation time series.

Parameter b is estimated with a distribution-free approach on a monthly bias using a 90-day window cetered on the interval. First, b is identified by matching the coefficient of variation (CV) of the corrected daily GCM precipitation (P^b) with the CV of observed daily precipitation (P_{obs}) for each month m:

Find b_m such that $f(b_m) = 0 = CV_m(P_{obs}(d)) - CV_m(P^{bm}_{contr}(d))$

$$= \frac{\sigma_m(P_{obs}(d))}{\mu_m(P_{obs}(d))} -) - \frac{\sigma_m(P^{bm}_{contr}(d))}{\mu_m(P^{bm}_{contr}(d))}$$

$$P^{*1}_{contr}(d) = P^{bm}_{contr}(d) \tag{2.21}$$

$$P^{*1}_{scen}(d) = P^{bm}_{scen}(d) \tag{2.22}$$

This is done with a root-finding algorithm using Brent's method. Therefore, the long term monthly mean of observed precipitation is matched with the monthly mean of the intermediary series $P^{*1}_{contr}(d)$ by using the standard linear scaling parameter.

$$P^{*}_{contr}(d) = P^{*1}_{contr}(d).\left[\frac{\mu_m(P_{obs}(d))}{\mu_m(P^{*1}_{contr}(d))}\right] \tag{2.23}$$

$$P^{*}_{scen}(d) = P^{*1}_{scen}(d).\left[\frac{\mu_m(P_{obs}(d))}{\mu_m(P^{*1}_{contr}(d))}\right] \tag{2.24}$$

e Delta-change correction of precipitation

The underlying idea of the widely used delta-change method (Bosshard et al., 2011; Graham et al., 2007) is to use the GCM-simulated future change for a perturbation of observed data rather than to use the GCM-simulations of future condition directly. The control run also known as baseline climatology, therefore corresponds to the observed climate and cannot be used for a proper evaluation. For the future scenario, the GCM-simulated anomalies between control and scenario runs are superimposed upon the observation time series (Teutschbein and Seibert, 2012). This is usually done on a monthly basis. A multiplicative correction is used for precipitation.

$$P^{*}_{contr}(d) = P_{obs}(d) \tag{2.25}$$

$$P^{*}_{scen}(d) = P_{obs}(d).\left[\frac{\mu_m(P_{scen}(d))}{\mu_m(P_{contr}(d))}\right] \tag{2.26}$$

Chapter 3

Data-driven method and time series prediction

In the past two decades, rapid development of data-driven methods has obtained considerable achievement in handling the complex process of real-world modeling. Soft computing and statistical models are two common groups of data driven models that could be employed to solve water resources and environmental problems. Data-driven methods are often inexpensive, accurate, precise, and more importantly flexible, which make them able to handle a wide range of real-world systems with different degrees of complexity based on our level of knowledge and understanding about a system. These methods are useful for various applications, such as hydrological prediction, flood forecasting, water quality monitoring, quantitative and qualitative modeling of water resources, climatic data analysis, and general function approximation (Araghinejad, 2013).

3.1 Artificial Neural Network (ANN)

ANN is a broad term covering a large variety of network architectures, the most common of which is a multilayer feedforward neural network. Fig.3.1 shows the general structure of an ANN model (Shahin, Jaksa, and Maier, 2008). The multi-layer feedforward neural network is the most popular application in many field studies which usually uses the technique of error back propagation to train the network configuration. The architecture of the ANN consists of a number of hidden layers and neurons in the input layer, and hidden layers in the output layer as described in Fig.3.1. ANNs with one hidden layer are commonly used in hydrologic modeling (Dawson and Wilby, 2001; De Vos and Rientjes, 2005) since these networks are considered to provide enough complexity to accurately simulate the nonlinear-properties of

the hydrologic process.

Neurons are mathematical expressions that filter the signal through the net. From the connected neurons in the previous layer, an individual neuron receives its weighted inputs that are usually summed along with a bias unit. The bias unit is used to scale the input to a useful range in order to improve the convergence properties of the neural network. The result of this combined summation is passed through a transfer function to produce the output of the neuron. This output is then passed through weighted connections to neurons in the next layer, where the process is repeated. The weight vectors connecting the different nodes of the network are found by the so-called error back-propagation method. During training, the values of these parameters are varied so that the ANN output becomes similar to the measured output on a known data set (Haykin, 1994; Bhattacharya, Price, and Solomatine, 2007). A trained response is achieved by changing the connections' weights in the network according to an error minimization criterion. A validation process can be used during training in order to prevent overfitting. Once the network has been trained to simulate the best response to input data, the configuration of the network is fixed and a test process is conducted to evaluate the performance of the ANN as a predictive tool (Bui et al., 2015).

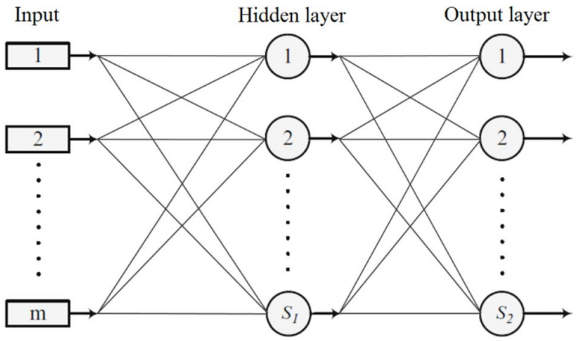

Fig. 3.1 Multilayer feedforward artificial network with one hidden layer

3.2 Seasonal ANN (SANN)

A seasonal time series forecasting problem can be thought of as a function approximation problem. So, SANN may improve on the ordinary ANN (Section 3.1) by taking into account the seasonal fluctuations of the series and successfully forecast with a proper ANN structure (Hamzaçebi, 2008). Using the s parameter for determining the input neurons number may help to make better predictions. The s parameter presents the series structure, such as;

monthly, etc... In this kind of network structure *ith* seasonal period observations are values of input neurons and $(i+1)th$ seasonal period observations output neurons values. The suggested model is called Seasonal Artificial Neural Network (SANN) using Levenberg-Marquardt (LM) learning algorithm. The input layer, $m = (k \times s)$ nodes, where s =12 (for monthly time series), and k is a coefficient representing the type of preprocessing method. The hidden layer consists of n = 3, 5, 8, 10 and 15 neurons, and the output layer with one node. The Tan-sigmoid function is used as transfer function in the hidden layer for all cases.

The SANN architecture is given by the following eq.3.1:

$$Y_{t+l} = \sum_{j=1}^{n} \mathbf{LW}_{jl} f \left(\sum_{i=1}^{m=ks} \mathbf{IW}_{ij} \mathbf{Y}_{t-i} + \mathbf{b}_j \right) + \mathbf{b}_l \tag{3.1}$$

where $Y_{t+l}\,(l = 1,2,\ldots,m)$ represents the predictions for the future s periods; $Y_{t-i}\,(i = 1,2,\ldots,m)$ are the observations of the previous s periods; $IW_{ij}\,(i = 1,2,\ldots,m;\ j = 1,2,\ldots,n)$ are weights of connections from input layer neurons to hidden layer neurons; $LW_{jl}\,(j = 1,2,\ldots,n;\ l = 1,2,\ldots,m)$, are weights of connections from hidden layer neurons to output layer neurons; $b_l\,(l = 1,2,\ldots,m)$ and $b_j\,(j = 1,2,\ldots,n)$ are weights of bias connections and f is the activation function, n is the number of neurons in the only hidden layer, and t is the current time step.

3.3 Long Short Term Memory (LSTM)

Though RNNs have proven successful on tasks such as speech recognition (Vinyals et al., 2015) and text generation (Sutskever, Vinyals, and Le, 2014), it can be difficult to train them to learn long-term dynamics, likely because of the vanishing and exploding gradients problem (Hochreiter and Schmidhuber, 1997). This phenomenon can result from propagating the gradients down through the many layers of the recurrent network, each of which corresponds to different time steps. LSTMs provide a solution by incorporating memory units that allow the network to learn when to forget previous hidden states and when to update hidden states with new information.

LSTMs extend RNN with memory cells, instead of recurrent units, to store and output information, easing the learning of temporal relationships on long time scales. The major innovation of LSTM is its memory cell which essentially acts as an accumulator of the state information. LSTMs make use of the concept of gating: a mechanism based on component-wise multiplication of the input, that defines the behavior of each individual memory cell. The

LSTM updates its cell state according to the activation of the gates. One advantage of using the memory cell and gates to control information flow is that the gradient will be trapped in the cell and be prevented from vanishing too quickly, a critical problem for the classic RNN model (Hochreiter and Schmidhuber, 1997; Pascanu, Mikolov, and Bengio, 2013). The input provided to an LSTM is fed into different gates that control which operation is performed on the cell memory: write (input gate), read (output gate) or reset (forget gate). The activation of the LSTM units is calculated like they are in the RNNs. The computation of the hidden value h_t of an LSTM cell is updated at every time step t. The vectoral representation (vectors denoting all units in a layer) of the update of an LSTM layer is denoted as input gate i_t, a forget gate f_t, an output gate o_t, a memory cell c_t and a hidden state h_t.

As research on LSTMs has progressed, hidden units with varying connections within the memory unit have been proposed. We use the LSTM unit as described in Figure 3.2, which is a slight simplification of the one described in Graves and Jaitly, 2014. The sigmoid nonlinearity which squashes real-valued inputs varies in a [0; 1] range, and the hyperbolic tangent nonlinearity, similarly squashing its inputs changes in a [-1; 1] range, the LSTM updates for time step t given inputs x_t, h_{t-1} and $c_{t-1}$are:

$$i_t = \sigma\left(W_{xi}x_t + W_{hi}h_{t-1} + b_i\right) \tag{3.2}$$

$$f_t = \sigma\left(W_{xf}x_t + W_{hf}h_{t-1} + b_f\right) \tag{3.3}$$

$$o_t = \sigma\left(W_{xo}x_t + W_{ho}h_{t-1} + b_o\right) \tag{3.4}$$

$$g_t = \phi\left(W_{xc}x_t + W_{hc}h_{t-1} + b_c\right) \tag{3.5}$$

$$c_t = f_t \odot c_t + i_t \odot g_t \tag{3.6}$$

$$h_t = o_t \odot (c_t) \tag{3.7}$$

where *i, f, o, c* and *g* are respectively the input gate, forget gate, output gate and cell activation, input modulation gate vectors; all of them are the same size as vector *h* defining the hidden value. Terms σ represent an element-wise application of the *sigmoid (logistic)* function. The term x_t the input to the memory cell layer at time; $W_{xi}, W_{xf}, W_{xo}, W_{xc}$ are weight matrices, with subscripts; b_i, b_f, b_o, b_c representing from-to relationships (the input-input gate matrix, the hidden-input gate matrix, etc.) are bias vectors; ϕ stands for an element-wise application of the *tanh* function; denotes $\odot$ elementwise multiplication.

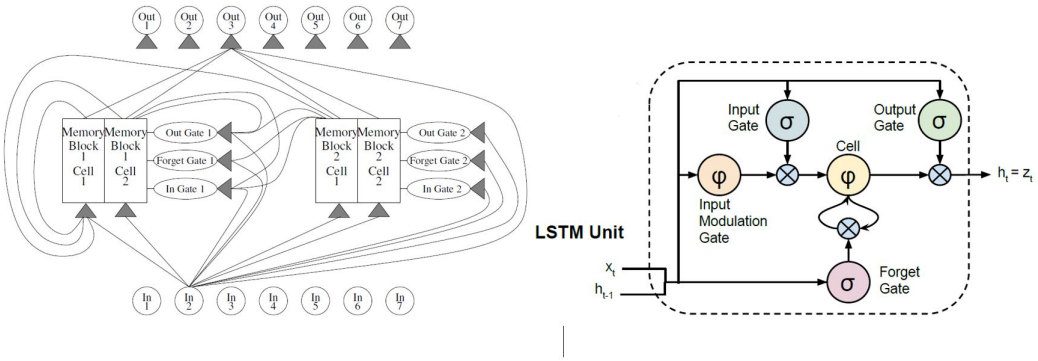

Fig. 3.2 A diagram of a LSTM network (left) and LSTM memory cell (right) (Donahue et al., 2015)

Chapter 4

Study area

4.1 Vietnamese Mekong Delta

The Mekong River is a major and the longest river in south-eastern Asia. From its source in China's Qinghai province near the border with Tibet, the Mekong generally flows southeast to the South China Sea, a distance of 4,200 km (2,610 mi). The Mekong crosses Yunnan Province, China, and forms the border between Myanmar (Burma) and Laos and most of the border between Laos and Thailand. It then flows across Cambodia and southern Vietnam into a rich delta before emptying into the South China Sea. In the upper course are steep descents and swift rapids, but the river is navigable south of Louangphrabang in Laos. The delta plain of the Mekong River Delta is about 62,520 km^2 of which 52,100 km^2 is located in Vietnam and the remainder in Cambodia. In Vietnam, the Mekong River Delta is occupied by eleven provinces with a population of 14.8 million. The region represents a national rice bowl providing agricultural products not only to Vietnam but also to other countries.

The Vietnamese Mekong River stems from the Cambodian border, where it splits into two primary distributaries, namely the Tien and Hau Rivers, with a total area of 19,500 km^2 (MRC, 2007a) (Fig. 4.2). The topography of the VMD is relatively flat; most of the elevations are approximately 0.5m to 1.0m above mean sea level. There is a complex channel network as a result of agricultural activities and the developments of transportation infrastructure over a long period of time. The total length of the channel network is about 91,000 km, and includes 193 spills, 409 reservoirs, 29 sluices, 749 floodplains and more than 20,000 kilometers of protection dykes that prevent early floods (Van et al., 2012; Tuan et al., 2007). The mean annual flow is 15,000 m3/s, the maximum discharge is about 60,000 m^3/s in the flood season and the minimum discharge is around 2,000 m^3/s in the dry season (MRC, 2005;

Trung et al., 2013). The VMD river network has highly complicated hydraulic conditions, influenced by the discharges at Kratie and from Tonle Sap Lake as well as the sea level along the South China Sea and the Gulf of Thailand.

The climate of the VMD has tropical monsoon characteristics, with two separate seasons per year. The rainy season normally runs from May to October, whereas the dry season ordinarily lasts from December to March (De, 2006). In general, the mean annual precipitation for the entire VMD is 1500 mm and its range varies from 1600 mm to 2400 mm/year. The total precipitation in the rainy season contributes nearly ninety percent of the annual precipitation (Huu-Thoi and Gupta, 2001). The average discharge in the dry season fluctuates extraordinarily, from 1,700 m^3/s to 6,000 m^3/s between January and May, causing water shortages for the irrigation of the 1.5 million hectares of agricultural cultivation (Tuan et al., 2007). There are two types of tidal regime, namely the semi-diurnal and diurnal tides affecting the hydraulic condition in estuaries of the East and West seas, respectively (Nguyen and Savenije, 2006). The salinity intrusion in the VMD—and in all the river networks has been substantial in recent years, particularly in the dry season, during which about 2.1 million hectares in the Mekong Delta suffered from salinity intrusion (Wassmann et al., 2004; Tuan et al., 2007). The tidal amplitude fluctuations in the South China Sea are between 1.0m and 3.5m, leading to changes in the daily water level in the rivers, especially in the dry season that is effect by the tidal regime (Van et al., 2012). The Tien River carries about 80% of the total discharge of the entire delta. The Hau River is linked to the Tien River by the Vam Nao River, and the annual discharge is about 1,500 to 6,500 m^3/s (MRC, 2007b).

The hydrological cycle of the VMD has specific characteristics driven by the tropical monsoon climate, with two prevalent directions: the Southwest and the Northeast Monsoons (Costa-Cabral et al., 2008; Delgado, Merz, and Apel, 2012). The Southeast direction prevails from May to September, while the Northeast Monsoon is active from November to February (Delgado, Merz, and Apel, 2012). The hydrological characteristics of the VMD with its two distinct flow hydrographs have developed through typical monsoon occurrences. Lager distributions of the annual discharge are significantly concentrated during the rainy season (July–December). Approximately 75 to 85% of the total annual flow in the rainy season leads to flooding in the large area in the downstream delta (MRC, 2005; Hoang et al., 2016). However, this flooding could beneficially contribute to the area's highly fertile alluviums and fish productivity (Eastham et al., 2008; Hapuarachchi et al., 2008).

Fig. 4.1 Study area of Vietnamese Mekong delta

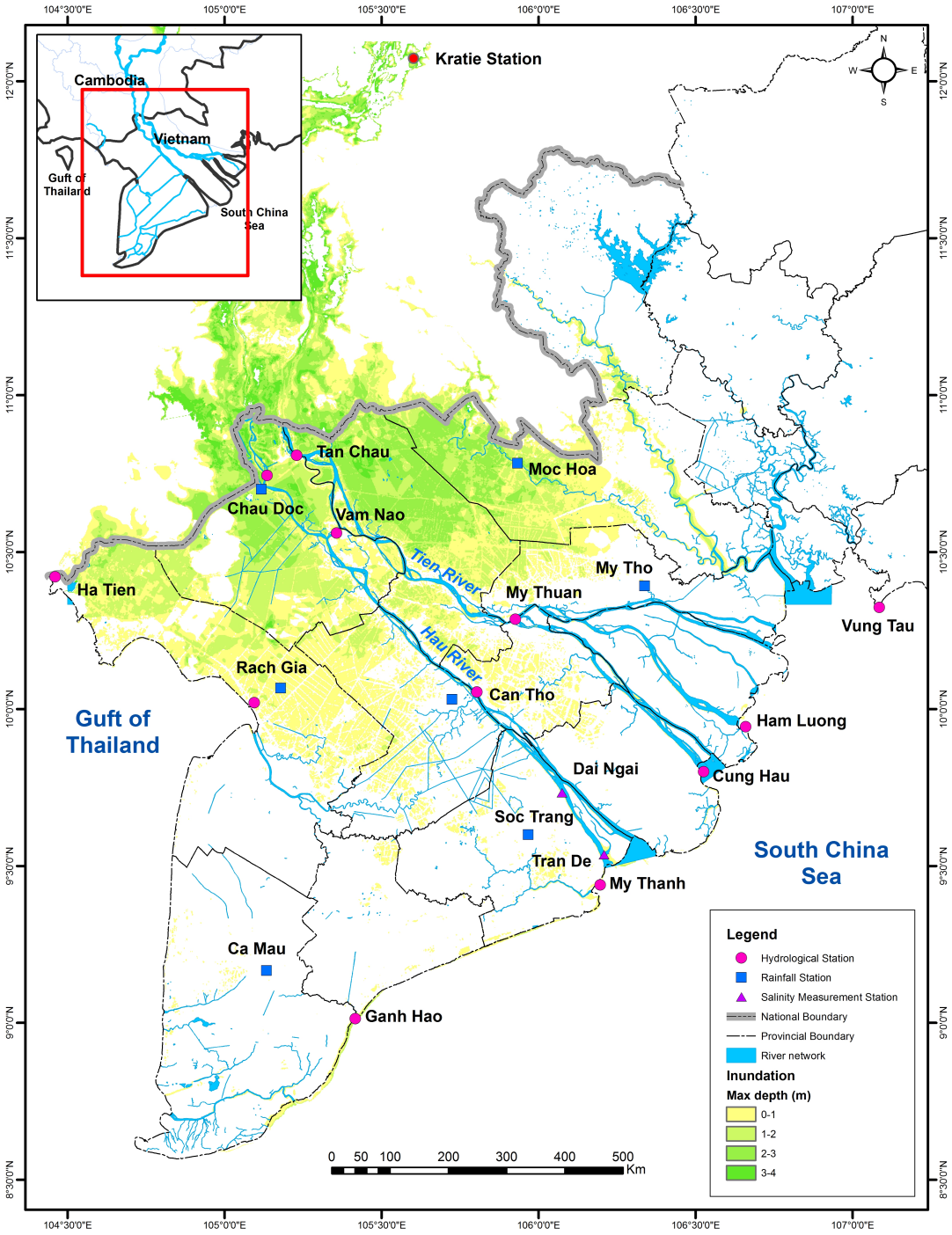

Fig. 4.2 The river network of Mekong delta

4.2 Data collection sources

Time series data of selected parameters were collected at provincial level. The data were collected from several agencies (water, bathymetry, and hydro-climate) and the data collecting institutions (General Statistic Office, Statistical Bureau, Statistic Division...). For hydro-climate data, data length has the duration of 1978 – 2011. Bathymetric data has the duration of 2010 by Department of rivers transportation management in Southern Vietnam. The summary of collected data was presented in Table 4.1 below.

The data is collected by several agencies as following:

- General Statistical Office (GSO);
- Vietnam Mekong river committee (MRC);
- Southern Regional Hydrometeorology Center (SRHMC);
- South Institute of Water Resources Planning (SIWRP),
- National Institute of Agricultural Planning and Projection (NIAPP),
- District People's Committee (DPC);

Hydro-climate data that have been selected from the specific stations have data lengths of at least 30 past years. The sea level data is collect at Vung Tau station with a length of 10 years.

Table 4.1 Data collection from secondary sources

No	Name of data	Length	Spatial scale	Sources
A	**Climate and water resource**			
1	Rainfall at 7 station in VMD	30 years	1978 – 2011	SRHMC
2	Evapotranspiration, Radiation	30 years	1978 – 2011	SRHMC
3	Wind speed, Humidity	30 years	1978 – 2011	SRHMC
4	Discharge at Kratie, Chau Doc, Can Tho	5 years	2005 – 2011	SIWRP
5	Water level at 10 stations	2 years	2010 - 2011	SIWRP
6	Water demand (domestic, irrigation and industry) and forecasting to 2030	5 years	2005 – 2011	SIWRP
B	**Geographical data**			
1	Bathymetry of estuary and offshore	1 years	2010 - 2011	DHI
2	Water level at Tan Chau station	2 years	2010 - 2011	SRHMC
3	Sea level at Vung Tau station	10 years	2001 - 2010	SRHMC
4	Cross section of Mekong river network	7 years	2005-2011	SIWRP
5	Digital map of Tien river	1 years	2011	SIWRP
6	Wind direction and speed from East Sea	1 years	2011	SIWRP

4.3 Research Methodology

This part describes step-by-step methodologies to achieve the objectives of the study. Fig 4.3 shows the methodology scheme to study the impact of climate change on hydraulic regime and salinity intrusion in Hau River, Vietnamese Mekong delta by through the use of upstream discharge variability, rainfall alteration and sea level rise by climate change.

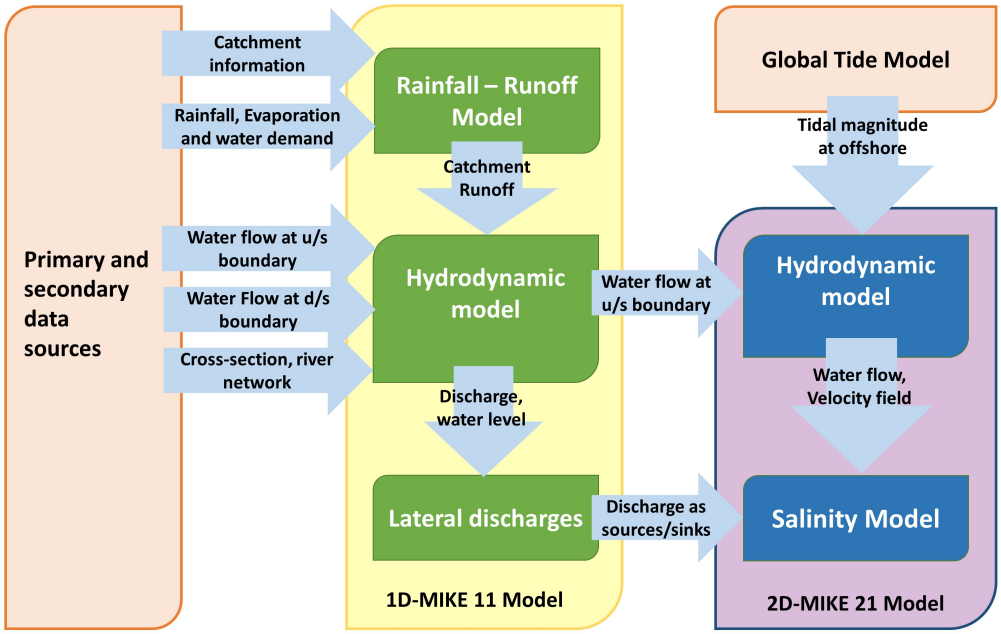

Fig. 4.3 The schema of research methodology (revised from Dasgupta et al., 2015)

To explain in detail the objectives and tools applied in this research, the research framework should be provided to clearly define all steps and methods used. The detail tasks and tools that obtain the main objectives are illustrated in Table 4.2.

Table 4.2 Research Framework

No.	Objectives	Sub-objectives	Tasks	Tools/Output
1	To forecast the amount of future rainfall in the study area under climate change with different scenarios from 5 GCM outputs.	• Rainfall prediction in Mekong delta based on measured hydrological data and rainfall obtained from 5 GCM models from CMIP5.	• Selecting of representative stations; • Analyzing and compilation raw data; • Data verification; • Apply different downscaling techniques and bias correction; • Analyzing the results and plotting.	• Secondary data from SRHMC, SIWRP; • Data from 5 GCMs, 2 RCP scenarios obtained from CMIP5; • MATLAB programming; • Statistical analysis of results; • Three bias correction methods.
2	To develop a new model of Artificial Neural network and Long Short Term Memory for predicting rainfall and runoff.	• Improve the skill of forecast for rainfall and rainfall – runoff in the Mekong delta	• Arrange meteorological data for training • Develop model of ANN and LSTM • Analyzing the correlation and select possible combination for training model. • Training model and analyze the results.	• Develop code for ANN and LSTM; • Rainfall data from Mekong delta (7 stations); • MATLAB and Python languages; • Rainfall prediction; • Rainfall – Runoff prediction.
3	To apply MIKE 11 model to simulate hydraulic regime for whole Mekong delta and the total volume of rainfall at the basin to use as the input of MIKE 21 model.	• Apply MIKE 11 HD software to simulate flow and water level in Mekong delta from Kratie to VMD	• River network and cross sections, • Setup time steps and simulation period • Discharge at Kratie and water level at outlet of Tien and Hau river; • Bed slop and resistance; • Boundary condition; • Wind condition and water use.	• The branches discharges and water level along Hau river; • Total rainfall from climate change converting to runoff in the main rivers.
4	To apply MIKE 21 model to simulate hydraulic regime and salinity intrusion in the Hau river under different scenarios of climate change, sea level rise and upstream discharge variations.	• Apply MIKE 21 HD and TR to forecast salinity intrusion at Hau river estuary when changing the upstream discharge and sea level rise.	• Bathymetry of Hau river estuary and offshore, • Simulation period (time steps) • Water level on river and sea level • Bed slop and resistance; • Boundary condition; • Sources and sinks from MIKE 11 output • Wind condition, sea level scenarios	• How far from salinity intrusion in different scenarios; • Hydraulic regime (water level, velocity distribution) on estuary; • Salt intrusion distribution: • Flushing time.

Chapter 5

Model applications

5.1 ANN, seasonal ANN and LSTM for rainfall prediction

5.1.1 Data collection

Monthly rainfall data obtained from the Ca Mau hydrological gauging station at Ca Mau province, Vietnam (Location: 9^o10'24" N latitudes and 104°42' - 105^o09'16" E longitudes) by the Southern Hydro-Meteorological Center was used to train and test all the models developed in this study. The rainfall data covers 39 years from 1971 to 2010. Three subsets of the data, training, validation and testing are required to build the model. To achieve this, the data from January 1, 1979 to December 31, 2004 (85% of total data) were used for training and validation, and the data from January 1, 2005 to December 31, 2010 (15% of total data) were used as the testing set.

A general statistical summary of the monthly rainfall data at Ca Mau Station and its subdivided periods are provided in Table. 5.1, including minimum, maximum, mean, standard deviation (S_d), skewness coefficient (C_s), and autocorrelations at 1 day lag to 3 day lag (R_1, R_2, and R_3). It should be noted that data driven methods as ANN perform best when they do not extrapolate beyond the range of data used for model training and when the extreme values of the available data are included in the training set. It can be seen from Table. 6.6, the extreme values of R is in the range of the training set. Skewness coefficients are low for all datasets, which is better suited for ANN models. High skewness coefficients generally have considerable negative effect on model performance (Altun, Bilgil, and Fidan, 2007). In general, we find that there is good similarity between the training the validation subsets, especially in terms of autocorrelation coefficients.

Table 5.1 The statistical analysis for training, validation, testing and all data sets

Statistical parameters	Training set	Validation set	Testing set	All data
Min	0	0	0	0
Max	782.1	748.7	656	782.1
Mean	198.29	223.798	196.655	202.43
S_d	170.266	176.683	166.183	170.53
C_s	0.568	0.559	0.437	0.543
R_1	0.568	0.480	0.629	0.565
R_2	0.297	0.239	0.339	0.298
R_3	-0.003	0.057	0.049	0.023

5.1.2 Model setup

5.1.2.1 Model selection

In this study, three different models are applied to predict rainfall in the following month. The three models are applied to predict monthly rainfall and evaluate the efficiency of these model (Fig. 5.1). Ranging the number of neuron from 3 to 15 in hidden layer and the number of memory blocks from 10 to 30 in LSTM ensure that the best structure of neural network can be determined during the training process.

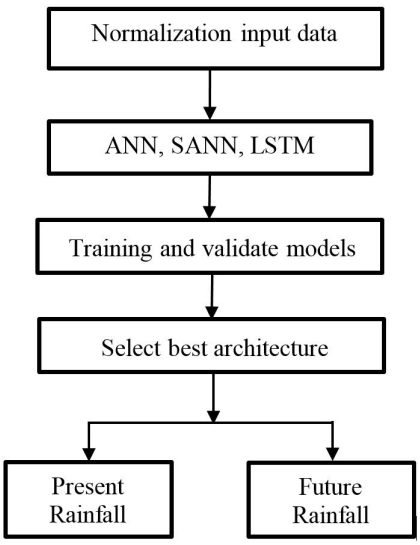

Fig. 5.1 The structure of study

The original data is divided into three sets of training, validation and testing sets. Finally, the divided data sets data are imposed to ANN or SANN, LSTM models to predict the rainfall. Since there is no especial rule for ANN SANN or LSTM models development, a trial and error method must be used to find the best network's configuration. However, using Kolmogorov's theorem, Marquez, White, and Gill, 2001 and Hornik, Stinchcombe, and White, 1989 proved that for many problems, only one hidden layer can be sufficient to ensure that the structure has the properties of a universal approximator given there are enough neurons in the hidden layer (Bui et al., 2015). Moreover, studies of Zhang, Patuwo, and Hu, 1998; Dawson and Wilby, 2001; and De Vos and Rientjes, 2005 further proved an ANN with only one hidden layer can be used for different hydraulic and hydrologic modelling. It is shown that these networks are considered to provide enough complexity to accurately simulate the nonlinear features of the hydrological processes, therefore increasing the number of hidden layers would not significantly improve the performance of network (Rajaee, 2011; Bui et al., 2015). It is also validated that the Levenberg-Marquardt method is by far the most powerful learning algorithm which may be used for neural network training (Schmitz, Zemp, and Mendes, 2006, Wu, Chau, and Li, 2009).

Another important concern is the type of selected activation function for nodes. The Sigmoid and linear activation functions are most frequently employed for hidden and output nodes, respectively, to make an ANN model more effective (Rajaee, 2011). As a result, we fixed the number of hidden layers, and the type of activation functions, and learning algorithm and investigate the optimum network architectures by only varying the number of hidden neurons. By minimizing the difference among the neural network predicted values and the desired outputs the optimum network architecture was selected. The training of the neural network models is stopped when either the acceptable level of error is achieved or the number of iterations exceed a prescribed value. Each modification of hidden neurons was tested with fifty trials, which served as the basis for performance assessment of mean values. After a trial and error procedure, an optimal ANN, SANN, and LSTM for rainfall prediction was found for each combination.

5.1.2.2 Model evaluation

Legates and McCabe, 1999 suggested that a perfect evaluation of the model performance should include at least one goodness-of-fit or relative error measure (e.g., correlation coefficient, R) and at least one absolute error measure (e.g. root mean square error, *RMSE* or mean

absolute error, *MAE*). We employ a range of statistical measures to evaluate the performance of our new model, including *R, RMSE,* and *MAE* as formulated below:

$$RMSE = \sqrt{\frac{1}{n}\sum_{i=1}^{n}(x-y)^2} \tag{5.1}$$

$$MAE = \frac{1}{n}\sum_{i=1}^{n}|x-y| \tag{5.2}$$

$$R = \frac{n\sum_{i=1}^{n}(xy) - \left(\sum_{i=1}^{n}x\right)\left(\sum_{i=1}^{n}y\right)}{\sqrt{\left[n\sum_{i=1}^{n}x^2 - \left(\sum_{i=1}^{n}x\right)^2\right]\left[n\sum_{i=1}^{n}y^2 - \left(\sum_{i=1}^{n}y\right)^2\right]}} \tag{5.3}$$

where x is the observed monthly rainfall, $y$is the predicted outcome based on various model combinations, and $n$is the total number of months in the time-series. The *R* expresses degree of similarity between predicted and actual data, where a value closer to 1 indicates greater similarity and values close to -1 indicate vice versa *RMSE* on the other hand, represents the average distance of a data point from the fitted line measured along a vertical line, *MAE* indicates how close predictions are to the measured outputs. Low RMSE and MAE values indicate high confidence in the model-predicted values.

5.1.3 Result and discussion

The three models previously mentioned were applied for predicting monthly rainfall time series at Ca Mau station, Vietnam. The LSTM, ANN and SANN to were to utilized to predict the monthly rainfall time series. The LSTM model was first applied and the results were compared with a single ANN, and SANN in terms of statistical performance. In general, the efficiency of LSTM models were examined in this paper. Tables 5.2 to 5.5 present the statistical performance indices of the three previously mentioned models, for the testing and all data set, respectively. As can be seen from these tables, the LSTM results yield a better performance than ANN and SANN for the testing phase. The obtained results indicate that deep learning LSTM can capture particular features of the data set.

According to four Tables, in Ca Mau rainfall data, the LSTM model trained with complex architecture including an input gate, output gate, forget gate and 30 memory blocks provides the best efficiency as described by the highest value of R = 0.9892 and the lowest RMSE =

24.150 (mm) and MAE = 17.315 (mm). For ANN, SANN models, the network trained with 5 to 8 neurons show acceptable results with the statistical performance including R, RMSE, and MAE are 0.8061, 98.311, 74.054 (mm) and 0.829, 92.886, 74.225 (mm), respectively. The results demonstrate that both ANN and SANN yield low performance in term of these statistical indices compared to those of the LSTM simulation. In general, ANN and SANN models have capacity to cope with the non-stationary time series data that may include seasonal features as rainfall but are less accurate than LSTM model for the same data set. This proves the advantages of using LSTM in sequence forecasting problems.

From Table 5.4 and 5.5, the accuracy of LSTM model depends significantly on numbers of memory blocks and numbers of loops. Increasing the number of memory blocks and numbers of loops may better captures the highlight pattern of input data, for example extreme peaks. The proposed LSTM model also applied dropout technique to overcome the overfitting problem during training model.

The temporal variations of the observed and predicted rainfall using the best performance of the three models are illustrated in Figs. 5.2 and 5.3. Moreover, the predicted rainfall are plotted against observed rainfall in these figures. As can be seen, the LSTM with 1 million loops and 30 memory blocks yield better results for rainfall prediction than the other two models. On the other hand, the results of these models are closer to 45^o straight line in the scatter plots compared to those of the others. It is also clear that LSTM results generally tend to overestimate measured data while ANN and SANN models almost under-estimate measured values. The most accurate result belongs to the LSTM, where the predicted peaks fit relatively well and consistent with the observed rainfall peaks.

Regarding to the LSTM performance, from Fig. 5.4, it can be seen that when increasing the number of LSTM blocks and loops, the model can capture the highlight characteristic of the data, for example the extreme peaks of sequences. Moreover, increasing in the number of loops leads to a significant reduction RMSE by around 70% while a slightly increase in correlation coefficient about 10%.

Table 5.2 The statistical performance of ANN and SANN models (Test data set)

Model	Statistical performance	Number of neurons 3	5	8	10	15
ANN	R	0.7948	0.8092	**0.8061**	0.7770	0.7248
	RMSE	103.9385	101.4842	**98.3109**	104.9657	114.1420
	MAE	84.3679	80.4982	**74.0538**	78.6600	82.7604
SANN	R	0.8300	**0.8287**	0.8049	0.8171	0.8112
	RMSE	94.8723	**92.8862**	99.5541	96.0473	97.0712
	MAE	78.8377	**74.2247**	79.1828	78.0073	76.7192

Table 5.3 The statistical performance of ANN and SANN models (All data set)

Model	Statistical performance	Number of neurons 3	5	8	10	15
ANN	R	0.7185	0.7389	**0.7496**	0.7323	0.7340
	RMSE	119.3717	116.1545	**112.7167**	116.2497	115.5481
	MAE	92.9199	90.6317	**82.9759**	85.3620	85.2603
SANN	R	0.8010	**0.8164**	0.8070	0.8200	0.8213
	RMSE	102.2606	**97.1078**	100.3804	96.7091	96.1686
	MAE	79.9284	**70.2974**	73.5328	73.3155	71.8607

Table 5.4 The statistical performance of different LSTM models (Test data set)

Model	Statistical performance	Number of memory blocks				
		10	15	20	25	30
Loops = 50,000						
	R	0.7015	0.8406	**0.8745**	0.7015	0.8650
	RMSE	105.6511	79.3030	**72.1195**	105.6511	74.7602
	MAE	73.1524	56.2781	**50.7898**	73.1524	48.8809
Loops = 100,000						
	R	0.9242	0.8550	0.9022	**0.9390**	0.8975
	RMSE	62.3216	86.7532	70.5206	**57.1235**	73.0849
	MAE	39.4369	67.1348	47.4715	**41.3648**	54.4961
Loops = 500,000						
	R	0.9784	0.8714	0.9586	**0.9900**	0.9651
	RMSE	34.5020	81.4141	47.0062	**24.4243**	42.8520
	MAE	24.8728	59.5547	33.5047	**18.9671**	30.9974
Loops = 1,000,000						
	R	0.8786	0.9584	0.9250	0.9058	**0.9892**
	RMSE	80.6690	47.1973	60.3078	71.5457	**24.1500**
	MAE	59.9050	34.6075	42.9468	53.1203	**17.3154**

Table 5.5 The statistical performance of different LSTM models (All data set)

Model	Statistical performance	Number of memory blocks				
		10	15	20	25	30
Loops = 50,000						
	R	0.6875	0.8238	0.8570	0.6875	0.8477
	RMSE	111.9902	84.0612	76.4467	109.8771	77.75061
	MAE	76.0785	58.5292	54.3451	78.2731	52.3026
Loops = 100,000						
	R	0.9057	0.8379	0.8841	0.9202	0.8795
	RMSE	66.0609	91.9584	74.7518	59.4084	76.0083
	MAE	41.0144	69.8202	50.7945	43.0194	56.6759
Loops = 500,000						
	R	0.9588	0.8539	0.9394	0.9702	0.9458
	RMSE	35.1920	89.5555	48.8865	24.9128	44.5661
	MAE	25.1215	66.7013	35.8500	20.2948	31.9273
Loops = 1,000,000						
	R	0.8610	0.9392	0.9065	0.8877	0.9694
	RMSE	82.2824	49.0852	63.3232	74.4075	24.8745
	MAE	61.1031	34.9536	45.9531	56.3075	18.0080

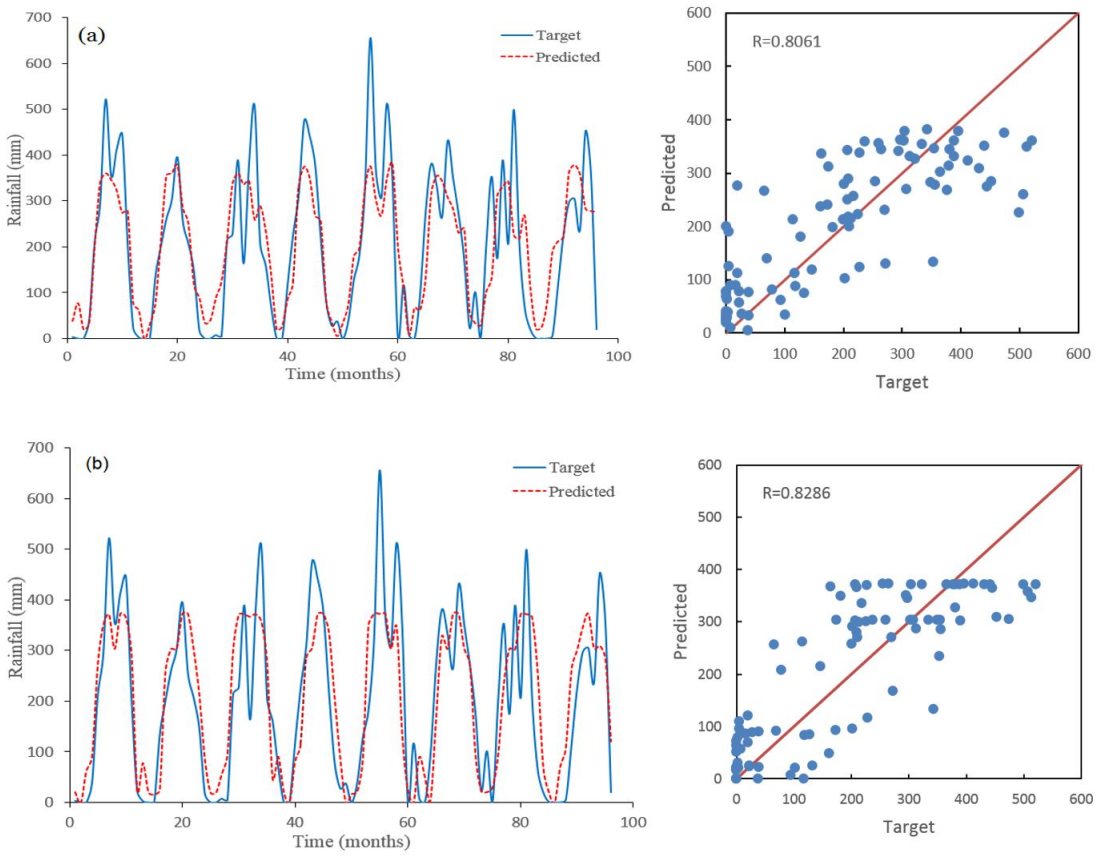

Fig. 5.2 Predicted rainfall using (a) ANN and SANN (b)

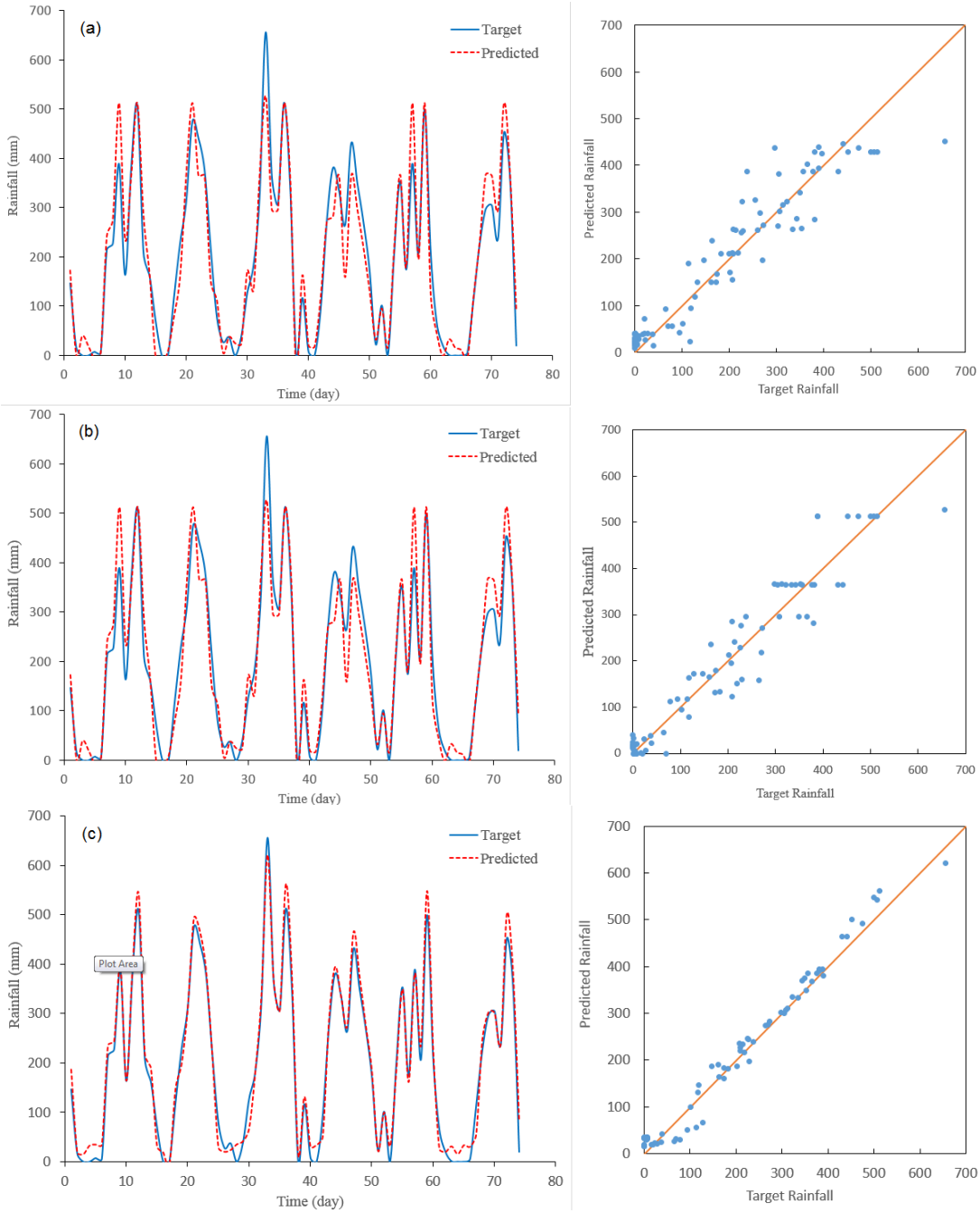

Fig. 5.3 Predicted rainfall using LSTM for the testing period; (a) 25 memory blocks with 100,000 loops, (b) 25 memory blocks with 500000loops, (c) 30 memory blocks with 1000,000 loops

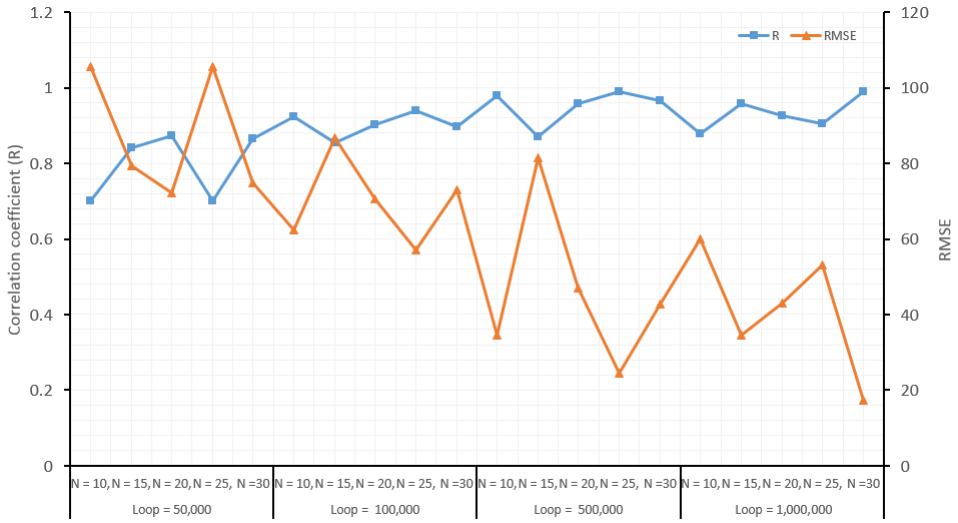

Fig. 5.4 Variations of correlation coefficient and RMSE respect to numbers of loops and memory blocks

5.2 ANN and LSTM for rainfall - runoff prediction

5.2.1 Data collection

Chau Doc and Can Tho, two rain gauge stations on the Hau River of the Vietnamese Mekong delta, are considered as case studies. The Hau River, a second branch of Mekong River, is located in Southern Vietnam. The daily collected data includes rainfall, runoff (better known as discharge). The data period of the Chau Doc station spans 16 years from January 1, 1996 to December 31, 2011, and the Can Tho station data spans 12 years from January 1, 2000 to December 31, 2011. The daily rainfall data and runoff data are measured at two rain gauges and two hydrological stations with the same respective names located at the upper region and middle of Hau River. The average discharge at Chau Doc is about 3200 m^3/s with an average annual rainfall of 1700 mm. At Cau Tho, the average discharge is about 9200 m^3/s with an average annual rainfall of 1300 mm. Fig. 5.5 demonstrates the rainfall and runoff time series in the two stations. The data represents various types of hydrological conditions, wthi flow ranging from low to very high for a long time, rendering; these data are relatively sufficient for ANN model. The entire input–output dataset in each station is divided into three subsets, namely a training set, cross-validation set and testing set with 70% of total data for training and 15% for cross-validation and 15% for testing. The training set serves the model training and the testing set is used to evaluate the performances of models. The cross-validation set has two functions: one is to implement an early stopping approach to avoid overfitting of the training data, and the second is to select best predictions from various ANN's runs. Moreover, ANN employs the hyperbolic tangent function as the transfer function in both hidden and output layers. Table 1 presents statistical information on rainfall and streamflow data, including mean (μ), standard deviation (S_x), skewness coefficient (C_s), minimum (X_{min}), and maximum X_{max}).

Table 5.6 Statistical information on rainfall and streamflow data

Hydrological stations and datasets	Statistical parameters				
	μ	S_x	C_s	X_{min}	X_{max}
Chau Doc					
Rainfall (mm)					
Original data	3.741	10.825	7.354	0	294.5
Training	3.746	11.084	8.260	0	294.5
Cross-validation	4.231	11.162	4.231	0	94.10
Testing	3.055	9.092	5.027	0	105.8
Runoff (m^3/s)					
Original data	2583	2146	0.649	133	8210
Training	2570	2153	0.658	133	8150
Cross-validation	2361	1901	0.607	214	6420
Testing	2868	2312	0.543	238	8210
Can Tho					
Rainfall (mm)					
Original data	4.254	10.908	5.769	0	230.4
Training	4.281	11.213	6.139	0	230.4
Cross-validation	3.801	8.763	3.103	0	60.90
Testing	4.232	10.975	4.872	0	109.0
Runoff (m^3/s)					
Original data	6371	4928	0.592	0	34190
Training	6165	4836	0.637	0	34190
Cross-validation	6968	4582	0.288	0	16600
Testing	6736	5581	0.601	0	19600

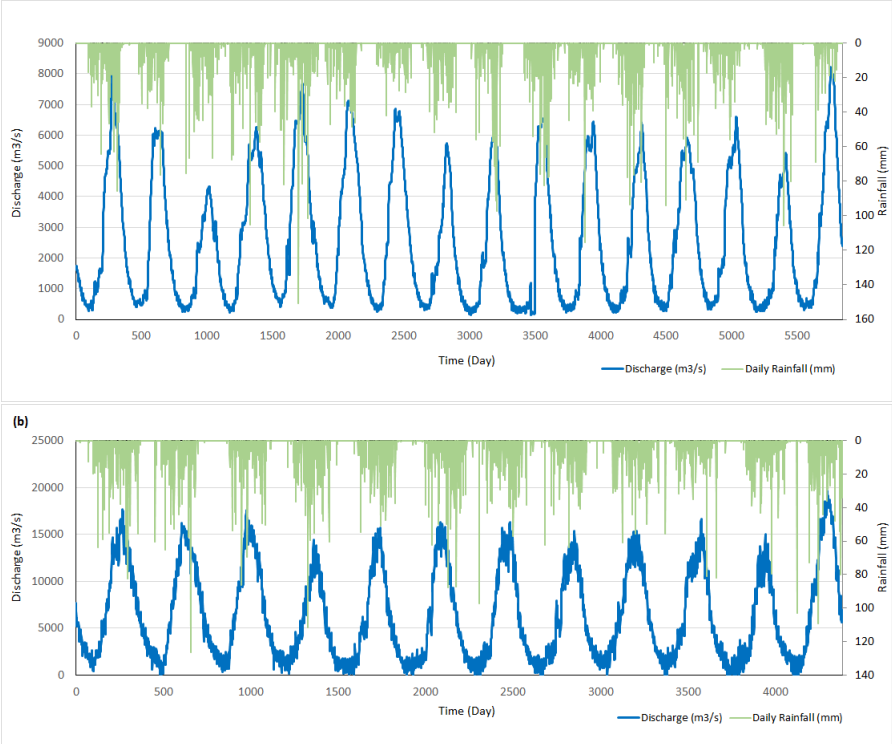

Fig. 5.5 Daily rainfall-runoff time series (a) Chau Doc and (b) Can Tho

5.2.2 Model setup

5.2.2.1 Potential input variables

Screening the possible variables for model inputs in the neural network method is an important step to select the optimal architectures of models. The causal variables in the rainfall–runoff relationship may include rainfall, evaporation, temperature, etc. The number of different variables depend on the availability of data and objectives of the studies. Most studies have applied rainfall and past discharges with different time steps and combinations as inputs (Xu and Li, 2002; Jeong and Kim, 2005; Senthil Kumar et al., 2005; Sivapragasam, Liong, and Pasha, 2001) while other studies attempted to apply other factors such as temperature or evapotranspiration, or relative humidity (Coulibaly, Anctil, and Bobee, 2000; Abebe and Price, 2003; Solomatine and Dulal, 2003; Wilby, Abrahart, and Dawson, 2003; Hu, Wu, and Zhang, 2007; Toth and Brath, 2007; Solomatine and Shrestha, 2009). However, some studies noted that evaporation or temperature as an input variable were unnecessary and may lead to noisy and chaotic results during the training model (Abrahart, See, and Kneale, 2001; Anctil, Perrin, and Andréassian, 2004; Toth and Brath, 2007). Anctil, Perrin, and Andréassian, 2004 pointed out that potential evapotranspiration did not improve the ANN

performance of rainfall-runoff model. In addition, Toth and Brath, 2007 also concluded that considering potential evapotranspiration data did not enhance model performance, and may instead yield worse results when compared to models that do not use this data. This may be explained by the fact that the addition of evapotranspiration (or temperature measures) input nodes increase the network complexity, and therefore the risk of overfitting (Wu and Chau, 2011). That being said, in the present study, we use rainfall and streamflow as final input variables in model development.

5.2.2.2 Designed models

This study developed three rainfall-runoff models as ANN and LSTM for the two hydrological stations on Hau River. The general representative data-driven model can be defined as:

$$\hat{Q}_t = f(X_t) = f\left(Q_{t-1}, Q_{t-2}, Q_{t-3}, \ldots, R_{t-1}, R_{t-2}, R_{t-3}\right) \tag{5.4}$$

where $\hat{Q}_t$ stands for the predicted flow at time instance t; Q_{t-1}, Q_{t-2}, Q_{t-3} is the antecedent flow (up to $t-1, t-2$ and $t-3$ time steps); R_{t-1}, R_{t-2} and R_{t-3} are the antecedent rainfall ($t-1, t-2$ and $t-3$ time steps). The predictability of future behavior is a consequence of the correct identification of the system transfer function of f(.). Based on Table 5.7, the auto-correlations (lag time) for discharge, the autocorrelation between Q and Q_{t-1}, Q_{t-2}, Q_{t-3} are still high while the autocorrelations for rainfall between R and R_{t-1}, R_{t-2}, R_{t-3} reduce significantly, meaning the later antecedent rainfall from $t-4$ time step does not contribute considerably to the forecast performance. Therefore, we consider the antecedent flow and rainfall from t to $t-3$ time step. Moreover, based on previous research, the appropriate antecedent flow and rainfall are limited to t – 4 time steps which significantly improves the model performance. Senthil Kumar et al., 2005 investigated 18 combination of input variables and found that the better model with $t-3$ time steps of the antecedent flow and current rainfall performed best. Several researches used cross-correlation analysis between rainfall and runoff, however, their approach only considers on a linear relationship between variables and not the nonlinear residual dependencies (Senthil Kumar et al., 2005). Wu and Chau, 2011 tested the appropriate lags for inputs using partial auto-correlation (PACF) and concluded that the proper lags for two data sets are lag 4 ($t-4$ time steps) for flow and lag 3 ($t-3$ time steps) for rainfall. Similar researches had aslo selected the antecedent flow and rainfall limited to t – 2 time steps for optimizing model performance (Jeong and Kim, 2005; Jain and Srinivasulu, 2006; Modarres, 2009; Machado et al., 2011).

ANN rainfall-runoff model was developed using a multilayer feedforward ANN with one hidden layer according to Kolmogorov's theorem. Marquez, White, and Gill, 2001 stated that with one hidden layer should be sufficient to ensure the structure has the properties of a universal approximator for various problems. Moreover, Dawson and Wilby, 2001, Zhang, Patuwo, and Hu, 1998; De Vos and Rientjes, 2005 further prove an ANN with only one hidden layer can be used for different hydraulic and hydrologic modelling. The input and target data were normalized in the range from zero to one because a sigmoid function purposed as the transfer function. From the input layer to the hidden layer, the log sigmoid function has been commonly used in hydrologic ANN models. From the hidden layer to the output layer, a linear function was purposed as the transfer function because the linear function is known to be robust for a continuous output variable. For the learning algorithm and the regulation procedure of traning models, this study used the Levenberg-Marquardt Back-Propagation (LMBP) algorithm for training models. It was also validated that the Levenberg-Marquardt method is the most powerful learning algorithm that can be used for neural network training (Schmitz, Zemp, and Mendes, 2006; Wu, Chau, and Li, 2009).

Since the appropriate number of hidden layers and dependent nodes for the models is unknown, a trial and-error method was used to find the network's best configuration. An optimal architecture was determined by changing the number neurons from 3 to 15 for ANN and 10, 15, 20, 25, 30 memory blocks for LSTM, with the goal of minimizing the difference between the neural network predicted values and the desired outputs. The training of the neural network models was stopped when either the acceptable level of error was achieved or the number of iterations exceeded a prescribed value. The neural network model configuration that minimized the MAE and RMSE and optimized the R was selected as the optimum, an analysis that was repeated several times. The ANN and LSTM architecture was modified by changing the number of hidden layers and its neurons, of the initial weights, as well as the type of input and output functions. Each modification was tested with one hundred trials, which served as the basis for performance assessment of mean values.

The LSTM rainfall-runoff model was developed based on the recurrent neural network but has a network structure is more complicated with input, output and forget gates in memory blocks. The input units are fully connected to a hidden layer consisting of memory blocks with one cell each. The cell outputs are fully connected to the cell inputs, to all gates, and to the output units. All gates, the cell itself and the output unit are biased. Bias weights to input and output gates are initialized block-wise: -0.5 for the first block, -1.0 for the second, -0.5 for the third, and so forth. Forget gates are initialized with symmetric positive values: +0.5 for the first block, +1 for the second block, etc. These are standard values that we use for all

experiments. All other weights are initialized randomly in the range [-0.1; 0.1]. The cell's input squashing function g is a sigmoid function with the range [-1.0; 1.0]. The squashing function of the output unit is the identity function.

A critical concern in the ANN and LSTM application is how to select the best model structure from the possible input variables and defining the number of hidden nodes. Unfortunately, there is no general rule to deal with this problem. Therefore, the trial-and-error procedure is a unique technique to handle this task. To select the input variables of ANN and LSTM, we propose the input combination based on correlation and lag analysis and the candidate input variables as rainfall and runoff at different time steps. There are six selected combinations of input variables for model training and the construction of model structure:

C1: $R(t-1), Q(t-1)$

C2: $R(t-1), Q(t-1), Q(t-2)$

C3: $R(t-1), R(t-2), Q(t-1), Q(t-2)$

C4: $R(t-1), R(t-2), Q(t-1)$

C5: $R(t-1), Q(t-1), Q(t-2), Q(t-3)$

C6: $R(t-1), R(t-2), Q(t-1), Q(t-2), Q(t-3)$

Table 5.7 The autocorrelation from 1 to 3 lag days for two data sets for discharge (Q) and rainfall (R) at Chau Doc and Can Tho stations

Lag days	Chau Doc		Can Tho	
	Q	R	Q	R
R_1	0.999	0.160	0.985	0.168
R_2	0.997	0.105	0.978	0.139
R_3	0.995	0.100	0.970	0.080
R_4	0.981	0.078	0.940	0.050

5.2.2.3 Evaluation of model performances

The evaluation of model performance is based on the statistical properties of model output. Legates and McCabe, 1999 found that the correlation coefficient (R) is an inappropriate measure in hydrologic model evaluation. Therefore we applied the correlation coefficient, a good index for presenting goodness-of-fit. Furthermore, Legates and McCabe, 1999 also

suggested that a complete assessment of model performance should include at least one absolute error measure (e.g., RMSE or MAE) to supplement a relative error measure. To better compare the performance of different models, the present study additionally uses another statistical index. The index, mean absolute percentage error (MAPE), is defined below. The MAPE is a statistical measure of predictive accuracy expressed as a percentage. The MAPE is useful for evaluating the performance of predictive models due to its relative values. MAPE effectively reflects relative differences between model results since it is unaffected by the size or unit of actual and predicted values (Kaveh, Bui, and Rutschmann, 2017). Four measures are therefore used in this study, and are listed below:

$$RMSE = \sqrt{\frac{1}{n}\sum_{i=1}^{n}\left(Q_i - \hat{Q}_i\right)^2} \tag{5.5}$$

$$MAE = \frac{1}{n}\sum_{i=1}^{n}\left|Q_i - \hat{Q}_i\right| \tag{5.6}$$

$$MAPE = \frac{1}{n}\sum_{i=1}^{n}\frac{\left|Q_i - \hat{Q}_i\right|}{|Q_i|} \times 100\% \tag{5.7}$$

$$R = \frac{n\sum_{i=1}^{n}\left(Q_i\hat{Q}_i\right) - \left(\sum_{i=1}^{n}Q_i\right)\left(\sum_{i=1}^{n}\hat{Q}_i\right)}{\sqrt{\left[n\sum_{i=1}^{n}Q_i^2 - \left(\sum_{i=1}^{n}Q_i\right)^2\right] \times \left[n\sum_{i=1}^{n}\hat{Q}_i^2 - \left(\sum_{i=1}^{n}\hat{Q}_i\right)^2\right]}} \tag{5.8}$$

Where n is the number of observations, $\hat{Q}_i$is predicted flow, $Q_i$represents observed flow.

5.2.3 Results and discussion

The prediction is performed by ANN and LSTM models for both hydrological stations and all input combinations. Tables 5.8 and 5.9 present the respective obtained results for ANN and LSTM models, respectively. According to Table 5.8, the ANN model using input data of combination 5 (C5) produces the best results for Chau Doc station in the testing period. In this combination, the ANN structure consists of 15 neurons in its hidden layer. The best result of ANN model for Can Tho station is obtained from the input combination 4 with 15 neurons in the hidden layer.

According to Table 5.9, for the Chau Doc station, the LSTM model trained using combination 5, with 20 memory blocks and 20,000 loops provides the best efficiency with a high

value of R = 0.9994 and the lowest RMSE = 89.571 m^3/s and MAE = 66.348 m^3/s in the testing phase. From this table, it is also seen that for the Can Tho station, the LSTM using input combination 2 performs better than the models using other combinations. This model uses 25 memory blocks and 10,000 loops.

Table 5.8 Performance of the ANN model for discharge estimation in both stations

Combination	C1	C2	C3	C4	C5	C6
Station	Chau Doc					
ANNs: Neurons in hidden layer	13	13	8	5	**15**	10
R	0.9991	0.9993	0.9993	0.9991	**0.9993**	0.9993
RMSE	89.009	79.582	81.719	89.220	**78.353**	81.313
MAE	66.111	56.197	58.797	66.597	**56.006**	58.401
Station	Can Tho					
ANNs: Neurons in hidden layer	14	14	13	**15**	4	10
R	0.9912	0.9906	0.9906	**0.9912**	0.9910	0.9910
RMSE	785.529	812.056	817.403	**785.525**	789.431	793.708
MAE	588.200	607.044	603.240	**587.317**	591.317	595.753

Table 5.9 Performance of the LSTM model for discharge estimation in both stations

Combination	C1	C2	C3	C4	C5	C6
Station	Chau Doc					
LSTM: Memory blocks	30	30	20	20	**20**	25
Number of loops	10,000	50,000	100,000	100,000	**20,000**	100,000
R	0.9992	0.9994	0.9994	0.9980	**0.9994**	0.9994
RMSE	104.907	96.405	97.760	155.187	**89.571**	94.784
MAE	80.535	71.237	75.468	117.602	**66.348**	71.802
Station	Can Tho					
LSTM: Memory blocks	20	**25**	25	10	15	30
Number of loops	10,000	**10,000**	10,000	10,000	10,000	10,000
R	0.9714	**0.9941**	0.9938	0.9710	0.9855	0.9858
RMSE	2084.928	**691.829**	712.482	2020.234	1021.185	1021.969
MAE	991.933	**534.328**	546.898	1263.875	790.801	792.322

Comparing Tables 5.8 and 5.9 shows that the LSTM model can significantly improve the prediction efficiency in the testing period for Can Tho station. According to these tables, the best LSTM model improves the RMSE, MAE, and R value from 785.525, 587.317, and 0.9912 to 691.829, 534.328, and 0.9941, respectively. However these values are not substantially improved using the LSTM model for the Chau Doc station in the testing period. For this station, the results of ANN and LSTM models are comparable with the ANN performing slightly better.

The temporal variations of the observed and predicted discharge using both models and the best input combinations (C5 and C4 for ANN, and C5 and C2 for the LSTM) for Chau Doc and Can Tho stations are respectively shown in Fig. 5.6 and 5.7. Moreover, the predicted discharges are plotted against observed discharges.

As seen in Fig. 5.8, the LSTM model yields better results for discharge prediction than those predicted by the ANN model. It is also obvious that both models underestimate the discharge peaks. However, in this case, the LSTM model performs better than the ANN model, and the results obtained by the LSTM model are closer to the 45°straight line in the scatter plots. The same conclusion is also obvious in the temporal plot where the LSTM model shows agree better with the peaks of the observed time series than the ANN model.

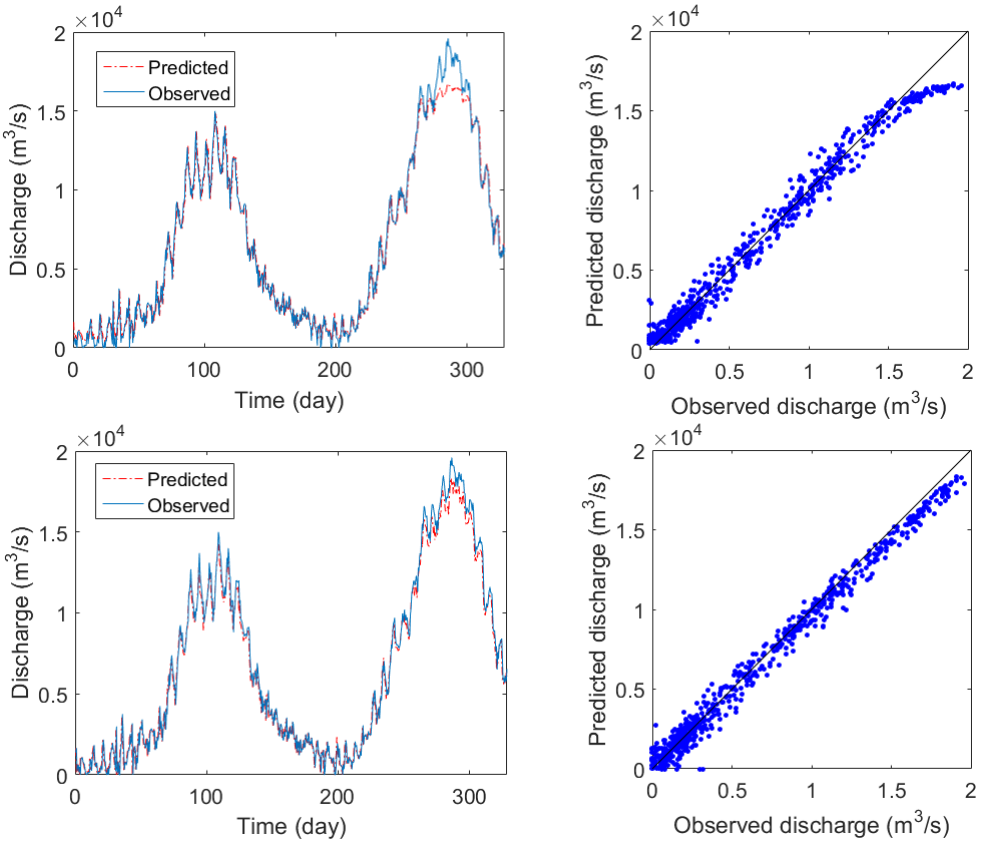

Fig. 5.6 Discharge values predicted for the Can Tho station in the testing period (a) ANN-C4, (b) LSTM-C2

Fig. 5.8 shows the performance index MAPE of the ANN and LSTM models for both stations and all attempted input combinations. As can be observed, the ANN models perform better than the LSTM for all input combinations in Chau Doc station. The LSTM model shows the lowest MAPE value (0.0096) using the second combination for the Can Tho station, while the lowest value obtained by ANN is 0.0101 which belongs to combination 4. For Chau Doc station, the lowest MAPE of the ANN is 0.0011 belonging to combination 2, while the lowest MAPE value of LSTM is 0.0018 when using combination 3. The difference

between two values for both models is very small. This proves that both models can work efficiently to predict rainfall-runoff relationship.

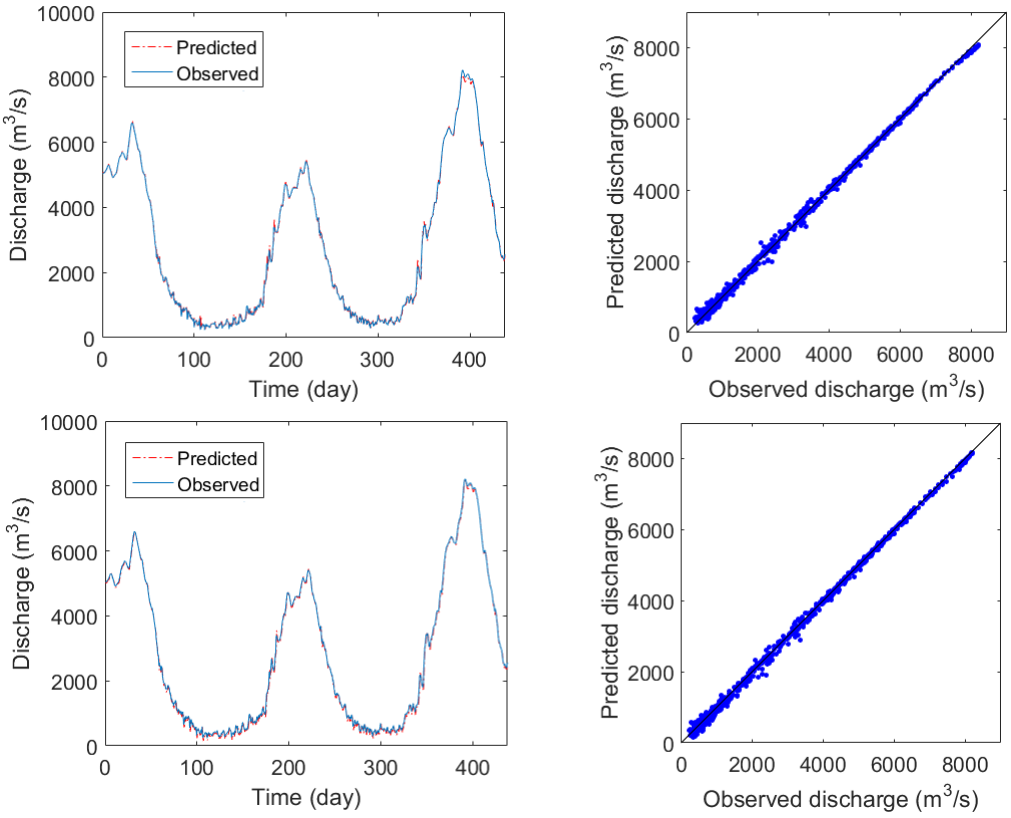

Fig. 5.7 Discharge values predicted for the Chau Doc station in the testing period (a) ANN-C5, (b) LSTM-C5

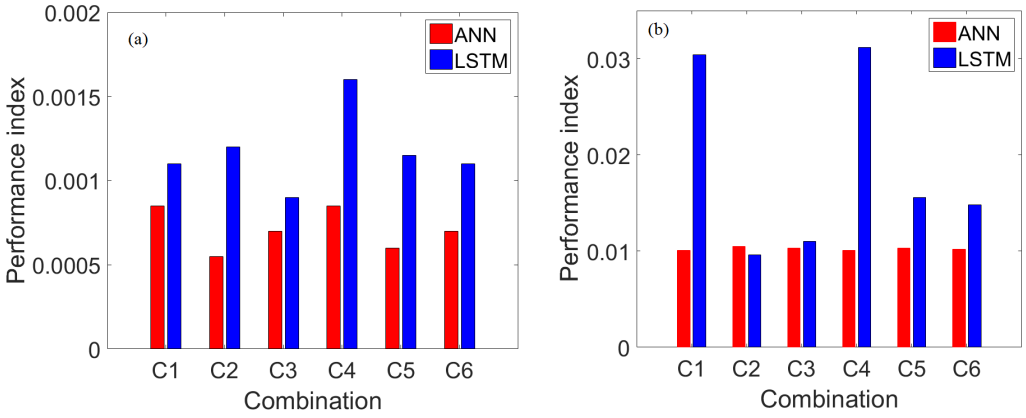

Fig. 5.8 Performance index MPAE for different input combinations (a) Chau Doc station, (b) Can Tho station

5.3 Statistical downscaling and bias correction for rainfall prediction

5.3.1 Bilinear interpolation and selection of GCM models

The Bilinear interpolation is usually applied in image transformation and manipulation techniques, as it is often necessary to employ some sort of interpolation or filtering to obtain a good image quality. The outputs of GCM models are gridded data with a spatial resolution in the range 100 – 300km of which is too coarse for impact assessments. To use the outputs of GCM models in impact studies, the downscaling techniques or bias correction should be applied. Improving the accuracy of the downscaling process, bilinear interpolation is used as a pre-processing technique to obtain finer resolution of GCM outputs and can be used for bias correction.

We can best understand bilinear interpolation by studying Figure 5.9. The green P dot represents the point where we want to estimate. The four red Q dots represent the nearest pixels from the original image. The color of these four Q pixels is known. In this example, P lies closest to Q_{12}, so it is only appropriate that the color of Q_{12} contributes more to the final color of P than the 3 other Q pixels. The calculation of function R_1 and R_2 as equation below:

$$f(R_1) \approx \frac{x_2 - x}{x_2 - x_1} f(Q_{11}) + \frac{x - x_1}{x_2 - x_1} f(Q_{21}) \tag{5.9}$$

$$f(R_2) \approx \frac{x_2 - x}{x_2 - x_1} f(Q_{12}) + \frac{x - x_1}{x_2 - x_1} f(Q_{22}) \tag{5.10}$$

After the two R values are calculated, the value of P can finally be calculated by a weighted average of R_1 and R_2.

$$f(P) \approx \frac{y_2 - y}{y_2 - y_1} f(R_1) + \frac{\mathrm{y} - y_1}{y_2 - y_1} f(R_2) \tag{5.11}$$

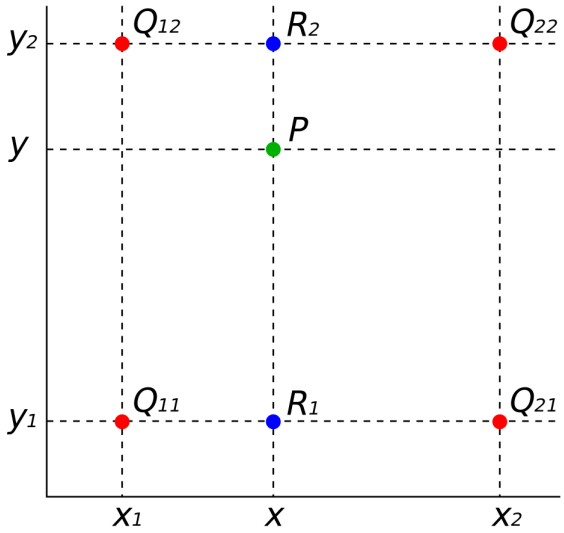

Fig. 5.9 Spatial interpolation of four points

The grid resolutions of GCM normally vary from 1.1^o to 2.5^o equal to 112 km to 276 km as described in Table 2.1. Proper selection of GCMs for impact assessments is important to reduce uncertainty and provide a plausible range of future climate change. The most recent CMIP5 climate projection was issued in 2013 to provide a multitude of GCMs for impact studies. We have based the selection of a proper GCM model in this research on several studies. Huang et al., 2014 assessed the CMIP5 models efficiency for the Mekong basin and suggested BCC-CSM1-1, CSIROMK3-6-0, HadGEM2-ES, and MIROC-ESM-CHEM as the better-performing models. Hasson et al., 2016 evaluated the GCM's performance in simulating seasonal precipitation specific to monsoonal activities for three major river basins in South and Southeast Asia, including the Mekong. They concluded that the MPI, MIROC5 and CSIRO-Mk3-6-0, CCSM4, CESM1-CAM5, GFDL-ESM2G, IPSL-CMAMR, MIROC-ESM, and MIROC-ESM-CHEM perform better than other GCMs. Furthermore, Sillmann et al., 2013 stated that ACCESS-1.0, CCSM4, MPI models, and HadGEM2-ES are amongst the better-performing models in climate extremes presentation. Based on these GCM evaluations, we selected five GCMs for this study as described in Table 5.17. The selection of grid resolution as presented in Figure 5.10.

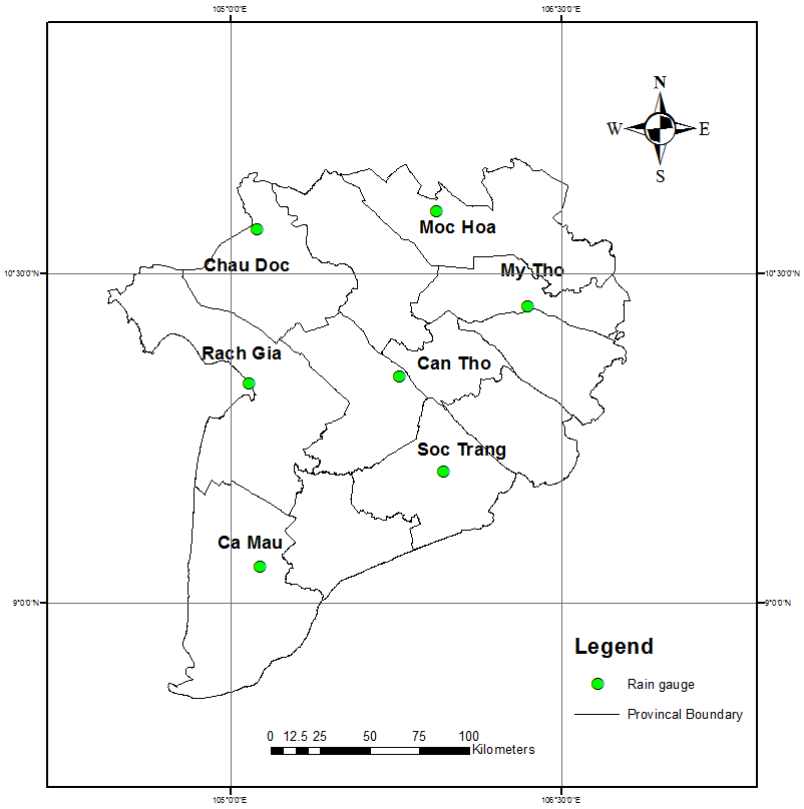

Fig. 5.10 Selection of grid size for VMD domain

5.3.2 Scheme of bias correction

Bias correction is another technique of statistical downscaling methods that is applied when adequate observations are available to adjust the model outputs. To improve the accuracy of forecasting of GCM models, bilinear interpolation to $0.5^o \times 0.5^o$ resolution for GCM's raw gridded data and process bias correction between GCM outputs and observed data for different locations were conducted (Fig. 5.10). In this study, we develop a robust and practical statistical bias correction including three distinct methods. These include linear scaling (LS), local intensity scaling (LOCI) and distribution mapping (DM) which we apply and validate using five GCM outputs over Mekong delta. The methodology described below was applied to the simulated daily precipitation data from five GCM models over Mekong delta interpolated onto the 50×50 km grid. Fig 5.11 described the procedure of bias correction in this study.

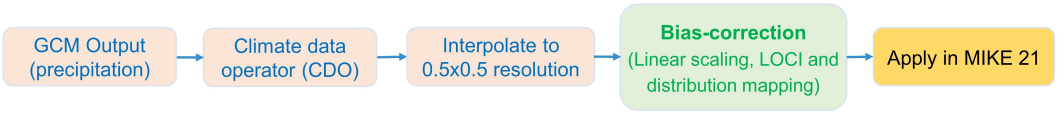

Fig. 5.11 The scheme of downscaling technique in this study

5.3.3 Statistical evaluation of bias correction procedures

According to the calculated performance measures, all precipitation-bias corrections improved the raw GCM simulations. Bias correction were applied for Can Tho, Chau Doc rain gauge stations. Based on the performance statistics, most bias correction methods performed equally well from March to December except January and February (Fig. 5.12). Only the local intensity scaling approach performed badly in two months, which was indicated by larger variability intervals in the calculated statistics. Furthermore, the local intensity scaling approach was not able to adjust the standard deviation to some extent, as apparent in January (Fig. 5.12 c & d). The other methods were able to improve the raw GCM precipitation much better and with less variability in the statistical measures. It should be mentioned that for the distribution mapping approach the current conditions coincide with the observed values by definition.

There were slight differences between the correction methods in the daily precipitation series' standard deviation, coefficient of variation (Fig. 5.13). Especially linear scaling and LOCI, both of which showed larger variability ranges and biases of a similar magnitude to the uncorrected precipitation. However, the major dissimilarities were identified by the probability of dry days and the intensity of wet days. Apart from the LOCI approach, which corresponded to the observations by definition, linear scaling and distribution mapping were able to adjust these two statistical measures of the daily precipitation series. Overall, all bias correction methods were able to correct monthly mean values of precipitation. The methods could be sorted according to their performance (Table 5.10) that describes their ability to match with the CDF fit (i.e., the calculated MAE). The distribution mapping performed best, followed by the linear scaling, and LOCI approach.

Table 5.10 The statistical performance of three methods for Chau Doc and Can Tho station

Model	Chau Doc			Can Tho		
	RMSE	MAE	R	RMSE	MAE	R
LS	6.95	4.84	0.993	8.96	5.94	0.994
DM	5.38	3.79	0.994	6.51	4.71	0.996
LOCI	8.64	6.34	0.991	7.46	5.31	0.993

Table 5.11 Best statistical performance (DM method) of bias correction for five GCM outputs at Chau Doc and Can Tho stations

Model	Chau Doc			Can Tho		
	RMSE	MAE	R	RMSE	MAE	R
ACCESS	6.90	4.65	0.992	8.30	5.85	0.994
CCSM	3.22	2.20	0.998	6.05	4.12	0.996
CSIRO	48.15	17.57	0.924	5.37	3.84	0.997
HadGEM	5.50	3.30	0.995	5.79	4.23	0.997
MPI	5.93	5.04	0.994	5.90	4.63	0.998

There were substantial differences in the ability of GCMs to reproduce precipitation data under current climate conditions (Teutschbein and Seibert, 2012). The biases were found to vary substantially depending on the analyzed climate variable and the locations. For monthly mean precipitation (Table 5.11), the ensemble mean fitted the observations well except for the CSIRO model with the Chau Doc station. In Chau Doc and Can Tho station, the GCMs tended to slightly overestimate in dry season. We obtained a robust signal, although the projections were more variable in January and February for CSIRO and MPI models. There was a strong tendency of all GCMs to simulate too many low-intensity rain events (drizzle). The ensemble means for the different station generally overestimated spring precipitation.

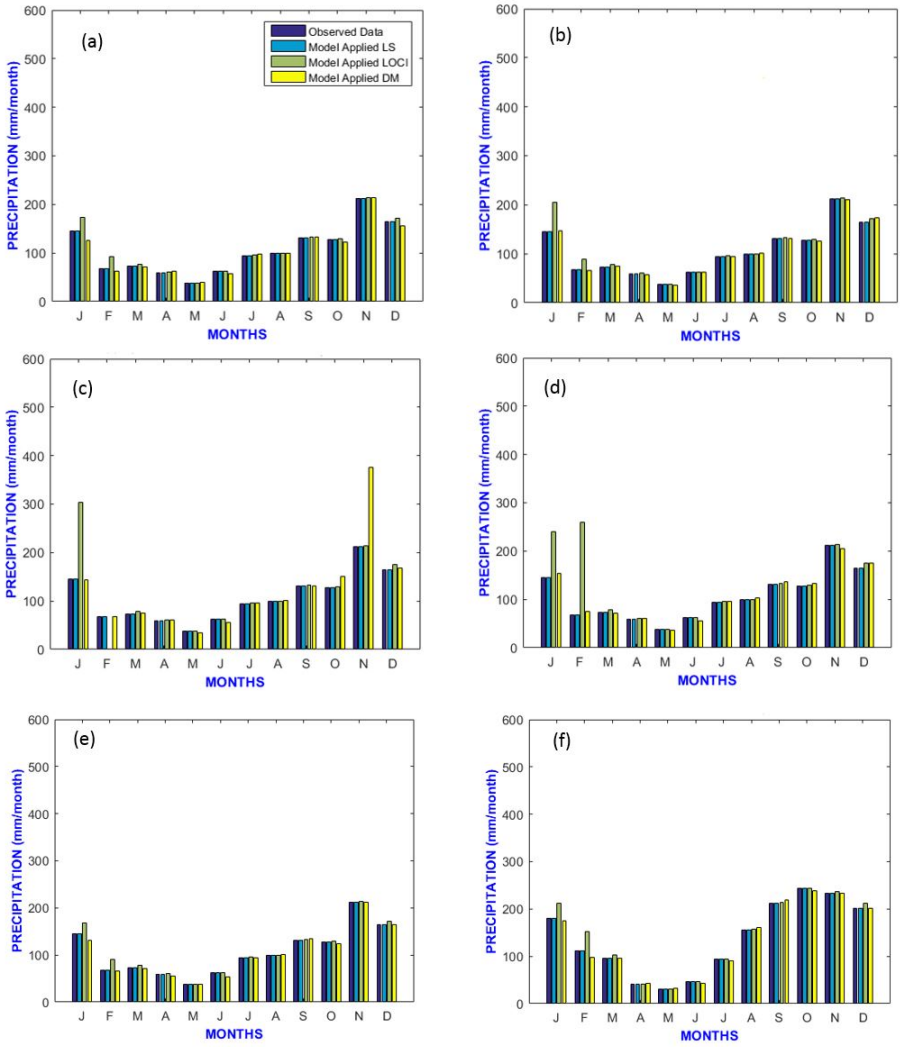

Fig. 5.12 Bias correction results for ACCESS model (a), CCSM (b), CSIRO model (c) MPI (d), HadGEM (e) for Chau Doc and (f) HadGEM for Can Tho station

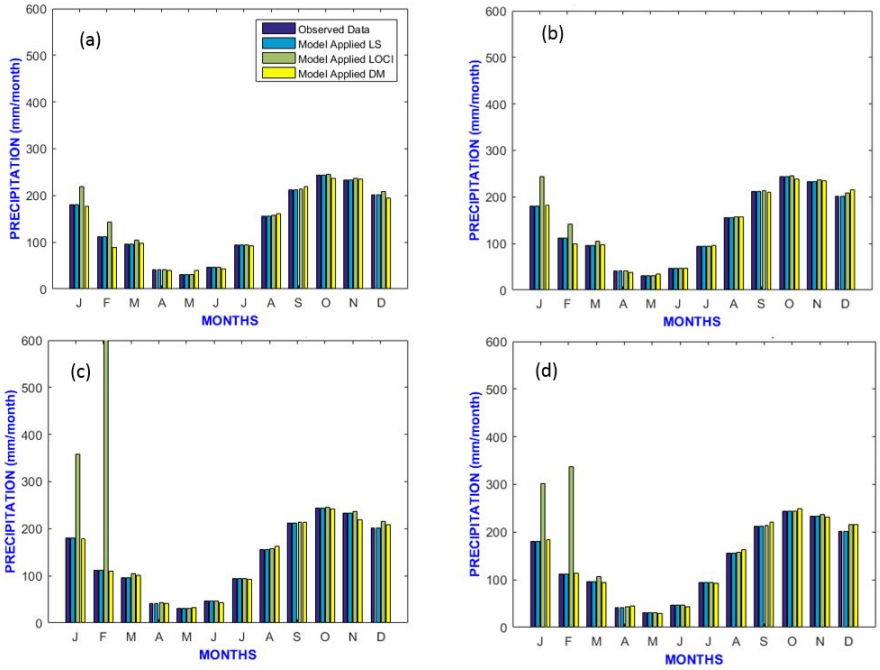

Fig. 5.13 Bias correction results for ACCESS model (a), CCSM (b), CSIRO model (c) and MPI (d) for Can Tho station

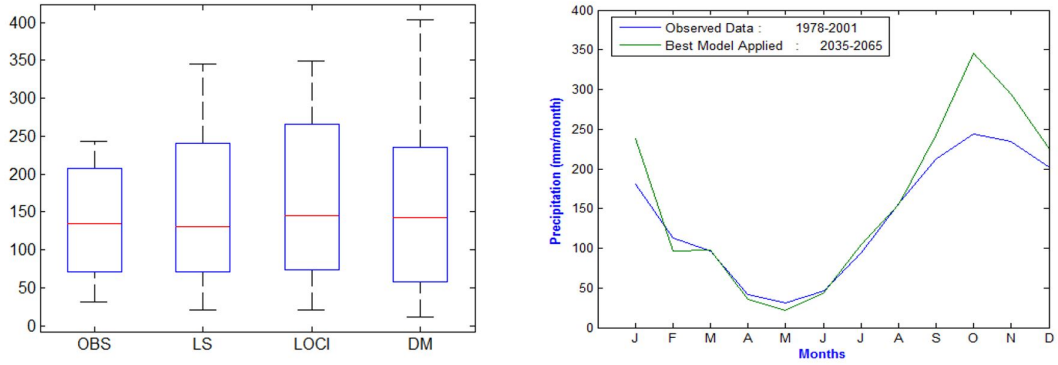

Fig. 5.14 Boxplot for annual precipitation for three methods in 1980-2011 and (b) Future averaged precipitation of three methods for Can Tho station

5.3.4 Statistical downscaling for rainfall using ANN and LSTM

5.3.4.1 Hydrological data

The observed daily precipitation data over a period of 33 years (1978– 2011), was taken from two main rain gauges of the Southern Hydro-Meteorological Center (SRHMC) for the

Vietnamese Mekong delta station, located in the South of Vietnam. Figure 5.15 shows the location of representative stations and the GCM resolution in VMD. The coordinates (latitude, longitude) for Chau Doc and Can Tho are 105^{o}07’30" E, 10^{o}42’20"N and 105^{o}47’00" E, 10^{o}02’00" N, respectively.

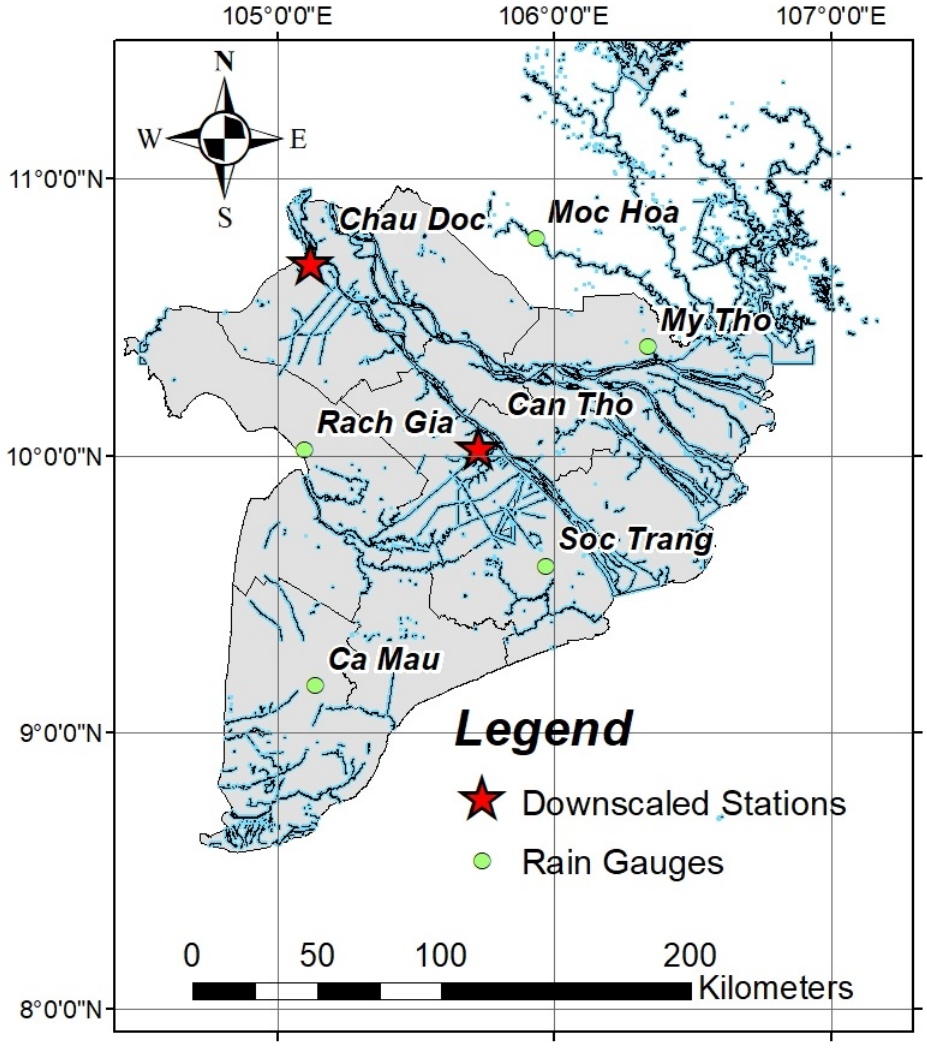

Fig. 5.15 The study are and downscaled meteorological stations

The precipitation scenarios can be generated from the most updated CMIP5 using five GCMs: ACCESS 1.0, CCSM4, CSIRO-Mk 3.6, HadGEM and MPI-ESM-LR (Huang et al., 2014; Basheer et al., 2016 and Sillmann et al., 2013) (see. Table 5.17). Although all GCMs contain similar levels of projected trends, different GCM models could provide different results because of GCM structures, mathematical equations used, and boundary conditions applied (Kingston, Thompson, and Kite, 2011). Therefore, as suggested by Todd et al., 2011)

and recommended by Wilby et al., 2004, the ensembles of CMIP5-GCMs were proposed to cover a range of plausible future scenarios and reduce these uncertainties. The daily total precipitation was obtained from an approximately $1.25^o \times 1.9^o$ resolution of five GCMs within two periods, from 1978 to 2001 and future period of 2036 - 2065. Bilinear interpolation was applied to downscale to the same resolution of $0.5^o \times 0.5^o$ grid before obtaining the normalization process for training model. Further, we selected two precipitation RCPs, namely RCP 4.5 and RCP 8.5. The RCP 4.5 is a medium scenario with a stabilization of radiative forcing to 4.5 Wm^2 by 2100 (Thomson et al., 2011). The RCP 8.5 is a high scenario with a radiative forcing reaching to 8.5 Wm^2 by 2100 (Riahi et al., 2011). We did not consider RCP 2.6 and RCP 6.0 because RCP 2.6 slightly affects the hydrology cycle due to low radiation forcing, and RCP 6.0 is close to the RCP 4.5 as well as in line with the range of RCP 4.5 to RCP 8.5 (Hoang et al., 2016). We expect to capture a reasonable range of climate change scenarios to simplify and reduce the combined scenarios.

5.3.4.2 Downscaling process

In this study, the overall methodology of proposed statistical downscaling process is displayed in Fig. 5.16. All the GCM daily precipitation for two present and future periods were interpolated to the same resolution $0.5^o \times 0.5^o$ grid through bilinear interpolation, prior to statistical downscaling. Subsequently, the GCM precipitation need to pass through standardization (normalization) to improve the efficiency of the LSTM, ANN training as well as avoiding training to get trapped in local minima. The GCM precipitation was used to train two models and obtain the nonlinear relationship from historical data and then we apply these equations to the future precipitation data. We use five GCMs under two Representative Concentration Pathways (RCPs)- RCP 4.5 and RCP8.5 scenario, to statistically downscale the precipitation at two hydrological stations for present (1978–2001) and future climates (2035–2065). The observed precipitation from 2002-2011 for Can Tho and Chau Doc stations are used to validate LSTM and ANN models. The outputs of the statistical downscaling of the GCMs include both the present-day (PD) and future datasets (FU) for two RCP4.5 and RCP8.5 scenarios. The observed data period of the Can Tho and Chau Doc station spans 33 years from January 1, 1978 to December 31, 2011. The GCM's precipitation from 1978 – 2001 was applied to train models and derived nonlinear relationship function. The entire input–output dataset in each station is divided into three subsets including a training set, cross-validation set and testing set. 70% of total data is allocated for training, 15% for cross-validation, and 15% for testing and observed precipitation from 2002 – 2011 was used to validate against models. The trained LSTM model through 3,000; 5,000; 8,000; 10,000 loop iterations with

20, 25, 30 neurons/cell memory blocks is applied to obtain projections of precipitation. The number of neurons in the ANN varies from 5, 8, 10, 12, 15 and are iterated 50 times to optimize the best architecture.

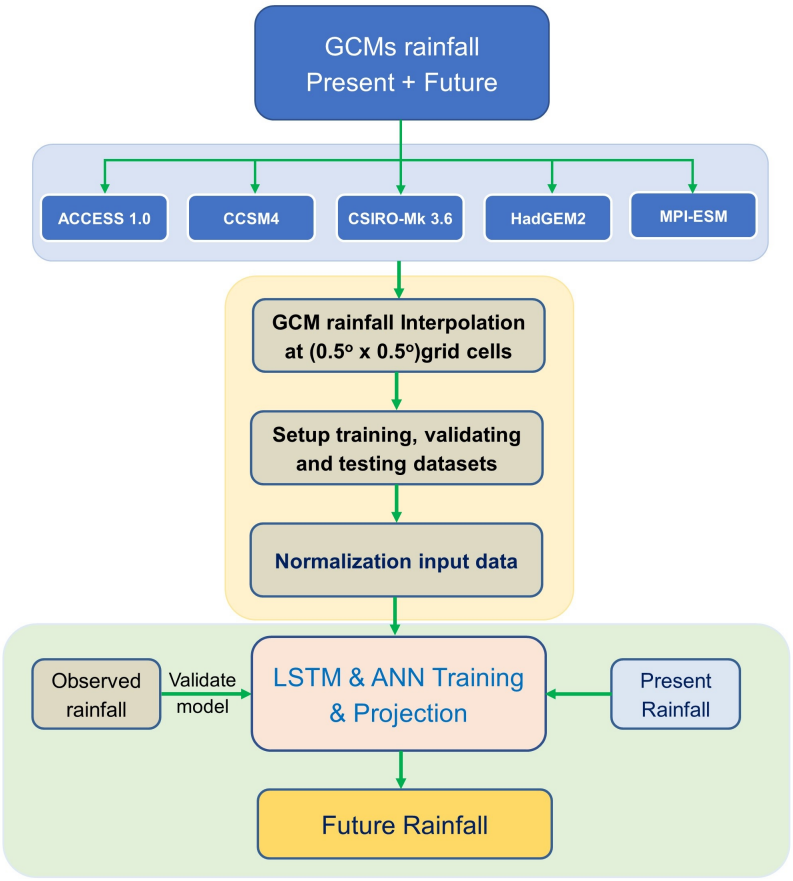

Fig. 5.16 Schematization of statistical downscaling using LSTM and ANN

5.3.4.3 Model training and validation

We use recurrent neural network (LSTM) and feed forward neural network (ANN) to evaluate the model efficiency with the testing data set. The training period for both models were set to 23 years, from 1978 to 2001, and with 8395 trained-values daily precipitation from five GCMs and observed data. Afterward, the observed precipitation at Can Tho and Chau Doc in a period of 2002 – 2011 are used to validate model to obtain corrected network for futre forecasting during 2035–2065. The performances of testing set for two models are is

evaluated using correlation coefficient (R), root mean square error (RMSE), mean absolute error (MAE).

The statistical indices (R, RMSE, MAE) for the five GCM precipitation correlated to the two hydrological stations for LSTM and ANN models are presented in Table 5.12 and 5.13, respectively. The statistical indices for LSTM simulation are relatively better for Chau Doc dataset than for Can Tho dataset with higher R and lower RMSE and MAE. The correlation coefficient for testing dataset with LSTM model at Chau Doc ranges from 0.908 – 0.974 while at Can Tho, the correlation coefficient varies from 0.916 to 0.957 (Table 5.12). The statistical performance for both Chau Doc and Can Tho stations are very reasonable with R >0.90. However, the statistical indices for ANN model are lower than the performance of LSTM. The correlation coefficient obtained from ANN model at Chau Doc is in the range of 0.605 – 0.856 whereas the correlation coefficient at Can Tho is falls between 0.665 to 0.846 (Table 5.13). Obviously, the performance of LSTM is considerably better than ANN, due to the highlight advantages of LSTM.

The scatter plots of the five GCM data during the testing periods using both LSTM and ANN models, for Can Tho and Chau Doc in daily scale are shown in Fig. 5.17 - 5.20. From Fig. 5.17 and Fig. 5.18, the LSTM simulations slightly underestimate the high peaks (blue dotted) for the five GCMs. It can be noted that considerable fluctuation between heavy precipitation days and dry days with zero values exist, meaning that the models may not capture the high peaks during training process even though the normalization process is applied before training models. On the other hand, the statistical performances between observed and predicted data of ANN for both hydrological stations is not good match with large dispersion and standard deviation (Fig. 5.19 & Fig.5.20).

Table 5.12 Statistical performances of LSTM model (testing data) for two precipitation stations under five GCM outputs

Statistics	ACCESS 1.0	CCSM4	CSIRO-Mk3.6	HadGEM2	MPI-ESM
Can Tho					
RMSE (mm)	1.6272	2.7049	1.9657	1.8098	2.7515
MAE (mm)	0.9726	1.3208	0.8504	1.0256	1.6925
R	0.9513	0.9225	0.9566	0.9561	0.9157
Chau Doc					
RMSE (mm)	1.4693	2.6243	1.5010	1.5689	2.2404
MAE (mm)	0.8186	1.2569	0.7129	0.9285	1.3664
R	0.9735	0.9081	0.9645	0.9578	0.9287

Table 5.13 Statistical performances of ANN model (testing data) for two precipitation stations under five GCM outputs

Statistic	ACCESS 1.0	CCSM4	CSIRO-Mk3.6	HadGEM2	MPI-ESM
Can Tho					
RMSE (mm)	3.5153	4.4907	3.1138	3.5465	4.3050
MAE (mm)	2.1463	2.6382	1.8028	2.1609	2.7228
R	0.7793	0.6650	0.8460	0.7613	0.6490
Chau Doc					
RMSE (mm)	3.2012	4.1824	2.5501	3.0868	0.6437
MAE (mm)	1.8635	2.4081	1.4421	1.8953	2.3447
R	0.7535	0.6045	0.8561	0.7544	0.6437

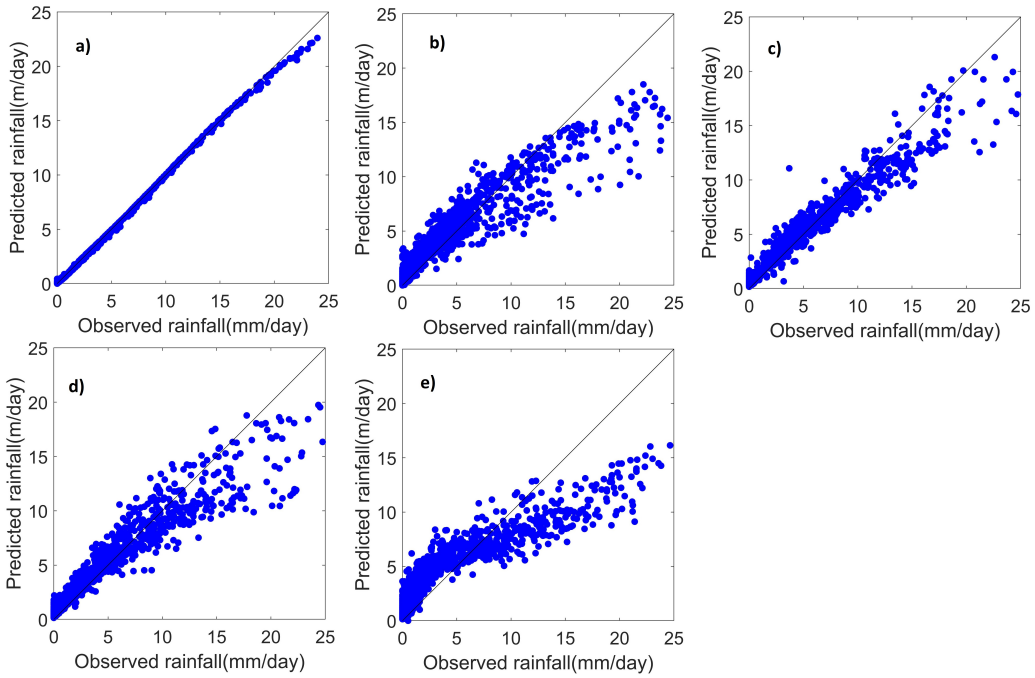

Fig. 5.17 Scatter plot of five GCM outputs correlated to daily precipitation at Can Tho station training by LSTM. a) ACCESS 1.0, b) CCSM4, c) CSIRO-mk3.6, d) HadGEM2 and e) MPI-ESM.

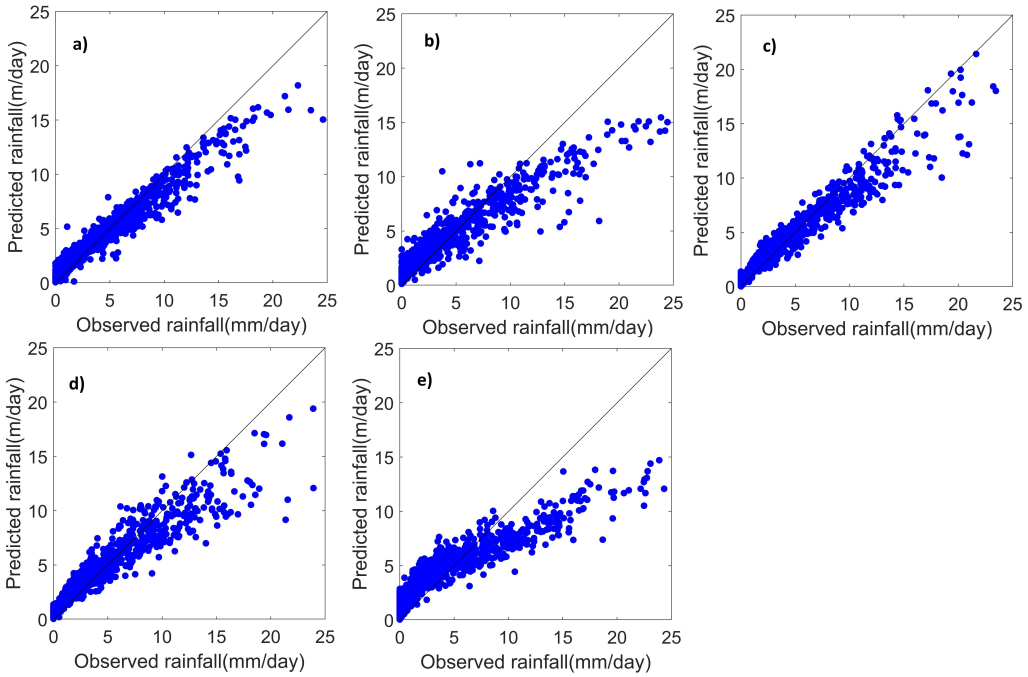

Fig. 5.18 Scatter plot of five GCM outputs correlated to daily precipitation at Chau Doc station training by LSTM. a) ACCESS1.0, b) CCSM4, c) CSIRO-mk3.6, d) HadGEM2 and e) MPI-ESM.

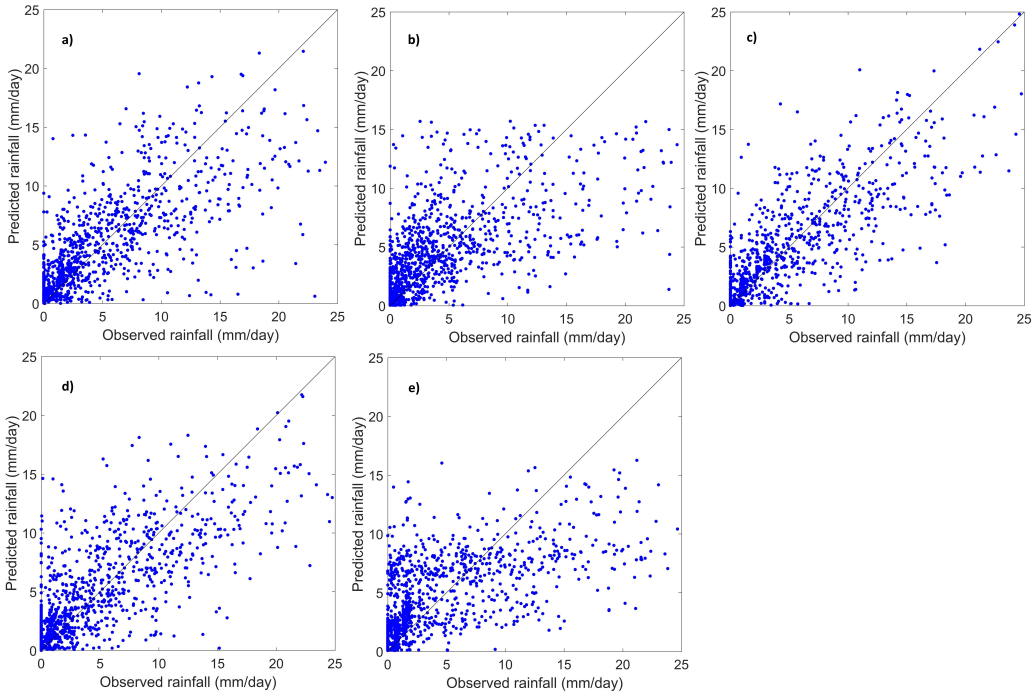

Fig. 5.19 Scatter plot of five GCM outputs correlated to daily precipitation at Can Tho station training by ANN. a) ACCESS 1.0, b) CCSM4, c) CSIRO-mk3.6, d) HadGEM2 and e) MPI-ESM.

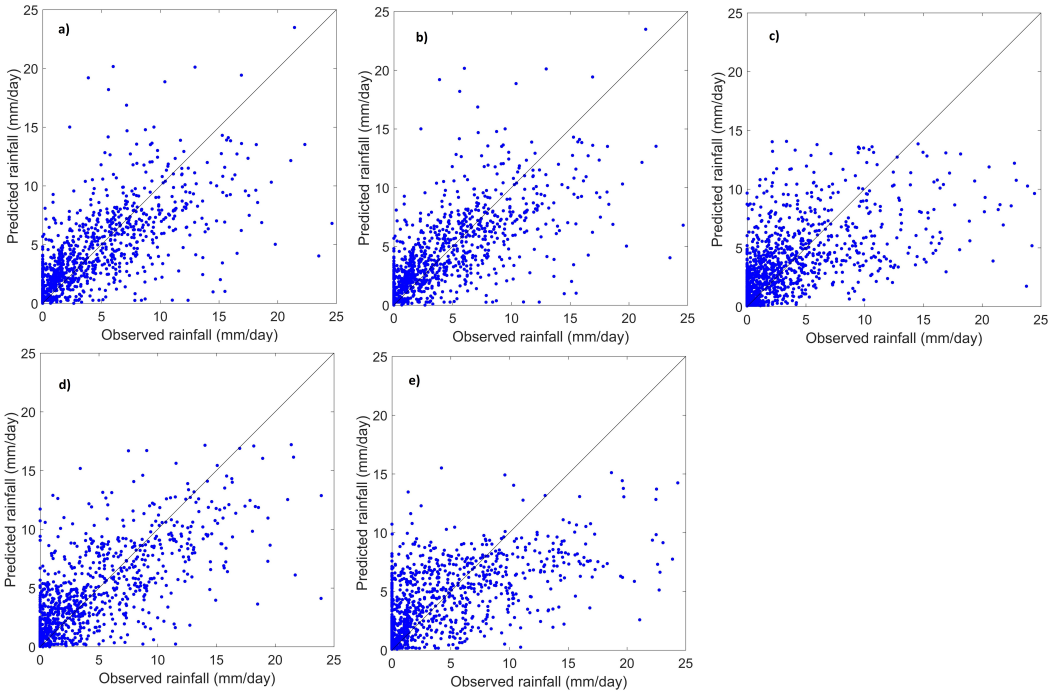

Fig. 5.20 Scatter plot of five GCM outputs correlated to daily precipitation at Chau Doc station training by ANN. a) ACCESS 1.0, b) CCSM4, c) CSIRO-mk3.6, d) HadGEM2 and e) MPI-ESM.

5.3.4.4 Future precipitation over VMD

In order to assess the future rainfall, downscaled five GCMs precipitation under two RCP scenarios were used in the study. These GCMs form an ensemble dataset, which could give a range of uncertainties of the future climate. Firstly, the comparisons of present-day climate and future precipitation are implemented for five GCM projections at two observed hydrological stations. Afterward, three statistical indices of rainfall extremes are tested and presented.

Future precipitation predictions from five downscaled models under two scenarios show that precipitation magnitude and intensity increase at Can Tho and Chau Doc from 2035 – 2065. According to the comparison of five downscaled models to observed data (Table 5.14), the precipitation at Can Tho during the dry season decreases by approximately – 9.3% to 22.3%. This result was made using the ACCESS 1.0 projections and considering RCP4.5 and RCP8.5, respectively. The worst-case scenario belongs to CSIRO-mk3.6 projection with precipitation decreasing by 15.9% and 28.1% when compared to baseline for RCP4.5 and RCP8.5, respectively. In contrast, only MPI-ESM projects an increase in precipitation at Can

Tho by 5.5%, and 10% in dry season under RCP4.5 and RCP8.5, respectively; and 19.7% and 26.6% under RCP4.5 and RCP8.5, respectively in wet season. Similarly, a projection by MPI-ESM for Chau Doc station generated an increase of precipitation in the range of 8.6% and 16.8% in dry season using RCP4.5 and RCP8.5, respectively and 19.4% and 29.2% in wet season under RCP4.5 and RCP8.5, respectively (Table 5.14).

Table 5.14 Percentage changes (%) of five GCMs downscaled precipitation compared to baseline (1978 – 2001) during dry and wet seasons for two hydrological stations.

Stations	ACCESS 1.0		CCSM4		CSIRO-mk3.6		HadGEM		MPI-ESM	
	RCP4.5	RCP8.5	RCP4.5	RCP8.5	RCP4.5	RCP8.5	RCP4.5	RCP8.5	RCP4.5	RCP8.5
Can Tho										
Dry season	-9.3	-22.3	-21.7	-14.5	-15.9	-28.1	12.1	-15.6	5.5	10.0
Wet season	34.1	32.8	14.4	17.2	-3.9	-4.1	36.9	30.0	19.7	26.6
Chau Doc										
Dry season	-13.7	-26.4	-18.8	-7.9	4.1	-14.5	16.7	-17.6	8.6	16.8
Wet season	31.6	33.2	19.1	27.9	18.4	11.1	32.3	31.7	19.4	29.2

Similar trends of decreasing precipitation in dry season also occured at Chau Doc station with a maximum decrease of 26.4% when using ACCESS 1.0 projections and considering RCP8.5. In all scenarios, the largest projected increases of precipitation in wet season during 2035 – 2065 is 33.2% using ACCESS 1.0 projections and considering RCP8.5. The projection with the lowest precipitaiton increase is 11.1% determined using CSIRO-mk3.6 projection under RCP8.5. It is observed that the average precipitation reduction across the five GCMs in dry season are -10%, -5.3% when compared to baseline at Can Tho, Chau Doc, respectively and an average precipitation increase across five GCMs in wet season are +20.4% and +25,4% at Can Tho and Chau Doc, respectively (Table 5.15). The results from five models outputs under two RCP scenarios indicate that precipitation will continue increasing in wet season and decrease in dry season during 2035 – 2065.

Table 5.15 Average precipitation and percentage changes (%) compared to baseline for dry and wet season at two hydrological stations.

Seasons	Precipitation (mm) in baseline (1978-2001)		Future projections (2035 – 2065) (mm)		Relative changes (%)	
	Can Tho	Chau Doc	Can Tho	Chau Doc	Can Tho	Chau Doc
Dry season	84.78	74.16	76.32	70.26	-10.0	-5.30
Wet season	190.25	138.08	228.98	173.13	20.4	25.4

The results for statistical downscaling from five GCMs including the present-day (PD) climate and their future projections (FU) and observed data from two hydrological stations are displayed in Fig. 5.21 and Fig. 5.22 as box plots of both datasets. These comparisons have been done to compare observed precipitation and GCMs projections. From boxplots of Fig. 5.21 and Fig. 5.22, it is obvious that median changes of the downscaled GCMs also indicate increases in precipitation over the future climate when compared to the present day. Especially, the boxplots of ACCESS and HadGEM clearly show an increasing trend in the future precipitation compared to the present-day conditions. Overall, there is an agreement in increasing precipitation during the wet season, for all five GCMs and decreasing precipitation during the dry season for both Can Tho and Chau Doc stations. The increase is different for all GCMs during the wet season, from lowest of CCSM4 – RCP8.5 (-7.9 %) to highest of ACCESS 1.0 – RCP8.5 (33.2%) (Table 5.14). The ensemble results between five GCMs is the average of the five, which is equal to 20.4 % and 25.4 % in wet season at Can Tho and Chau Doc, respectively. This signifies that Vietnamese Mekong Delta might experience more flooding conditions during the rainy season in the future.

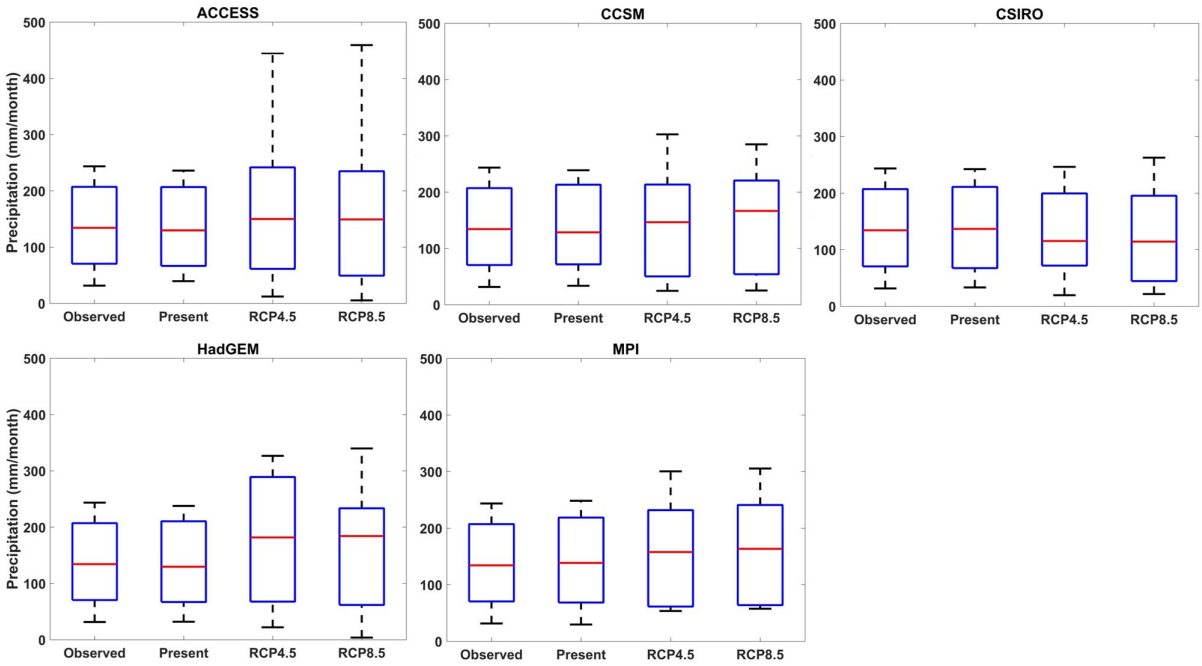

Fig. 5.21 Boxplot for rainfall at Can Tho station, observed, present (1978-2001) and RCP4.5 and RCP8.5 for five GCM outputs.

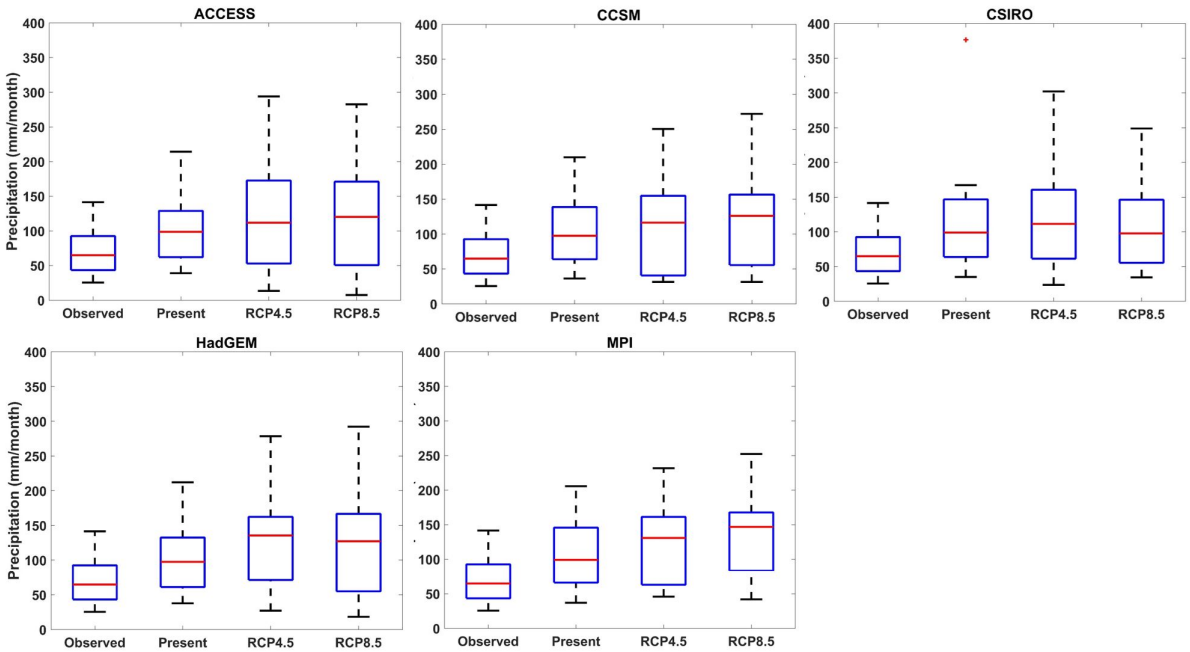

Fig. 5.22 Boxplot for rainfall at Chau Doc station, observed, present (1978-2001) and RCP4.5 and RCP8.5 for five GCM outputs.

5.3.4.5 Change in extreme precipitation indices

Comprehensive assessment of climate change not only consider mean values but also take into account extreme events to understand mean and variability. As recommended by the European Commission-funded project (STARDEX), we select 3 indices to evaluate future precipitation including Annual maximum wet day frequency (Prcp, day); 95th percentile of precipitation (P95p, mm) and maximum 5-day consecutive rain (R5d, mm) (Vu et al., 2016).

The relative changes, for these indices, were calculated from the projected precipitation (2035–2065) with respect to the present day (1978-2001) for Can Tho and Chau Doc stations as presented in Fig. 5.23 – 5.25. We use Cumulative Gamma Distribution Function (CDF) to present three statistical indices for both present day and future, so it is easy to visually compare the differences between current and future climate. The distributions were calculated for the fitted cumulative gamma probability distribution functions of these indices for baseline period (plotted as dashed line) and future period (continuous line). The present day climate is abbreviated as 'PD', and the future 'FU'. Each downscaled GCM is displayed in different colors and line patterns, for better visualization. There are ten curves in each statistical index plot to represent both present-day and future climates as per the five downscaled GCMs. Results indicate that the overall trend for the future wet indices (Prcp, P95p, R5d,) are on the increase. However, maximum 5-day consecutive rain (R5d) index in Fig. 5.25 shows significant differences between two RCP scenarios at both Can Tho and Chau Doc stations. Especially, the projections of CSRIO-mk3.6 model for R5d index (blue color) are far from other GCMs results. This means that this model may have different structure and mathematical expression; the results therefore could increase uncertainties for further basin assessment. Generally, the maximum 5-day consecutive rain index at the two hydrological stations discovers that future climate is likely to be dominated by increases in the precipitation during the rainy season. These can have strong implications as an increase in intensity of extreme rainfall events over the Mekong delta during rainy season may induce large flooding and inundation of the area.

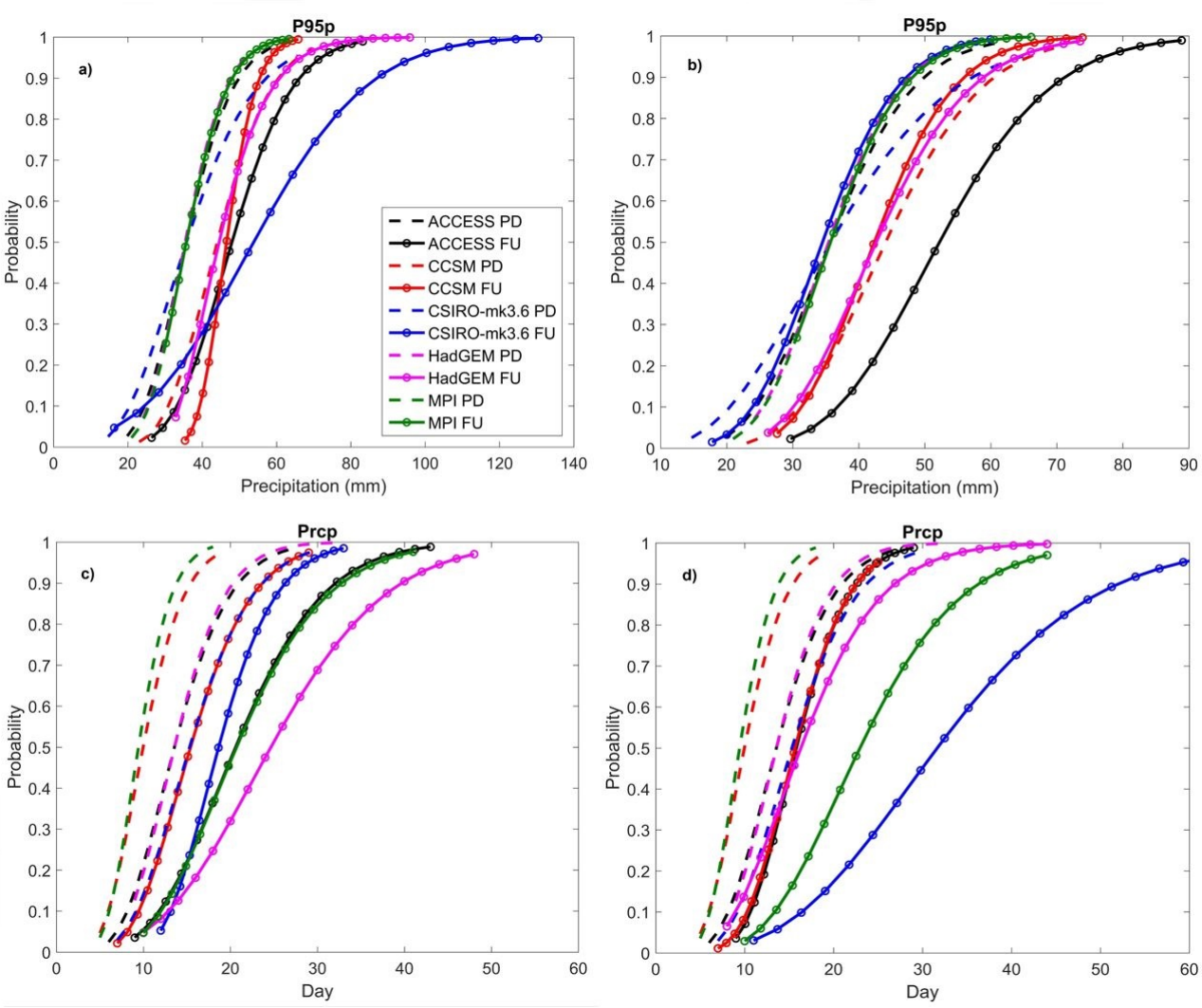

Fig. 5.23 Cumulative gamma distribution function of statistical indices for downscaled rainfall at Can Tho, both present (1978-2001) (PD) and projection (FU) for five GCMs under two RCP. (a) P95p - RCP4.5 (b) P95p -RCP8.5, (c) Prcp - RCP4.5 and (d) Prcp- RCP8.5

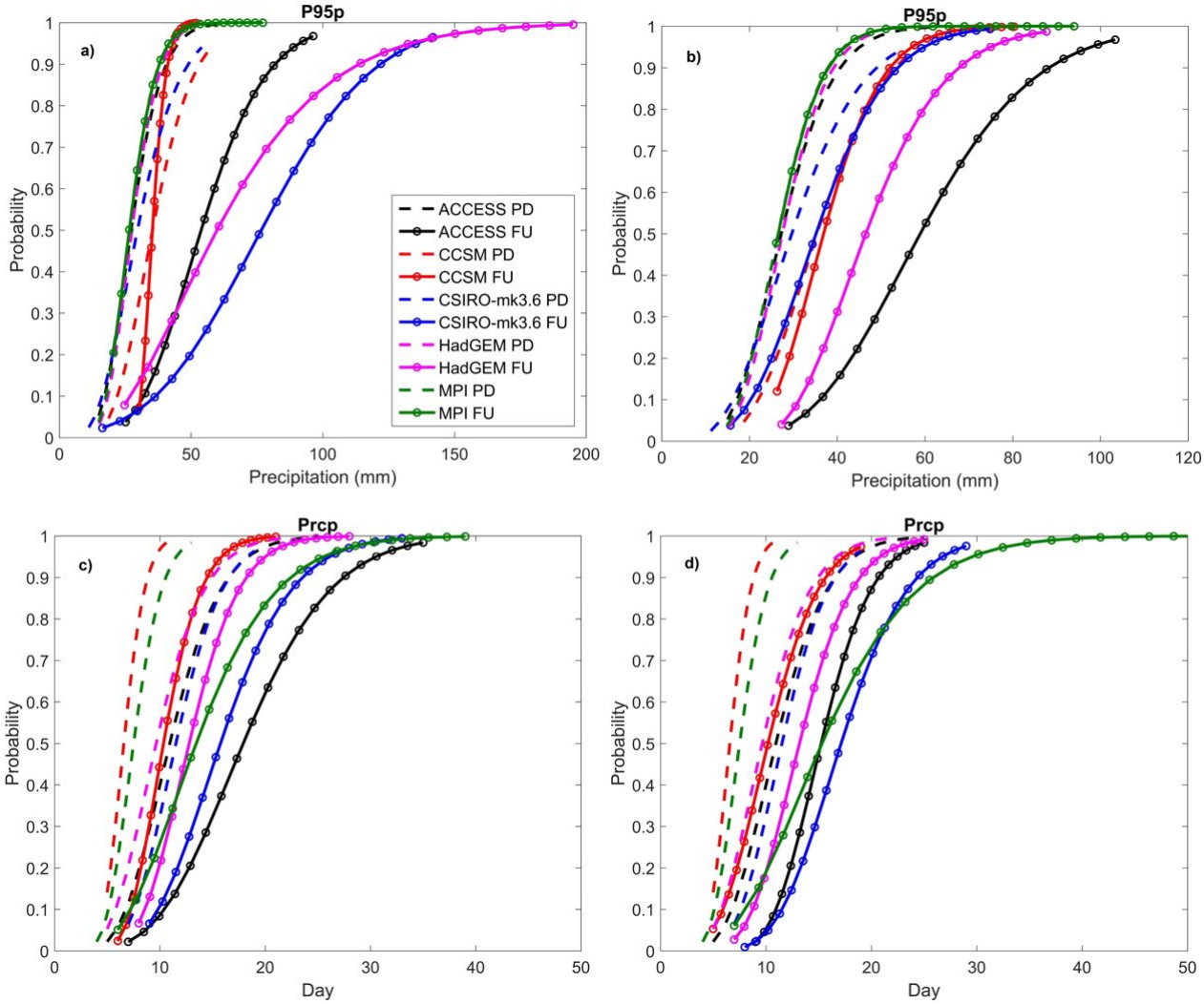

Fig. 5.24 Cumulative gamma distribution function of statsitical indices for downscaled rainfall at Chau Doc, both present (1978-2001) (PD) and projection (FU) for five GCMs under two RCP. (a) P95p - RCP4.5 (b) P95p -RCP8.5, (c) Prcp - RCP4.5 and (d) Prcp-RCP8.5

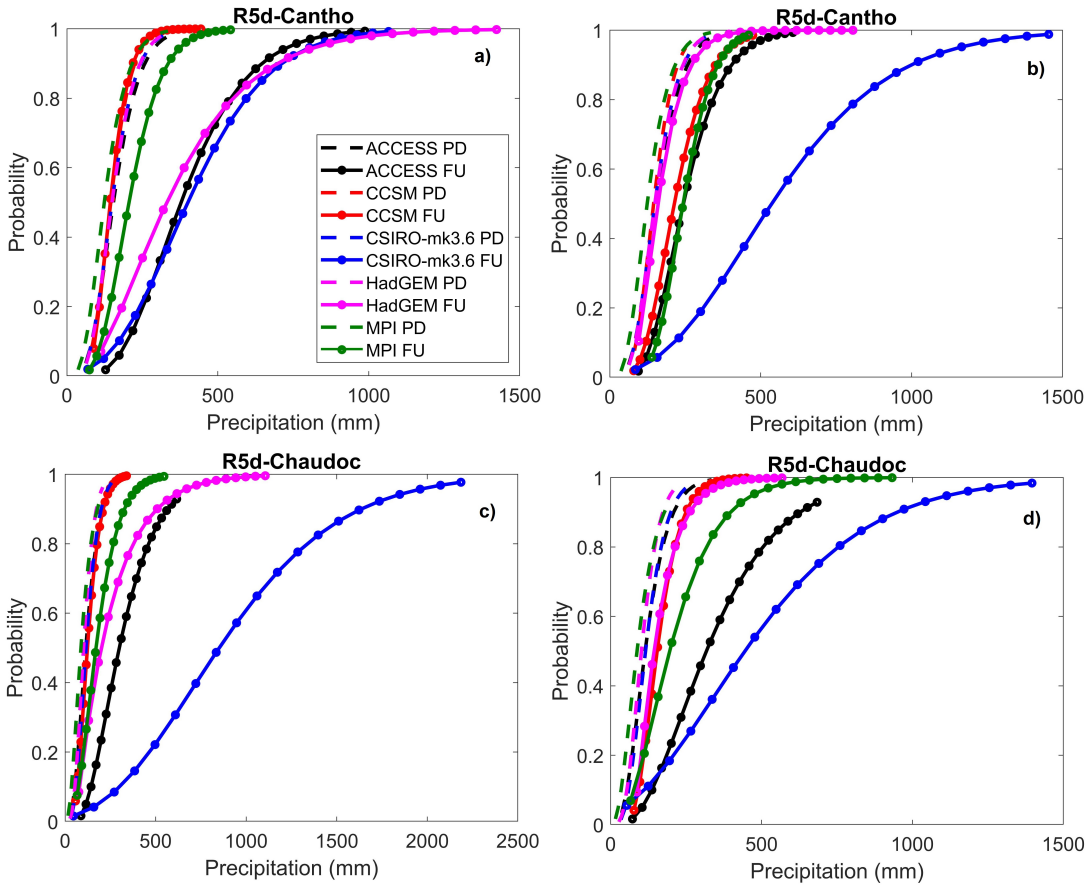

Fig. 5.25 Cumulative gamma distribution function of maximum 5-day consecutive rain for downscaled rainfall at Can Tho and Chau Doc, both present (PD) and projection (FU) for five GCMs under two RCPs. (a) R5d - RCP4.5-Cantho, (b) R5d -RCP8.5-Cantho, (c) R5d - RCP4.5-Chaudoc and (d) R5d- RCP8.5-Chaudoc

5.4 1D-MIKE 11 model for hydraulic regime of lower Mekong delta

5.4.1 Data collection

5.4.1.1 River network and hydraulic data

The river network, digital cross sections and topography of the VMD was provided by Southern Institute of Water Resources Research (SIWRR) and has been frequently updated from 1999 to 2010 from data collected on several field campaigns between 2005 and 2010.

The hourly discharge and water levels at ten stations were collected from the Vietnam's Southern Regional Hydro-meteorological Center (SRHMC) and SIWRR. The water demand data for agriculture, industry and domestic use were collected from the Southern Institute for Water Resources Planning (SIWRP) in the period from 2005 to 2011. The water level time-series was measured at 10 main stations: Vung Tau, Vam Kenh, Binh Dai, An Thuan, Ben Trai, My Thanh, Ganh Hao, Song Doc, Rach Gia, and Xeo Ro (see station location in Figure 5.26). The hourly discharges were used for model calibration and validation at Chau Doc, Tan Chau, Can Tho, and My Thuan stations during 2009 – 2011 period.

Table 5.16 Input data for the simulations

Input data	**Observed**	**Projection (if any)**
Precipitation	Daily precipitation at 7 stations (see Fig. 1) Period: 1978 - 2011 Source: SRHMC	Projected precipitation based on statistical downscaling and bias-correction approaches Period: 2036-2065 Source: CMIP5
River discharge at Kratie	Daily discharge Period: 1978-2011 Source: MRC & SIWRR	Four scenarios with annual changes of -20%, -15%, -10% and +10%, respectively
River discharge	Hourly discharge and water level at 10 stations (see Fig. 1) Period: 2005-2011 Source: SIWRR	NA
Sea water level	Period: 2005-2011 Source: SIWRR	Two scenarios with +23 cm and +35 cm relative sea level rise
Hydraulic network (cross sections, main rivers and channels)	Period: 2005-2011 Source: SIWRR	
Water withdrawal for irrigation and domestic uses	Period 2050 - 2011	2030 – 2050

5.4.1.2 Hydrological data

Daily observed precipitation data during a period of 33 years (1978–2011) were taken from 20 rain gauges of the Southern Regional Hydro-meteorological Center (SRHMC). The daily evapotranspiration was calculated using the averaged mean value of all gauging stations in the VMD during a period of 3 years (2009–2011). We selected seven rain gauge stations that were spatially distributed over the whole delta to represent the rainfall features of the VMD (see Fig. 5.26). All seven rain gauges were compared to the APHRODITE (Asian Precipitation Highly Resolved Observational Data Integration Towards Evaluation) dataset (Yagatai et al., 2012) and showed good consistency between two datasets.

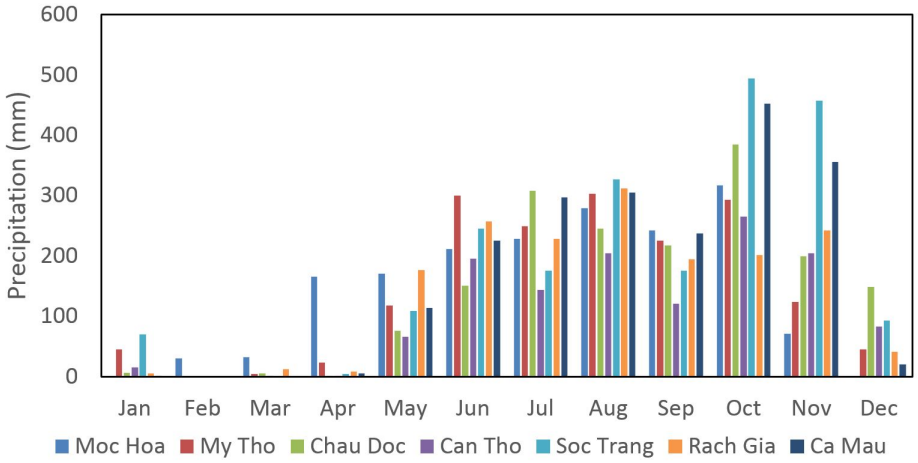

Fig. 5.26 Measured precipitation in 2011 at seven main stations

5.4.1.3 Rainfall projection data

The precipitation scenarios were developed from output data of five CMIP5 GCMs namely ACCESS 1.0, CCSM4, CSIRO-Mk 3.6, HadGEM and MPI-ESM-LR (Huang et al., 2014; Basheer et al., 2016 and Sillmann et al., 2013) (see. Table 5.17). To account for possible disagreement between individual GCMs (Kingston et al., 2011); we used a relatively large GCM ensemble, which covers a wide range of plausible future scenarios (Todd et al., 2011). The daily total precipitation data were obtained from the GCMs at spatial resolutions of $1.25^o \times 1.9^o$ for two periods, from 1978 to 2001 and from 2036 to 2065. Bilinear interpolation was applied to downscale to a $0.5^o \times 0.5^o$ grid before applying bias correction.

Future climate scenarios for precipitation were generated using the best methods of bias correction, including Linear Scaling (LS) (Lenderink, Buishand, and Deursen, 2007,

Local Intensity Scaling (LOCI) (Schmidli, Frei, and Vidale, 2006) and Distribution Mapping (DM) (Sennikovs and Bethers, 2009; Block et al., 2009). These methods are based on the assumption that the relationship between the global mean precipitation and the response pattern is linear and stationary or time invariant (Piani et al., 2010). Detailed information on these three bias correction methods is available in Teutschbein and Seibert, 2012.

Table 5.17 Emission scenarios and spatial resolution of different GCMs

GCM	**Abbreviation**	**Country**	**Original Spatial Resolution**
ACCESS 1.0	ACCESS	Australia	$1.25^o \times 1.875^o$
CCSM4	CCSM4	NCAR/USA	$0.94^o \times 1.25^o$
CSIRO-Mk 3.6	CSIRO	Australia	$1.875^o \times 1.875^o$
HadGEM2-ES	HadGEM2	Hadley/UK	$1.25^o \times 1.875^o$
MPI-ESM-LR	MPI	Germany	$1.875^o \times 1.875^o$

Daily precipitation data during the future period of 2036-2065 from five GCMs (Table 5.17 and two RCPs (Table 5.20) are statistically downscaled to station scale using bias correction methods. The corrected data are then compared to the monthly averaged observations spanning the period (1978-2001) at the two stations (Can Tho and Chau Doc) and to each other (Fig. 5.27). The statistical performances of daily precipitation for five GCMs are relatively good with the best method being Distribution Mapping. Since we only assessed hydrological changes for the VMD, we excluded the upper area from Kratie Station (i.e. North of latitude 12.47^o N) for studying the projection of future precipitation. In general, the monthly precipitation in the VMD is projected to decrease in dry seasons (Jan – June) and increase in rainy seasons (July – Dec.) in all GCM and RCP simulations (Fig. 5.28). That means, in the future there could be more drought in dry seasons and higher flooding in rainy seasons in the VMD. All GCMs project higher monthly precipitation, where we find more of an increase in the RCP8.5 than the RCP4.5. In particular, the RCP8.5 ensemble shows an increase of 6.1% to 57.13% and a decrease of -0.66% to -31.28% whereas the RCP4.5 ensemble projects an increase of 8.03% - 34.33% in rainy seasons and a decrease of -6.1% to -19.79% in dry seasons. Among five GCMs and RCPs the monthly average precipitation trends significantly differ. The lowest basin-average precipitation in dry seasons is projected by the CSIRO-RCP4.5; a similar trend is seen in the HadGEM-RCP8.5 projections while the ACCESS-RCP4.5 and RCP8.5 project the largest increase in precipitation of +88.52%. Projected results using ACCESS show considerable ranges of precipitation in both dry and

rainy seasons. The general tendencies of projected precipitation are relatively similar for all GCMs and scenarios. However, projected results from the CSIRO model (for both RCP4.5 and RCP8.5) show somewhat different results as compared to the rest of the GCMs. The calculated results show a larger range of basin-wide precipitation changes under the RCP8.5 (i.e. between -87.39% and +88.52%) compared to that under the RCP4.5 (i.e. between -19.79% and 34.33%).

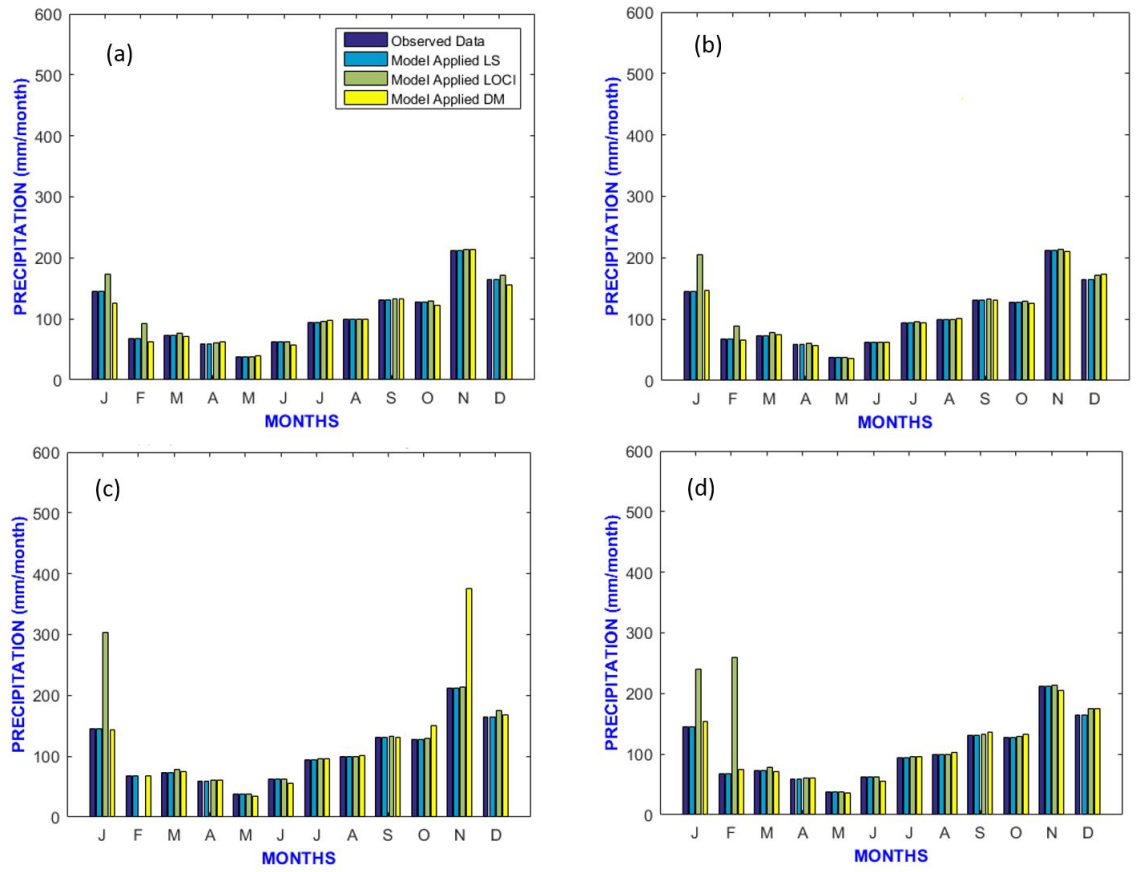

Fig. 5.27 Bias correction results for ACCESS model (a) and CCSM (b), CSIRO (c) and HadGEM- GCM models (d) at Can Tho station

All scenarios have a large variation of precipitation between rainy and dry seasons (Fig. 5.28). CSIRO-GCM projection is lower than baseline for both RCP4.5 and RCP8.5 scenarios, while four other GCM projections exhibit obvious increased trends during the rainy season. Similar consequences in terms of trend and magnitude are proved by downscaling and bias correction for Chau Doc station, but are not presented here because of limited pages. Finally, the spatial patterns of precipitation change show a considerable deviation between

the individual GCM projections. The among in projected precipitation highlight the high degree of uncertainty in reproducing future precipitation cycles in the VMD.

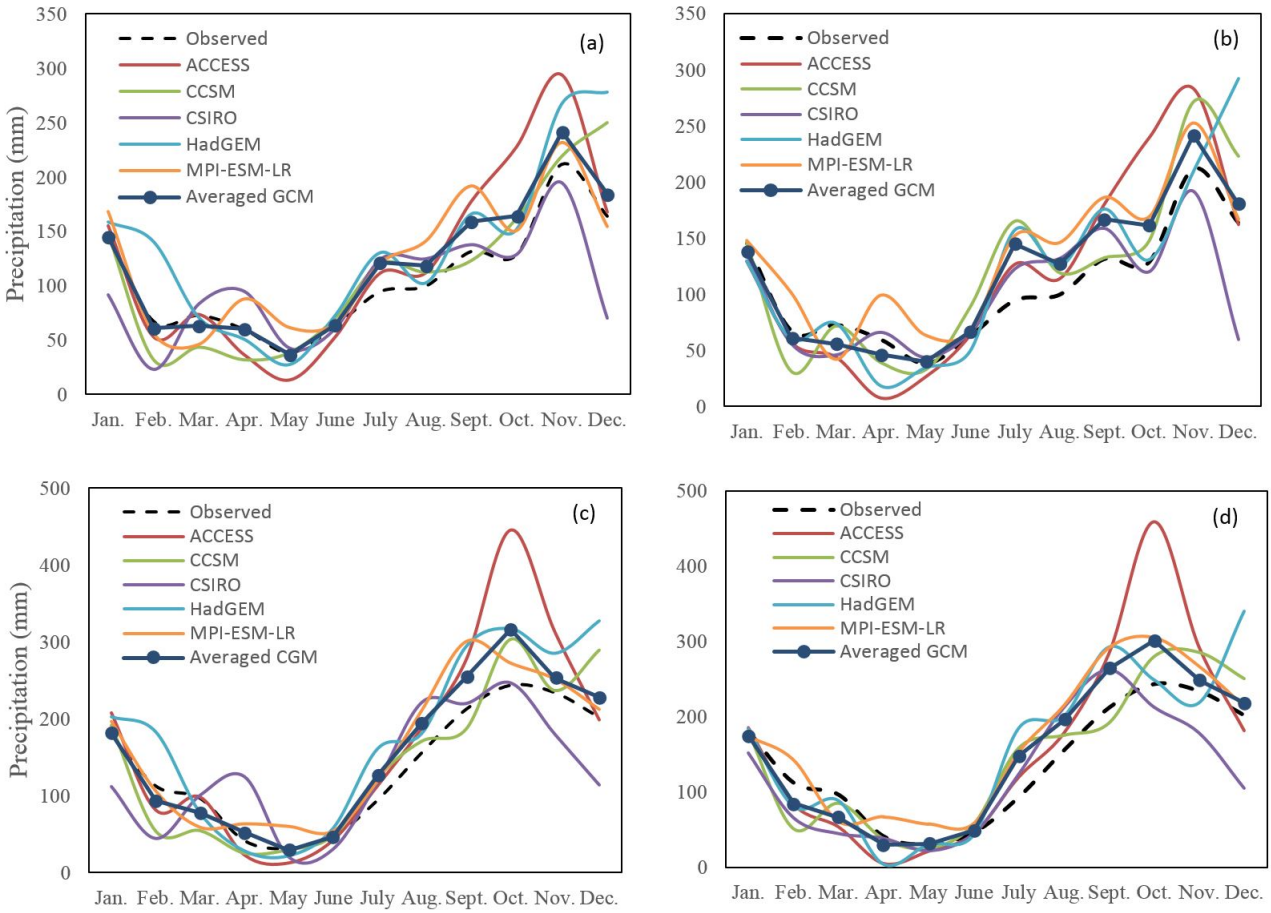

Fig. 5.28 The prediction of precipitation in Chau Doc station for (a) RCP4.5 and (b) RCP8.5 scenarios and Can Tho station for (c) RCP4.5 and (d) RCP8.5 scenarios

5.4.1.4 Upstream discharge variation and sea level rise

To assess the Mekong Delta's future hydraulic regime, we developed four scenarios of changing boundary conditions accounting for future sea level rise, upstream river discharges and in-delta precipitation (Table. 5.20). Sea level rise scenarios were based on the regional projection proposed by MONRE (2012). Our sea level rise scenarios project average increase of 23 cm during the 2030 – 2040 period and 35 cm during the 2050 – 2060. Scenarios for upstream river discharges were based on projection results conducted by Lauri et al., 2012 and Hoang et al., 2016. Lauri et al., 2012 modelled the Mekong's flows under future climate change and reservoir developments during 2032-2042, a study that indicated the discharge at Kratie will range from -11% to $+15\%$ for the wet season and -10% to $+13\%$ for the

dry season. The changes in discharge due to planned reservoir operations result in 25–160% higher dry season flows and 5–24% lower flood peaks at Kratie. Hoang et al., 2016 assessed climate change impacts on river discharges using a large ensemble of the CMIP5 climate change scenarios. Their study projected annual discharge changes ranging between -3% to +5% at Kratie for the 2036-2065 relative to 1971-2000 periods. However, both studies of Lauri et al., 2012 and Hoang et al., 2016 did not involve the other anthropogenic factors such as irrigated land expansion, urbanization, and inter-basin water transfer. All these factors will likely have significant impacts on the flow, especially low flow during the dry season (Hoanh et al., 2010; MRC, 2010). In addition, Kingston, Thompson, and Kite, 2011 discovered that the flow will alter from -17.8% to 6.5% under 2^oC scenario by HadCM3-GCM. It can be understood that the different results of these researches is due to wide range of boundary condition and time scale considerations. We therefore selected a range of annual discharge change at Kratie between -20% and +10% for our scenarios to expand the plausible range of hydrological variability. These changes were then applied on the hydrograph of 2011 to develop four upstream discharge scenarios. Lastly, precipitation scenarios were based on the downscaled and bias corrected GCM data. Further, we selected two precipitation RCPs, namely RCP 4.5 and RCP 8.5. The RCP 4.5 is a medium scenario with a stabilization of radiative forcing to 4.5 Wm^2 by 2100 (Thomson et al., 2011). The RCP 8.5 is a high scenario with a radiative forcing reaching to 8.5 Wm^2 by 2100 (Riahi et al., 2011). All in all, the two consider RCPs are expected to cover a realistic range of future climatic and hydrological changes in our study.

5.4.2 Model setup

5.4.2.1 MIKE 11

The MIKE 11 HD is a model for one dimensional unsteady flow computation and can be applied to looped networks and quasi-two dimensional flow simulation on floodplains. The model has been designed to perform detailed modelling of rivers, including special treatment of floodplains, road overtopping, culverts, gate openings and weirs. It is capable of using the 1D Saint-Venant equations. The solution of the continuity and momentum equations is based on an implicit finite difference scheme. Boundary types include water level (h), flow discharge (Q) and Q/h relation. The water level must be specified at either the upstream or the downstream boundary of the model. The flow discharge can be applied to either the upstream or the downstream boundary condition, and can also be applied to the side tributary flow (lateral inflow). The lateral inflow is used to describe runoff. The Q/h relation

can only be applied to the downstream boundary. MIKE 11 is a modelling package for the simulation of surface runoff, flow, sediment transport, and water quality in rivers, channels, estuaries, and floodplains. The most commonly applied hydrodynamic (HD) model is a flood management tool simulating the unsteady flows in complex rivers and channel systems. It has been successfully applied in different river basins around the world.

Reliable predictions of the hydraulic regime of the upper basin, as affected by dam constructions and changing hydrological cycle due to climate change and other water bodies, are needed to develop watershed management plans (Hoanh et al., 2010; MRC, 2010) and to predict plausible future variability due to the factors driving the changes. Among others, the MIKE 11 model has been widely applied by local and international institutions and universities also in Vietnam to evaluate the impact of climate change on salinity intrusion (Hoanh et al., 2010; Johnston and Kummu, 2012). For example, Luu et al., 2010 applied MIKE 11 to simulate the hydrological regime and water budget of the Red River Delta. Manh et al., 2014 conducted the sediment transport and sediment deposition in the Mekong Delta using 1D MIKE 11 and the quasi-2D hydrodynamic model has been developed by Dung et al., 2011. In a similar manner, Doan et al., 2014 employed MIKE 11 to simulate the influence of river flow and salinity intrusion on the Mekong River estuary.

During the setting up of the 1D models there are several obstacles that need to be dealt with, as follows: (1) numerous closed dike systems with different crests were constructed to protect agricultural fields. The question is how to deal with the hydraulic interaction of water storage between the block compartments and the branches and main rivers. The solution is to convert all floodplains into artificial branches that have shallow and wide cross sections that have been extracted directly from the Digital Elevation Model (DEM) with a horizontal resolution of 90m, and link those branches to the channels by control structures (Dung et al., 2011). (2) There are also a multitude of internal water exchanges for irrigation, industry and domestic uses. Calculation of water demands for different purposes should be considered by taking into account diverse aspects and potential sources.

5.4.2.2 Boundary conditions and modelling scenarios

Boundary conditions used for the VMD model forcing include discharge at Kratie for the upper boundary, sea water level in both the West and East seas for the lower boundaries, and wind, rainfall, as well as evapotranspiration over the whole domain. In addition to the discharge of the Tonle Sap and other tributaries in Cambodia, the flows from Sai Gon and

Dong Nai river basins were also incorporated as upper boundary conditions. Sea water levels at lower boundaries were based on the mean average forecasted tide in both East and West seas for the period of 2009-2011. The precipitation was calculated and transferred to runoff by using the distributed NAM model (rainfall-runoff model). As topic is lesser importance part to this study, the details of structure and parameters in NAM model are not presented in this part. The description of this model is available in Dang, Cochrane, and Arias, 2018. The water demand in the VMD for 120 sub-basins was calculated by the SIWRP based on irrigation, domestic and industry requirements and has been updated up to the year 2010. Because the water demand is in terms of daily withdrawal discharges for 120 sub-basins are considered as inputs of distributed sources in the model.

5.4.3 Model calibration and validation

The MIKE 11 model provided hourly water levels and mean velocities at every cross sections of the network. The observed discharge and water level were applied for model calibration during the period from January to December 2011, and for model validation during the period from January 2009 to December 2010 because catastrophic flooding occurred in 2011 and tremendous drought in 2009-2010.

The entire VMD model was calibrated by adjusting the Manning's coefficient for three main areas: the upper and middle areas as well as the area near the sea. The result of this adjustment is shown in Table 5.18. Chau Doc, Tan Chau, Can Tho, and My Thuan gauging stations were used as the main calibration locations, being the most important stations with the most accurate data. Moreover, the model performance was tested by using two data sets including the flood event in 2000 and the driest year in 2005. The match between simulated and observed discharges and water levels was evaluated using the Nash-Sutcliffe efficiency coefficient E (Nash and Sutcliffe, 1970), root mean square error (RMSE) and correlation coefficient (R). The robustness of the calibrated model was then validated for the period of 2009-2010 by using the previously calibrated parameters and comparing the model accuracies between the validation and the calibration period at all four main river stations mentioned above.

Due to relatively large and highly complex networks with numerous human activities in the study domain, calibration of the model by adjusting the parameters is not an easy task. A successful model calibration can be quantified by obtaining a good agreement between

calculated results and observed data.

The model agreement between the modelled and observed data is good at four main stations (Chau Doc, Tan Chau, Can Tho, and My Thuan) for the calibration period (Fig. 5.29 & 5.30) but the coefficient E values at Vam Nao, Long Xuyen stations had the lowest values. The lower E values can be partially explained the transfer of water use between internal compartments for agricultural activities and inter-exchange water between main rivers and compartments for both calibration and validation periods. (Table. 5.19). Generally, the agreement between observed and modelled time series was good for both the calibration and validation periods (i.e. E = 0.84 to 0.98). We therefore concluded that the model is suitable for predicting future hydraulic regime changes in the VMD.

Table 5.18 The calibrated Manning coefficients in the distinct parts of the river system

Components	Manning coefficient range	Remark
1. Main Tien and Hau river	n = 0.017- 0.030	
	n = 0.028-0.030	Chau Doc to Long xuyen
• Upstream river		
	n = 0.022-0.026	Long xuyen to Can Tho
• Middle delta		
	n = 0.017-0.022	Dai Ngai to Tran De
• Near the sea		
2. Primary channels	n = 0.022-0.030	
3. Field channels	n = 0.028-0.032	
4. Floodplain	n = 0.028-0.032	

Table 5.19 Statistical performances of the model for discharge and water level simulated with daily time-step

Stations	Calibration (2011)			Validation (2009-2010)		
	E	RMSE (m)	R	E	RMSE (m)	R
Chau Doc	0.93	0.46	0.98	0.91	0.49	0.98
Tan Chau	0.91	0.31	0.98	0.89	0.34	0.93
My Thuan	0.86	0.19	0.96	0.86	0.23	0.95
Can Tho	0.85	0.23	0.96	0.84	0.21	0.96
Vam Nao	0.84	0.26	0.93	0.83	0.22	0.88
Long Xuyen	0.87	0.42	0.91	0.89	0.46	0.85
Discharge	E	RMSE (m3/s)	R	E	RMSE (m3/s)	R
Chau Doc	0.95	514.5	0.97	0.92	625.3	0.96
Tan Chau	0.93	2946	0.96	0.91	3203	0.95
Can Tho	0.93	2491	0.97	0.94	2679	0.96
My Thuan	0.87	2503	0.96	0.88	2160	0.97

Table 5.20 Four selected scenarios for discharge alteration, sea level rise and precipitation scenarios

Modelling scenarios	**Sea level rise (cm)**	**Changes upstream discharge**	**Precipitation scenarios**
Original source	MONRE 2012, CMIP3	Kingston et al. 2011 and Lauri et al. 2012 (CMIP3); Hoang et al. 2016 (CMIP5)	Following Hoang et al. 2016 (CMIP5)
Scen. 1	23	+10%	RCP 4.5, 8.5
Scen. 2	23	-10%	RCP 4.5, 8.5
Scen. 3	35	-15%	RCP 4.5, 8.5
Scen. 4	35	-20%	RCP 4.5, 8.5

Table 5.21 Statistical performance of the bias corrections of five GCMs

GCM-Models	Can Tho			Chau Doc		
	RMSE (mm)	MAE (mm)	R	RMSE (mm)	MAE (mm)	R
ACCESS	8.30	5.85	0.994	6.90	4.65	0.992
CCSM	6.05	4.12	0.996	3.22	2.20	0.998
CSIRO	5.37	3.84	0.997	48.15	17.57	0.924
HadGEM	5.79	4.23	0.997	5.50	3.30	0.995
MPI	5.90	4.63	0.998	5.93	5.04	0.994

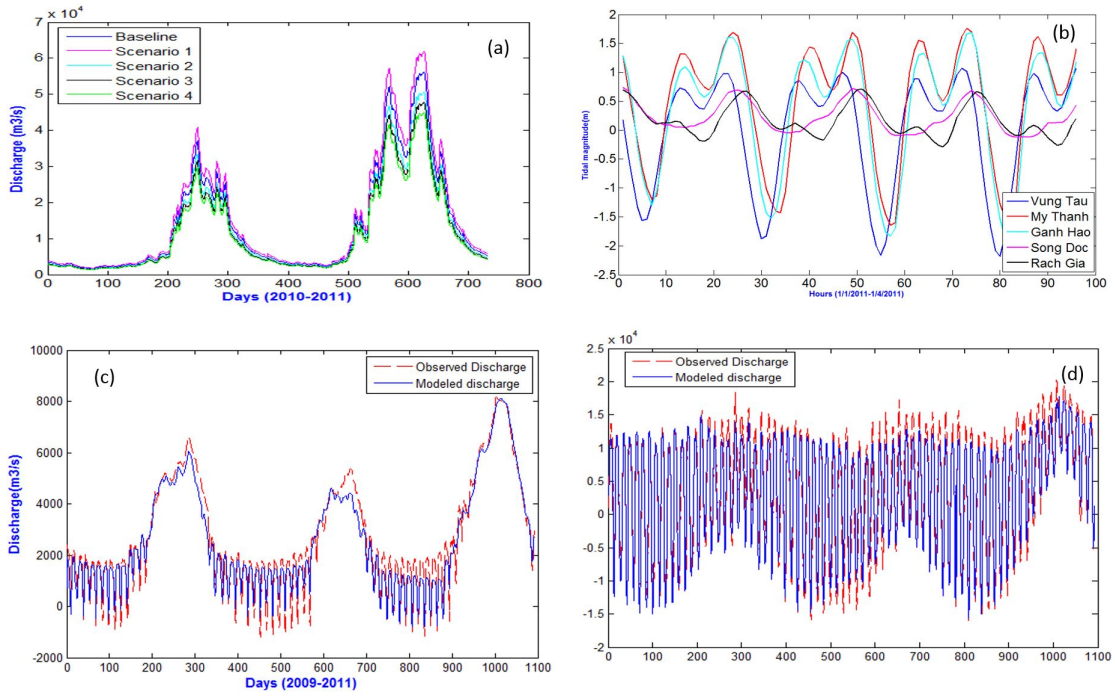

Fig. 5.29 Daily discharge scenarios at Kratie (2010 – 2011) (a); Representative tidal level at East and West Sea (b); Daily discharges at Chau Doc (c) and Can Tho (d) for calibration and validation periods (2009-2011).

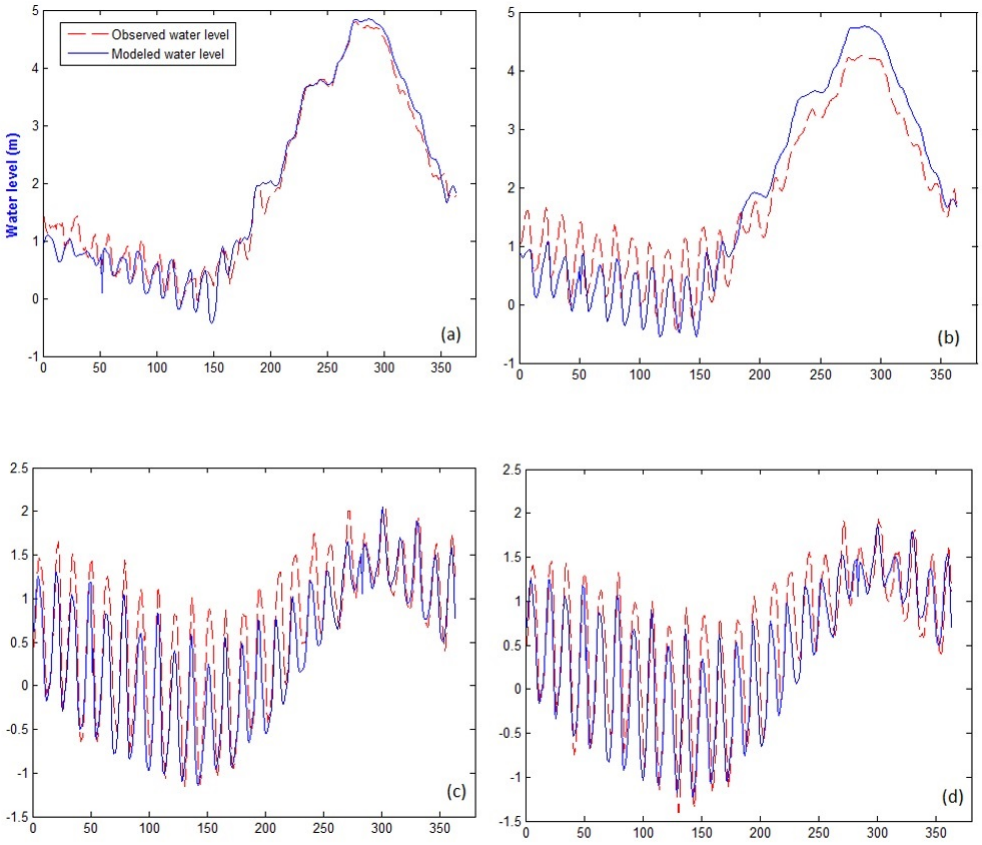

Fig. 5.30 Calibrated daily water levels at Tau Chau (a), Chau Doc (b), Can Tho (c) and My Thuan (d) in 2011

5.4.4 Model results

The impacts of climate change, sea level rise, and upstream flow variation at Kratie are assessed by modelling four scenarios presented in the following sections 5.4.4.1 – 5.4.4.4. The statistically downscaled GCM outputs and three bias-correction approaches for precipitation (LS, LOCI and DM) are used to create inputs for the hydrodynamic model. For climate change scenarios, we selected the baseline (1978-2001) and future period (2036-2065) based on available data and reliable assessment. The hydrodynamics model runs using combination of GCMs outputs, RCP ensembles of precipitation, upstream flow changes and sea level rise scenarios.

The simulations of the hydraulic regime were based on four scenarios described in Table 5.20. This section presents changes in the daily river discharges at the Tien and Hau Rivers as a result of Kratie's flow variations and in-delta precipitation change. Daily changes are

presented for all four mainstream stations (Chau Doc, Tan Chau, Can Tho, and My Thuan). We limit the remaining results to four representative stations to preserve the focus of the paper. For each scenario, an analysis of the future hydraulic regime in terms of seasonal, annual discharges and water levels is presented separately, as follows:

5.4.4.1 Scenario 1: 10% increase Kratie's discharge and 23cm sea level rise

We consider the discharge at Kratie in 2011 as the baseline and simulate the predicted hydrodynamic for the 2036 – 2065 future scenarios. Figure 5.31a presents the simulated daily discharge of four main stations mentioned above. Overall, the model predicts substantially lower discharges in the dry season and also in the early stages of the flooding season at Tan Chau, My Thuan and Can Tho stations. For instance, the different ranges of monthly discharges vary from -20.2% to 122.2%, -5.0% to +19.7%, -18.1% to +18.1% and -39.6% to +117.8% compared to the baselines at Chau Doc, Tan Chau and My Thuan and Can Tho, respectively (Table 5.23). The predicted discharge at Chau Doc exhibits an increase from 9.2% to 122.2% during the wet season. In contrast to the predicted directions, the three remaining stations (Tan Chau, Can Tho and My Thuan) have a decreasing trend of daily discharge in both dry and rainy seasons. In general, the annual flows of all stations tend to decrease: by 9.6%, 30.3%, 38.2% and 42.3% for Chau Doc, Tan Chau, My Thuan and Can Tho, respectively.

Figure 5.31a shows changes in daily water level compared to baseline in scenario 1. Overall, the model projects higher water levels at Tan Chau and Chau Doc stations during the rainy season and decreasing levels in the dry season, approximately 0.04m to 0.5 m and -0.03 m to -0.41 m. respectively. However, the decrease in the water level at Long Xuyen and Can Tho ranges from 0.1 m to 0.3 m and 0.08m to 0.23 m, respectively. Although the Kratie discharge increased by 10% in Scenario 1, the discharges at Tan Chau and Chau Doc reduced up to 40% (Table. 5.22). These contrasting trends could be attributed to the increasing in future water demand for irrigation, domestic and industry. Additionally, reduced discharges are due to the decrease in the local precipitation. Slight increases in the water levels at Tan Chau and Chau Doc (0.19 m and 0.03 m, respectively) are attributed to sea level rise. From Table 5.22 and 5.23, the annual averaged water level at Tan Chau station slightly increased but the annual averaged discharge decreased significantly. This is due to the substantially decreased discharge in dry season but not so much in wet season, so the average values of discharge at Tan Chau are negative. However, the differences of monthly water level at Tan

Chau between dry season and wet season are small, so the averages of water level are only slightly increased.

5.4.4.2 Scenario 2: 10% decrease in Kratie's discharge and 23cm sea level rise

The results of simulation under scenario 2, presented in Fig. 5.31b and Fig. 5.32b, show the differences of projected discharges and water levels at the considered stations located on the Tien and Hau Rivers. In this scenario, the discharges at Tan Chau, Can Tho, and My Thuan decrease dramatically in both dry and wet seasons whereas the discharge at Chau Doc decreases only in the dry season and increases by 32.92% in the wet season. The changes of the daily discharge at these stations vary from -11% to -94.3%, -6.8% to -89.8%, -5.4% to -87.5% for Tan Chau, Can Tho, and My Thuan, respectively. In addition, the relative changes in annual discharges reduce to -38.2% at Tan Chau, followed by -48.4% at Can Tho and -51.2% at My Thuan (Table 5.22).

The average water levels at Tan Chau and Chau Doc decrease by 0.2 m and 0.19 m in the dry season, respectively while the predicted water levels at Long Xuyen, Can Tho and My Thuan decrease by of 0.46 m, 0.2 m, and 0.15 m in the rainy season, respectively.

5.4.4.3 Scenario 3: 15% decrease in Kratie's discharge and 35cm sea level rise

From Table 5.23, the relative changes of annual discharges reduce to -40.64 % at Tan Chau, followed by -27.234 % at Chau Doc, -51.27% at Can Tho and -54.03 % at My Thuan compared to baseline. the relative changes of discharge in dry season at these stations vary from -68.7%, -68.5 %, -100.1 % and -82.5 % for Tan Chau, Chau Doc, Can Tho, and My Thuan, respectively. The calculated results showed that, generally, the annual discharges at all considered stations were slightly reduced compared to the results for scenario 2. The differences in relative changes between scenarios 2 and 3 are approximately 2.45% to 3.75%, while the flow discharge at Kratie decreased relatively by 5% and the water level at the downstream boundary increased relatively by 12cm.

In this scenario, the water levels at all considered stations slightly increased, approximately 0.06 – 0.10m compared to scenario 2, while the water level at the downstream boundary increased relatively by 12 cm. It can be surmised that the tidal level is the main driving force behind water level changes near sea stations (i.e. Can Tho and My Thuan).

5.4.4.4 Scenario 4: 20% decrease in Kratie's discharge and 35cm sea level rise

To investigate the impact of upstream discharge and climate change in the VMD, the most extreme scenario 4 was generated to compare with other cases. Figures 5.31d and 5.32d present the discharges and water levels at four considered stations. The discharges at these stations will decrease substantially during the dry season, with a large range of relative changes from -69.16% to -100.2% (Table. 5.23), while the discharges will slightly reduce, from roughly 7.7% to 29.7%, except for an increase of 7.3% at Chau Doc station during the wet season. The discharge at Can Tho will be considerably diminished at a double rate, up to 100%, compared to baseline. The water levels at all considered stations will decrease slightly compared to scenario 3.

Table 5.22 Annual averaged discharges and water level changes during the time period (2036 – 2065) compared to baseline

Scenarios	Relative changes of annual averaged discharge (%)				Relative changes of annual averaged water level (m)			
	Tan Chau	Chau Doc	Can Tho	My Thuan	Tan Chau	Chau Doc	Can Tho	My Thuan
Scen. 1	-30.3	-9.5	-38.2	-42.3	0.19	0.03	-0.01	0.04
Scen. 2	-38.2	-23.5	-48.4	-51.2	0.09	-0.25	-0.08	-0.01
Scen. 3	-40.6	-27.2	-51.3	-54.0	0.10	-0.24	0.02	0.08
Scen. 4	-42.9	-30.9	-53.9	-56.3	0.02	-0.31	0.01	0.07

Table 5.23 Annual averaged changes in seasonal river discharges at four stations for 2036 – 2065, relative to baseline 2011

Scenarios	Relative changes in dry season (%)				Relative changes in wet season (%)			
	Tan Chau	Chau Doc	Can Tho	My Thuan	Tan Chau	Chau Doc	Can Tho	My Thuan
Scen. 1	-66.5	-65.7	-99.5	-79.7	5.8	46.6	23.2	-4.9
Scen. 2	-68.0	-68.0	-99.9	-81.2	-8.3	21.0	3.2	-21.1
Scen. 3	-68.7	-68.5	-100.1	-82.5	-12.5	14.0	-2.4	-25.5
Scen. 4	-69.2	-69.1	-100.2	-82.9	-16.6	7.2	-7.7	-29.7

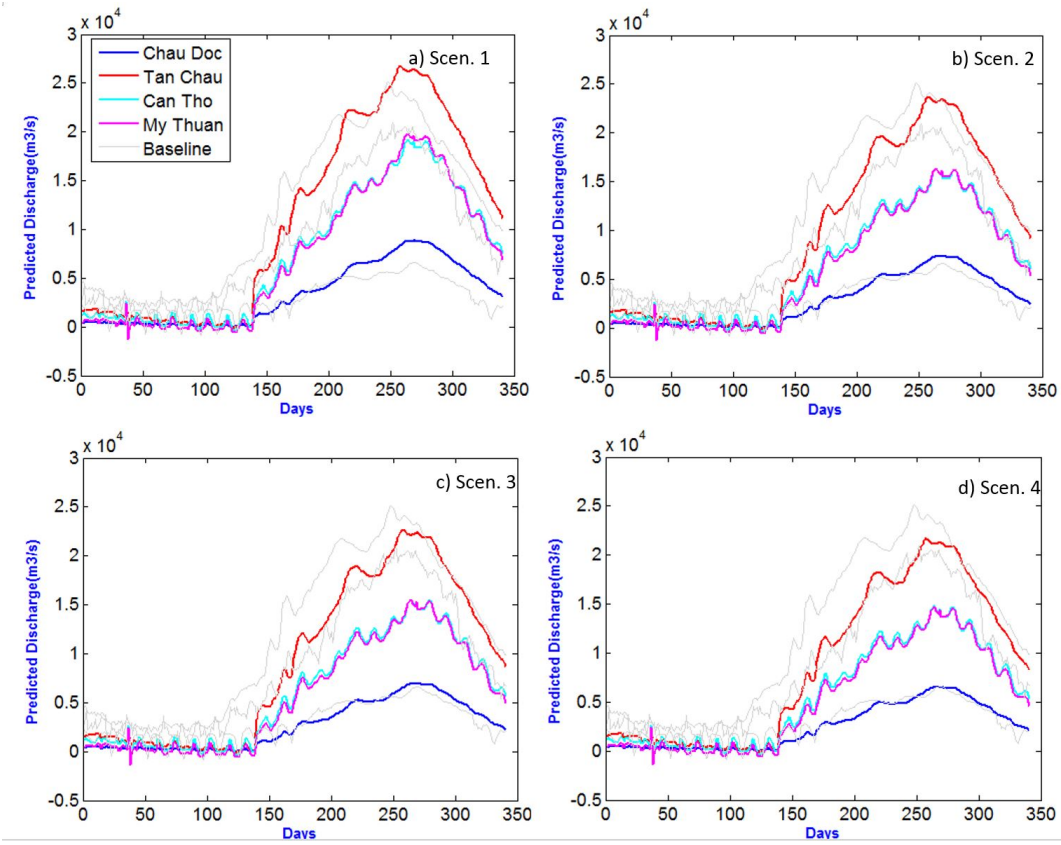

Fig. 5.31 Predicted daily discharges at four stations during the period 2036 – 2065 and for four scenarios

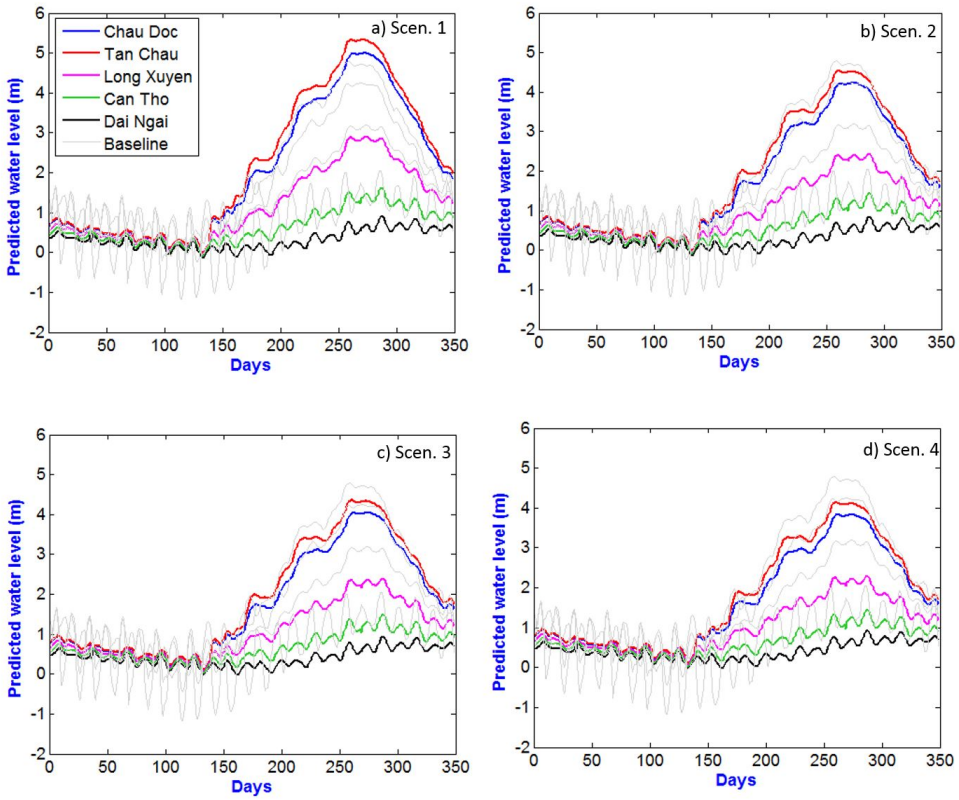

Fig. 5.32 Predicted daily water levels at four stations during the period 2036 – 2065 and for four scenarios

5.4.5 Discussion

5.4.5.1 Impact of climate change on precipitation

Climate change is predicted to alter rainfall patterns on a global scale, particularly in the Mekong Delta (Lauri et al., 2012; Hoanh et al., 2010). Changes in hydrological circulation in terms of rainfall and runoff depend on both local characteristics and large scale climate oscillations (Field et al., 2014). Precipitation is the primary driving force to change the runoff, surface water and hydraulic regime at the basin level. According to the downscaled results and bias corrections of the GCMs used in this paper, precipitation in the VMD is broadly projected to decrease in the dry season and increase in the wet season (Fig. 5.28). However, the downscaled results of five GCMs show large differences in projections through all RCP simulations, indicating high uncertainty not only in the magnitude, but also in the direction of hydrological behaviors due to climate change. It is therefore necessary to apply ensembles of GCMs and RCP scenarios to cover appropriate ranges of climate change (Christensen

et al., 2007).

Improvement of spatial resolutions and performances in the CMIP5 climate change scenarios has provided the motivation to conduct a new simulation and gain an updated perspective to the current knowledge of the VMD. As a result, our study provides updates of and insight into climate change in the VMD, driven by five CMIP5-GCMs and various downscaled and bias correction methods. Furthermore, the results also contribute to the ongoing study of the effect of climate change on salinity intrusion in Tien and Hau Rivers by using 2D models. Although the VMD is relatively large and highly complex, we attempt to focus only on main factors that deal with the climate change issue. In general, our derived precipitation, downscaled from five GCMs and three bias correction methods, is in line with findings from most previous studies (Hoanh et al., 2010; Lauri et al., 2012; Vastila et al., 2010) for the whole Mekong Basin. However, as Hoanh et al., 2010 and Vastila et al., 2010 only used one GCM, their study results did not reflect the uncertainty. Kingston, Thompson, and Kite, 2011 and Eastham et al., 2008 compared seven and eleven GCMs, respectively, but non-downscaling was applied to reduce bias and uncertainties.

Moreover, a various research (Hoang et al., 2016; Manh et al., 2014; Dung et al., 2011) has been conducted, focusing on the Vietnamese Mekong Delta, to provide detailed descriptions of current and future hydrological conditions. It is difficult to compare these studies to our results for accuracy because of different boundary conditions and assumptions. However, despite differences in GCM selection, downscaling approaches, boundary conditions and modelling applications, similar trends of an increased precipitation during the wet season have been clearly and confidently confirmed by Dinh et al., 2012 and Van et al., 2012.

5.4.5.2 Impact of both upstream flows and climate change

Because of the limited scope of this study, we have considered four scenarios with different flows at Kratie station, based on the study conducted by Lauri et al., 2012. Our investigation is also based on the premise of the previous studies carried out by Van Manh et al., 2015 and Van et al., 2012 to focus on climate change and the hydraulic regime in the VMD.

Lauri et al., 2012 conducted research to consider the impacts of climate change and reservoir operations, using both separate and cumulative assessments. The annual discharge changes varied from a decrease of 4% to an increase of 12%, as indicated in their findings. These results are similar to those in the study of Hoanh et al., 2010. Therefore, we consider

the range of variabilities of discharge at Kratie from +10% to -20% to be plausible for possible future scenarios. Our results show large differences of discharges throughout all RCP scenarios at the four main considered stations. For example, the magnitudes of the monthly discharge significantly vary between all scenarios. The discharge in Hau River is likely to increase from 7.25% to 46.66% for four scenarios in the wet season and decrease by approximately 67.8% in the dry season, while other discharges (i.e. Tan Chau, Can Tho, My Thuan) may decrease significantly in both dry and wet seasons throughout scenarios 2, 3, 4. It can be explained that the hydraulic regime in the VMD are strongly influenced by the upper hydrological conditions (i.e. building and planning dam construction, changes in land use, climate change, etc.).

Two available studies (Van et al., 2012 and Manh et al., 2014) were conducted on sediment dynamics and flood propagation in the VMD for the different time frames. Manh et al., 2014 used a baseline of 2000-2010 and a future period of 2050-2060 and Van et al., 2012 applied a baseline of 2000 and forecasted a period of 2050, whereas our study employed a baseline of 2011. Moreover, Manh et al., 2014 concentrated mostly on sediment transport, while Van et al., 2012 focused more on immediate spatial flooding during the monsoon season. However, to some extent, the increasing trends of flooding during the wet season are similar in both studies due to sea level rise and increases in precipitation.

5.4.5.3 Limitation, remaining challenges and further research

The scope of this paper is to assess the VMD's hydraulics responses to the upstream discharge boundary, climate change related to changing precipitation, and sea level rise. This is the first step in the impact assessment process related to water management. In order to fully understand the environmental, social and economic impacts, further study should be considered to assess all relevant factors, including hydrology, ecosystems and anthropogenic activities (Commission, 2010; Lamberts and Koponen, 2008). For example, irrigation expansion, inter-basin water transmission, land use changes and urbanization (Pech and Sunada, 2008) might significantly contribute to changes in hydrology and water resources. Moreover, due to a limited availability of evapotranspiration data we therefore choose climate change models do not include it. We acknowledge the limitation of lacking this information, as evapotranspiration may substantially contribute to the hydrology of this region.

One limitation of this study is to create different scenarios using the predicted discharge at Kratie given by Lauri et al., 2012 without new updated simulations of the upper hydrological

regime for current and future conditions. However, the results of this paper may be considered acceptable because of its plausible range of different scenarios. Another limitation is that we did not consider all meteorological stations in the VMD for downscaling of climate data; to maintain the focus of the paper we attempted to downscale only the main rainfall stations belonging to the Tien and Hau Rivers. Finally, our study has shown that the MIKE 11 model is able to simulate the hydraulic regime of the VMD with a relatively good accuracy. Nevertheless, there are uncertainties as a result of inaccuracies in input data, model structure, parametrization (Lauri et al., 2012) and the complexity of the VMD system.

5.5 2D-MIKE 21 model for salinity intrusion in Hau River estuary

5.5.1 Data collection

Distributed hydrological models are frequently applied in water resources assessments at the Mekong basin level, but little attention is paid to the hydraulic regimes in the estuaries due to the highly complex river-estuary-ocean interactions. The existing modelling frameworks are not well-designed to cope with the complex hydrodynamic relationship between river flow, tides and anthropogenic activities. To address this challenge, we propose a combination of hydrological models and hydrodynamic models. Therefore, the objective of this study is to integrate 1D-MIKE 11 and 2D-MIKE 21 hydrodynamic models to investigate the hydraulic regimes of and salinity intrusion in specific river sections, namely the Hau River, which stretches between Can Tho and Tran De and Dinh An estuaries. To achieve this objective, we first applied a 1D model to simulate the entire hydrodynamic of the VMD with different scenarios of upstream discharge and downscaled precipitation from five GCMs using two RCP scenarios from CMIP5. We used the simulated discharges by MIKE 11 simulation as described in Duong *et al.* (2018). Next, we employed statistical downscaling and bias-correction treatments, as shown in detail in the paper "Modelling Seasonal Flows Alteration in the Vietnamese Mekong due to Kratie Discharge Changes, Rainfall and Sea Level Rise". The outputs of the downscaled daily precipitation for 2036–2065 were used in a rainfall-runoff model required to simulate runoff for 1D hydrodynamic simulations. Finally, we used the results of Can Tho and branch discharge along the Hau River from the MIKE 11 simulation as a boundary condition of the 2D hydrodynamic model to force it include river-estuary-ocean interaction simulations. As such, our modelling framework allows one

to evaluate the combined impacts of changing upstream discharges, the variabilities of precipitation and sea level rise from climate change on salinity intrusion in Hau River, VMD.

5.5.1.1 Hydrological and hydraulic data

The hydrological input data for the MIKE 11 model includes river discharges at the delta inlet at Kratie (Cambodia), outlet water levels, precipitation, evapotranspiration and water demands for agriculture, industry and domestic sectors in the entire VMD. The hourly Kratie discharge and hourly water levels at 10 major stations, including Vung Tau, Vam Kenh, Binh Dai, An Thuan, Ben Trai, My Thanh, Ganh Hao, Song Doc, Rach Gia and Xeo Ro, were measured from 2009 to 2011 and all input data is summarized in Table 5.24. More details about these data can be found in Duong et al. 2018.

The daily precipitation scenarios for boundary conditions in the MIKE 11 model were generated from the CMIP5 using five GCMs: ACCESS 1.0, CCSM4, CSIRO-Mk 3.6, HadGEM and MPI-ESM-LR, with two RCP4.5 and RCP8.5 scenarios (Table 5.25). The bilinear interpolation was applied to downscale climate data to $0.5^o \times 0.5^o$ resolution before applying the bias correction. Future precipitation change scenarios were generated using three bias correction methods, including Linear Scaling (Lenderink, Buishand, and Deursen, 2007), Local Intensity Scaling (Schmidli, Frei, and Vidale, 2006) and Distribution Mapping (Sennikovs and Bethers, 2009; Block et al., 2009). The motivations for selecting the GCMs and RCP scenarios were explained in detail in Hoang et al., 2016 and Duong et al., 2018.

The hydraulic data for the MIKE 21 model consists of hourly discharge at Can Tho station, offshore tidal levels and salinity concentration at Tran De and Dai Ngai stations, in the years 2011 and 2010 for calibrating and validating the models, respectively. The tidal levels in the years 2010 and 2011 were derived from the Global Tidal Model in the MIKE Zero Toolbox and were calibrated with tidal levels data at My Thanh station, provided by the Institute of Coastal and Offshore Engineering (http://www.icoe.org.vn/index.php). Furthermore, the branch discharges along the Hau River were simulated from the MIKE 11 model, for five main intakes, including Mang Thit, Rach Mop, Cau Quan, Nga Bay and Dai Ngai. The future discharges at Can Tho were simulated from MIKE 11 with four scenarios of upstream discharges at Kratie and precipitation in the VMD.

Regarding the wind data for the MIKE 21 simulation, there are two dominant wind directions; the wind blows south-west in the wet season and northeast in the dry season, with stronger speeds as a result of the monsoon in the South China Sea. The average north-east wind speed varied between 3 and 6 m/s, and the maximum speed was approximately 15–20

m/s towards the east, blowing from the sea. The predominant wind directions were calculated and are shown in Table 5.26.

Table 5.24 Main input data for the hydrological simulations

Model	Input data	Observed	Projection (if any)
MIKE 11	Precipitation	Daily precipitation from 7 stations (locations in Fig. I) Period: 1978 - 2011 Source: SRHMC	Projected precipitation based on downscaled and bias-corrected GCM simulations. Period: 2036-2065 Source: CMIP5
	River discharge at Kratie	Daily discharge data Period: 2078-2011 Source: MRC + SIWRR	NA
	River discharge in the Mekong Delta	Daily discharges and water levels at 10 stations (locations in Fig I) Period: 2005-2011 Source: SIWRR	NA
	Sea water level and tides	Period: 2005-2011 Source: SIWRR	
	Hydraulic network	Period: 2005-2011 Source: SIWRR	
MIKE 21	Discharges at Can Tho	Hourly discharge Cali. Period 2011 Vali. Period 2010 Source: SRHMC+DHI	Future Period 2036-2065
	Tidal magnitudes	Period 2010-2011 Source: SRHMC+DHI	Future Period 2036-2065
	Branches discharges	Five main channels/rivers connecting Hau river Period 2010-2011	

SRHMC: Southern Regional Hydro-meteorological Center, SIWRR: Southern Institute of Water Resources Research.

Table 5.25 Downscaled GCMs, emission scenarios used, and spatial resolution of each GCM

GCM	**Abbreviation**	**Country**	**Spatial Resolution**
ACCESS 1.0	ACCESS	Australia	$1.25^o \times 1.875^o$
CCSM4	CCSM4	NCAR/USA	$0.94^o \times 1.25^o$
CSIRO-Mk 3.6	CSIRO	Australia	$1.875^o \times 1.875^o$
HadGEM2-ES	HadGEM2	Hadley/UK	$1.25^o \times 1.875^o$
MPI-ESM-LR	MPI	Germany	$1.875^o \times 1.875^o$

Table 5.26 Direction of Wind, Southern Vietnam (SIWRR, 2011)

Month	Jan.	Feb.	Mar.	Apr.	May	June	July	Aug.	Sept.	Oct.	Nov.	Dec.
Direction	NE	NE	E	SE	SE	SW	SW	SW	SW	NW	ENE	NE

Note: E = east; ENE = east-northeast; NE = northeast; NW = northwest; SE = southeast; and SW = southwest.

Salinity data was used for calibrating and validating the MIKE 21 model for the years 2011 and 2010, respectively. The salinity concentration in the Hau River significantly changed during the dry season and reached its largest value between March and May (see Figure 5.33. The Dinh An and Tran De estuaries are characterized by an irregular semi-diurnal tide, which has a strong effect due to tidal oscillations (Nguyen, 2013, Duy Vinh et al., 2016). Similar to salinity, the discharge at Can Tho shows considerable fluctuation within one day, and the diurnal differences are evident. The salinity and tidal levels showed phase differences, with the maximum salinity at the Dai Ngai station occurring during the spring tide. The maximum salinity in 2011 at the Tran De station was about 23.0 PSU (practical salinity unit; 1 PSU equals 1%■) and the minimum value was 0.5 PSU (CGIAR, 2016). The salinity concentration at Dai Ngai station was smaller than Tran De because this station was located about 31 km further inland. In 2011, the maximum value of salinity level in Dai Ngai reached 11.0 PSU, and minimum values varied between 0.0 and 0.5 PSU.

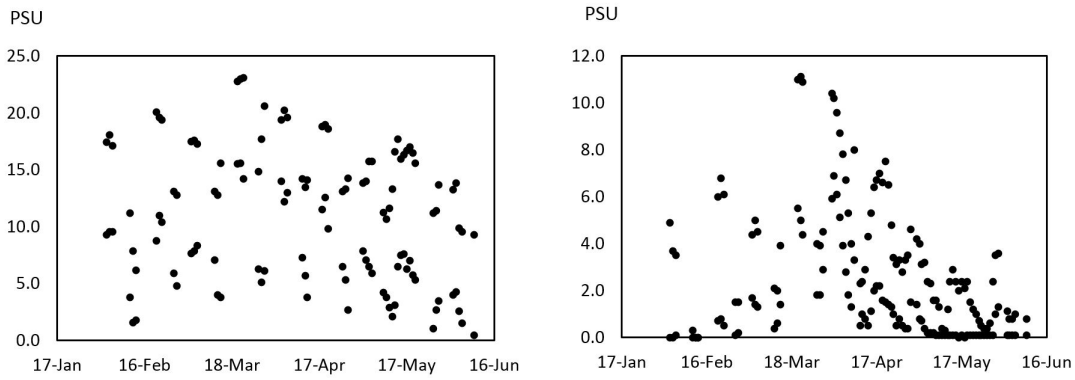

Fig. 5.33 The salinity concentration at Tran De (a) and Dai Ngai (b) stations in the year 2011

5.5.2 Model setup

5.5.2.1 Model schematization

The detailed bathymetry in numerical modelling plays a critical role in achieving accurate hydrodynamic simulations. In the present study, the bottom topography data in the coastal area and the Hau River estuary were obtained from the DHI Vietnam (Danish Hydraulic Institute), the Department of Transportation in Ho Chi Minh City, and the Southern Institute of Water Resources Research (SIWRR). The modelling domain in the horizontal plane covers 100×110 km including the main river stream and the coastal sea. The greatest depth in the study area is 20 m below mean sea level, near the south-east corner of the modelling domain in the coastal sea. It is important to consider the model stability by satisfying the Courant–Friedrich–Levy number: the selection of time step (Δt) and grid step (Δx) is crucial in order to balance the trade-off between numerical stability and computational time. The simulation grid cell selection for the study area is flexible mesh (FM) or unstructured mesh, where triangular cells of bathymetry are used to optimize the simulation, with small sizes in river domain and larger sizes in offshore settings. The triangular element sizes are about 80–100 m in the river and 800–1000 m offshore, with the total triangular being 35,000 elements and 28,000 nodes. Bathymetry was constructed with the MIKE zero tool and obtained from an updated digitizing map in 2011 from the Southern Institute for Water Resource Planning and DHI Vietnam. The bathymetry and grid resolution is presented in Figure 5.34.

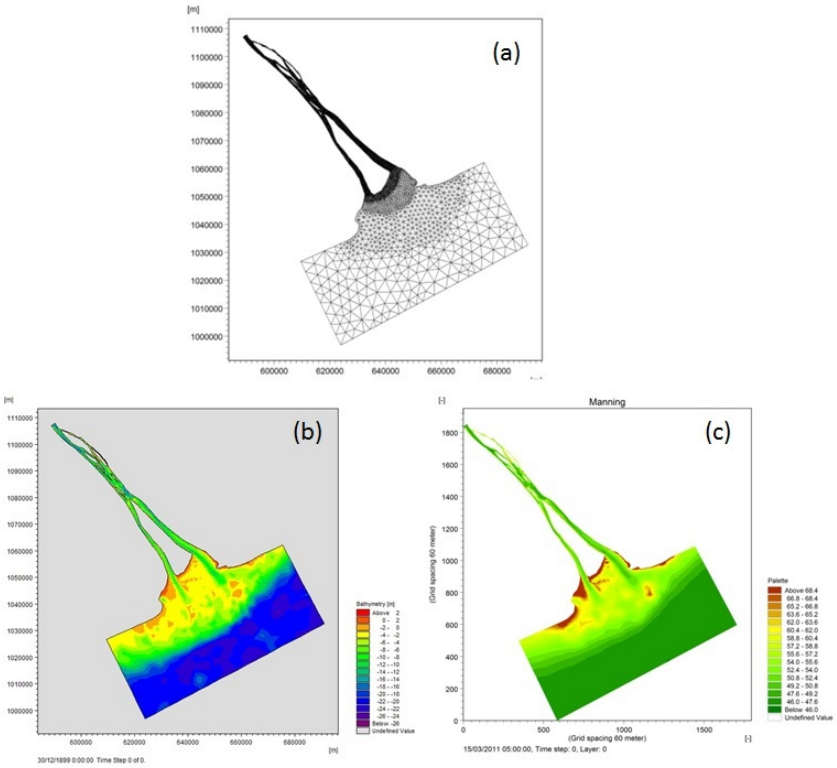

Fig. 5.34 a) Mesh; b) Bathymetry and c) spatial Manning number distribution

5.5.2.2 MIKE11 hydrodynamic model

The MIKE 11 is an unsteady 1-dimensional hydrodynamic model, which is based on one-dimensional equations and solves the vertically integrated equations regarding conservation of continuity and momentum. The solution of continuity and momentum equations are employed as an implicit finite difference scheme with a 6-point Abbott scheme (Abbott and Ionescu, 1967). The main governing equations are Saint-Venant equations (Shooshtari, 2008). In order to effectively simulate floodplain and field areas, and to connect main channels and rivers, we employed the quasi-2D modelling approach developed by Dung et al., 2011. The rice fields and the floodplain are considered to be artificial channels or "virtual channels", having wide cross sections and were extracted from the digital elevation model (DEM). The calibration process of these channels and crest of dikes was explained in detail in Manh et al., 2014 and Dung et al., 2011.

5.5.2.3 MIKE21 hydrodynamic model

The MIKE 21 is a dynamic modelling system applicable for coastal and estuarine environments. The MIKE 21 comprises several modules, including the hydrodynamic module, advection–dispersion module, spectral wave module, and transport module. This model is based on the numerical solution of the two dimensional incompressible Reynolds-averaged Navier–Stokes equations with the assumptions of Boussinesq and hydrostatic pressure. It comprises continuity, momentum, temperature, salinity and density equations (MIKE21 and MIKE3 Flow Model, 2009).

This study applies MIKE 21 with two modules, namely hydrodynamic (HD) and transport modules (TR), using a flexible mesh. The mutual interaction between the flow, wind, and velocity and sea tide is considerable. The wind is specified as a spatially constant value for the entire domain and temporally variable values. The schematic presentation of the modelling framework is shown in (Fig. 5.35).

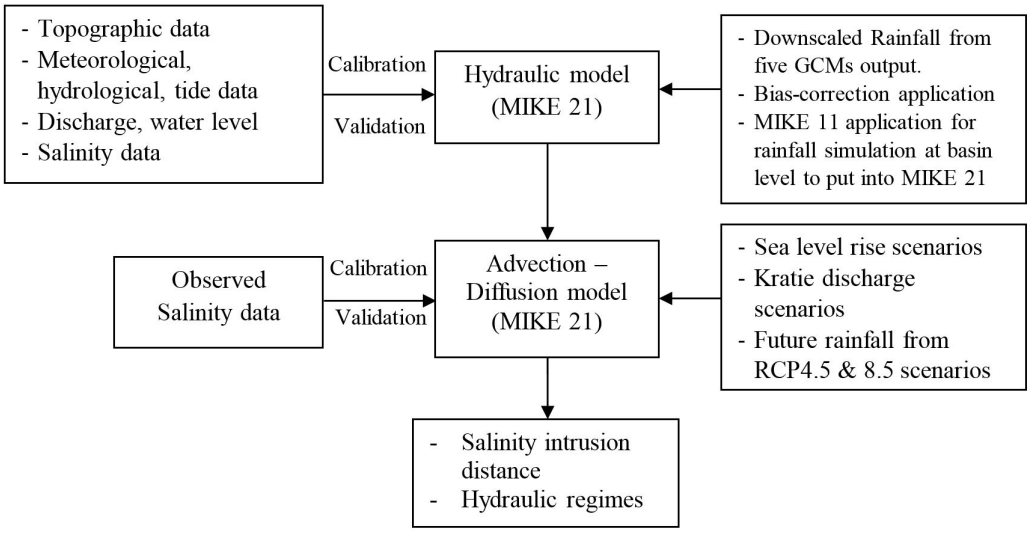

Fig. 5.35 The research methodology for combined modelling

5.5.2.4 Model parameterization

The model parameters to be defined for the HD model are the roughness coefficient (n), or Manning number, and for the AD model, the horizontal dispersion coefficient (D_h), eddy viscosity, Courant–Friedrich–Levy (CFL) and Smagorinsky coefficient. In order to realistically reproduce the physical phenomena of river mechanics, the Manning number is

defined as a function of water depth (h) and bed river type, and can be calculated based on depth and drag coefficient (David, 2010; Soulsby, 1997) (see Figure 5.34c). In the MIKE 21 manual, the Manning number was defined via the drag coefficient in below equation with g as gravity constant:

$$C_d = \frac{g}{\left(Mh^{1/6}\right)^2},$$

which C_d can define through total water depth and empirical drag coefficient (at 1m above the bed) for different bottom types (from mud to gravel):

$$C_d = \left(\frac{1}{0.32h}\right)^{1/7} C_{100}$$

$C_{100} = 0.022 \div 0.0047$, and a table of full empirical drag coefficients can be found in Soulsby, 1997. The Manning numbers were available for each grid and varied from estuary to upstream river in the entire domain. The range of the Manning number varied from 20 to 40 $m^{1/3}/s$, and depends on grainsize (rippled sand – gravels) and water depth (shallow to deep water) during model calibration. We adjusted the Manning number throughout the revision of C_{100} by defining the type of riverbed and seabed. The eddy viscosity was defined in a Smagorinsky formulation and was adjusted during calibration with a range 0.25–0.27, with an initial value of 0.28.

5.5.2.5 Boundary condition

For the delta-wide modelling with MIKE 11, we proposed four scenarios to cover future changes of upstream discharges, sea level rise and in-delta precipitation changes, and used these scenarios as boundary conditions for our modelling exercises (5.27). More detailed information about rationales and designs of the scenarios can be found in Duong et al. 2018. Results from the Mike 11 modelling, particularly the discharge data at Can Tho, were then used as boundary conditions for the salinity intrusion simulation using MIKE 21. The changes in upstream discharges at Kratie are selected with a range of +10% to -20% relative to baseline discharge in 2011, based on literature review on projected future flow changes of Lauri et al., 2012 and Hoang et al., 2016. Notably, both studies did not consider the other anthropogenic factors such as irrigated land expansion, urbanization, and inter-basin water transfer. In addition, other studies (Kingston, Thompson, and Kite, 2011; Thomson et al., 2011) show different ranges of future hydrological changes due to differences in GCM outputs and climate change scenarios selection. Therefore, we extended the range of inflow

changes at Kratie to capture possible future hydrological alterations in the upper Mekong Delta. For the climate change scenarios, we selected two RCPs for precipitation, namely RCP4.5 and RCP8.5.

Our sea level rise scenarios were obtained from the scenarios provided by the Ministry of Natural Resources and Environment. We selected an average of the predicted sea level rise, resulting in an increasing 23 cm between 2030 and 2040 and 35 cm between 2050 and 2065 (MonRE, 2009). For the MIKE 21 simulation, the hourly discharges at the Can Tho station were taken from the MIKE 11 simulation with four distinct time series of flows. The predicted sea levels were calculated linearly based on the averaged multi-annual tidal magnitudes from the global tidal model (Andersen and Knudsen, 2009). The seawater density was assumed to be constant and the salinity level at sea was predicted to remain at 35.0 PSU in the future condition. There are two approaches to obtaining the sea level rise condition. One is to impose an instantaneous elevation of sea level at coastal sea boundaries by applying linear adjustment of the mean sea level from the long observed sea level; the other is to run the hydrodynamic model over a long period to obtain predicted sea level. In this study, we obtained the sea level rise projection from the Vietnamese Ministry of Natural Resources and Environment (MONRE) and applied linear adjustment for predicted sea level rise during the 2036–2065 period.

The boundary condition for the MIKE 21 modelling includes the upstream hourly discharge at Can Tho station and tidal magnitude at downstream boundaries in the coast (Figure 1). To obtain salinity boundary conditions under future sea level rise and to reduce the influence of the boundary conditions on the in-delta modelling, a larger offshore domain that covers Hau estuary and adjacent shelf area was used. Secondly, five river branches connecting to the Hau River include Mang Thit, Rach Mop, Cau Quan, Nga Bay and Dai Ngai, were simulated as the sources and sinks. Thirdly, wind speeds and directions data were collected at the Vung Tau hydrological station and applied for the entire domain. Finally, time series of water level at My Thanh, Dai Ngai and Tran De stations were measured during 2010–2011 for model calibration and validation. For salinity at downstream boundaries, we set up the salinity concentration as 35.0 PSU and assumed the salinity in upstream to be 0.1 PSU.

Table 5.27 Four scenarios of changing of discharges and sea level rise, precipitation

Scenarios	**Sea level rise (cm)**	**Changes upstream discharge**	**Precipitation scenarios**
Scen. 1	23	+10%	RCP 4.5, 8.5
Scen. 2	23	-10%	RCP 4.5, 8.5
Scen. 3	35	-15%	RCP 4.5, 8.5
Scen. 4	35	-20%	RCP 4.5, 8.5

5.5.2.6 Computation of Flushing Time

The flushing time can be determined by the freshwater fraction approach (Lauff, 1967; Dyer, 1997), which can be determined from the salinity distributions. This technique provides an estimation of the time scale over which contaminants and/or other material (saltwater in this study) released in the estuary are removed from the system. Using the freshwater fraction method, the flushing time (Tf) in an estuary can be expressed as:

$$T_f = \frac{F}{Q} = \frac{\int_{vol} f.d(V)}{Q}$$

where F is the accumulated freshwater volume in the estuary, which can be calculated by integrating the freshwater volume, d(V), in all the sub-divided model grids over a period of time. In estuaries with unsteady river flow and tidal variations, F and Q are the approximate average freshwater volume and average freshwater input, respectively, over several tidal cycles for a period of time. The term "f" is the freshwater content or the freshwater fraction, which is described by:

$$f = \frac{S_o - S}{S_o}$$

where S_o is the salinity in the ocean and S is the salinity at the study location.

5.5.3 Model calibration and validation

5.5.3.1 Model calibration

The MIKE 21 FM-HD and TR models were first calibrated with the observed averaged water level and salinity concentration at the middle cross section of the Hau River's estuaries. The

calibration period was from January to December 2011 for hydrodynamic simulation, and six months from January to June 2011 for salinity simulation. The water levels measured at My Thanh and Dai Ngai were used to calibrate the model. In the inlet of the model at Can Tho station, initial salinity values were set at 0.1 PSU (%■). In the outlet of model (offshore), the salinity concentration was set at 35 PSU.

Several parameters of the HD and TR modules of MIKE 21 were adjusted to improve model performance. The calibration process aims to match simulated results and observed data, including water level and salinity concentration in different locations, by changing the Manning number and CFL in MIKE 21 HD and TR. In the simulations we applied a value of 0.8 for CFL-number and Smagorinsky coefficient within the range 0.25 and 0.27. Model calibration results have achieved the realistic results and indicated that the selected parameters were reasonable, as shown in Figure. 5.36. To compare the observed and simulated water levels and salinity concentrations, the latter were taken at the center point of the cross section, as mean values for comparing with observed values. The performance indices include mean absolute error (MAE), root mean square error (RMSE) and correlation coefficients (R). The comparison between modelling results and observed salinity data also reveals a strong correlation and an excellent prediction, with the R-value higher than 0.8 (Table 5.28).

Figure 5.37 compares the observed and simulated salinity concentrations at the Tran De and Dai Ngai stations. The simulated salinity time series compared favorably with the discrete salinity measurements at the two aforementioned stations. Overall, the model reflected the large dynamic variation of salinity between 0 and 30 PSU over a tidal cycle, with decreasing values of mean salinity as freshwater discharge increased.

5.5.3.2 Model validation

The MIKE 21 model was further validated with the calibrated parameters, focusing on water levels and salinity concentration. The time series data of hourly discharge at the Can Tho station in 2010 was used as upstream boundary conditions to drive the model simulations. The hourly tidal values taken from a global tide model were adopted as a forcing function at the coastal sea boundaries. The hourly tidal data and daily freshwater discharges were collected from SIWRR and the Southern Regional Hydro-Meteorological Center (SRHMC). The water level and salinity concentrations from Tran De and Dai Ngai stations were employed to evaluate the model. The comparison of observed data and simulated results for water level and salinity concentration is verified to check the model's performance.

Figure 5.38 compares the simulated water levels and observed data with the time series at

My Thanh and Dai Ngai during the period between 29 April and 11 May 2010. In general, the modelling results show realistically simulated water level variations. The comparison demonstrates the model's capability to reproduce the water levels, even under large variations of daily freshwater influx from the upstream Can Tho station. To compare the observed and simulated water levels and salinity concentrations, the simulated water level and salinity were taken at the center point of the cross section, as mean values for comparing with observed values. Overall, the model satisfactorily simulated the water level at My Thanh and Dai Ngai on the Hau River. The calibrated model parameters were, therefore, adopted for our modelling exercises and scenario analyses.

Table 5.28 displays the performance of the model simulation and measured data for water levels and salinity concentration. The performance indices include mean absolute error (MAE), root mean square error (RMSE) and correlation coefficients (R). The MAE values in calibration and validation for water level at My Thanh and Dai Ngai, respectively, are 0.23 and 0.11 m and 0.26 m and 0.14 m. The RMSE values for water level at My Thanh and Dai Ngai, respectively, are 0.29 and 0.13 m for calibration and 0.31 m and 0.16 m for validation. R values at My Thanh and Dai Ngai are 0.923 and 0.997 for calibration and 0.913 and 0.967 for validation, respectively. The comparison between modeling results and observed data in water level indicates a strong correlation and an excellent prediction. Through the model validation, the calibrated parameters are adopted in the model for prediction.

Table 5.28 Statistical performance of calibration result at three station

Stations	Calibration(2011)			Validation (2010)		
	RMSE (m)	MAE (m)	R	RMSE (m)	MAE (m)	R
Water level at My Thanh	0.29	0.23	0.923	0.31	0.26	0.913
Water level at Dai Ngai	0.13	0.11	0.997	0.16	0.14	0.967

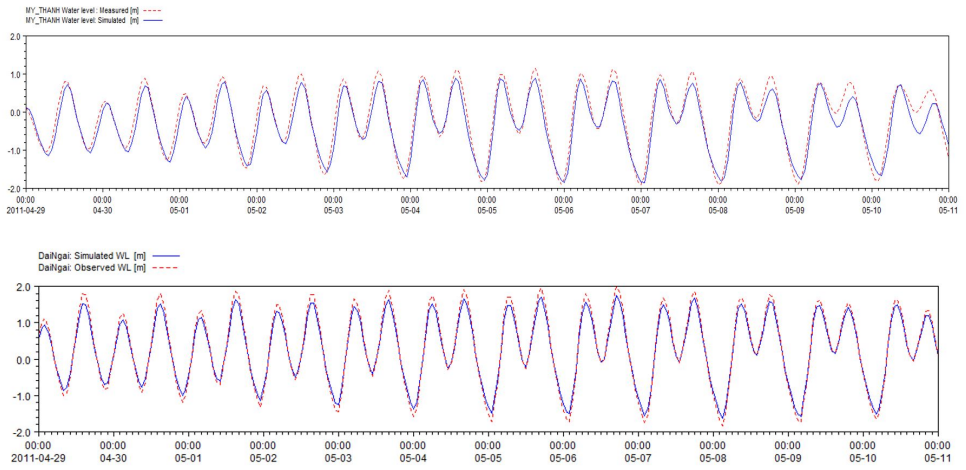

Fig. 5.36 Calibration of water level at My Thanh (a) and Dai Ngai station (b)

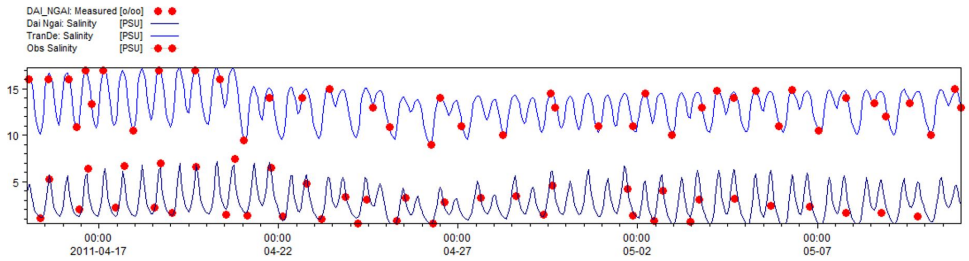

Fig. 5.37 Calibration of salinity concentration at Tran De and Dai Ngai stations

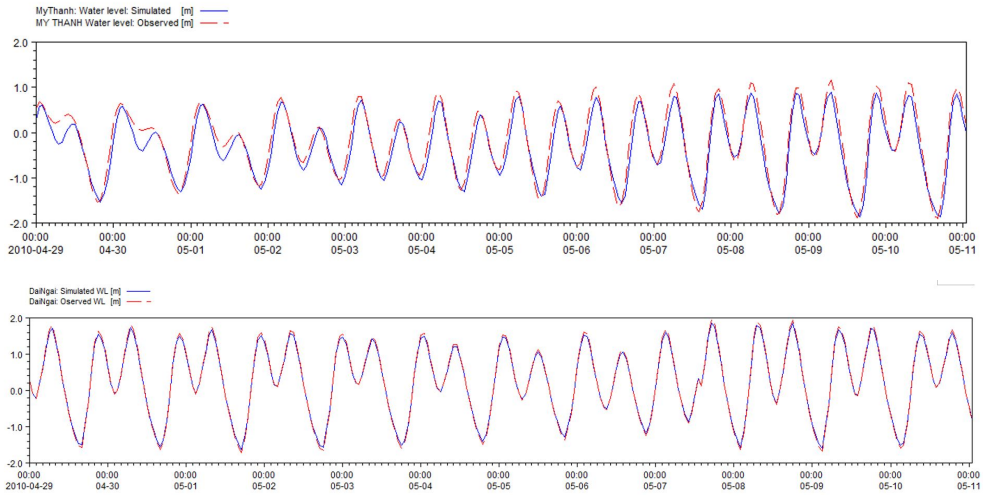

Fig. 5.38 Validation of water level at My Thanh and Dai Ngai station

5.5.4 Results and discussion

5.5.4.1 Changes in salinity intrusion

Simulating the spatial variations of salinity in the estuary and further upstream of the Hau River shows the detailed changes in the salinity dynamics under different discharges, sea level rise (SLR) and rainfall scenarios. The discharge at Can Tho varied significantly throughout the year, with a maximum discharge less than 20,000 m^3/s in the wet season and a minimum discharge of -15,000 m^3/s (Figure 5.39). The inverse flow direction in the dry season is caused by the tidal flow. Discharges at Can Tho were influenced not only by the upstream flow from Tan Chau, Vam Nao, but also by tidal regimes from the East Sea. The tidal feature in South China Sea is semidiurnal asymmetry; the peak spring tide reaches 3.0 m between December and January every year and reaches its lowest levels from June to August with a variability of around 0.5 m.

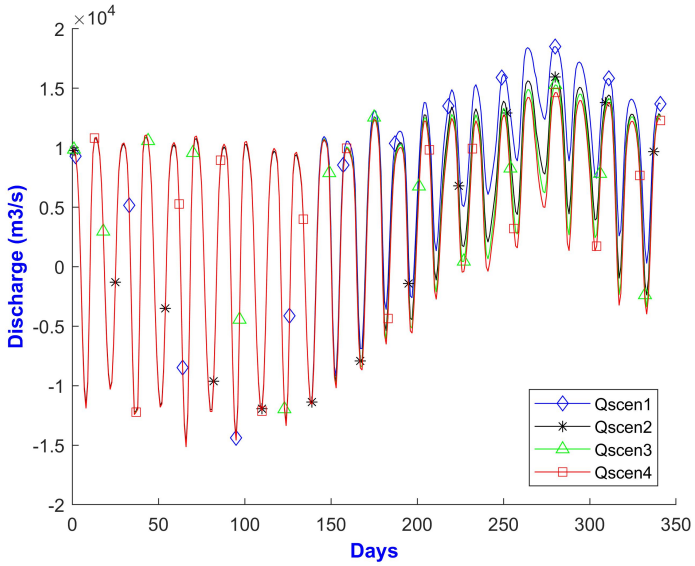

Fig. 5.39 Discharge at Can Tho for four scenarios obtaining from MIKE results

In order to quantify the spatial variations in the salinity concentrations along the river, the minimum and maximum difference in salinity concentrations between the baseline and four scenarios was calculated and is presented in Table 5.29

Figure 5.40 and 5.41 presents the spatial distributions of maximum and average salinity levels along the Hau River estuary under the four scenarios, respectively. The result shows radical changes in the salinity levels across the entire estuary. Compared to the reference isohaline of 4.0 PSU, the salinity profile with 4.0 PSU moves farther upstream by 48.55,

49.13, 49.16 and 49.18 km from Scenario 1 to Scenario 4, respectively (Table 5.30). The relative changes compared to the baseline are 3.29, 3.87, 3.90, and 3.92 km for the four scenarios, respectively (Table 5.31). Scenario 4 shows the farthest salinity intrusion, which is explained by strong upstream discharge reduction and substantial sea level rise of 35 cm (5.42). Similarly, Scenario 1 shows weaker salinity intrusion from the sea compared to other scenarios. This is explained by slight increases in the upstream discharge and the sea level rise of 25 cm. Figure 12 presents the salinity distribution under four scenarios at different points along the river: from the river mouth (My Thanh station) to upstream (Can Tho station) in spring tide (Fig. 5.43a) and neap tide simulations (Fig5.43b). The mean values are taken at the middle point of the cross-section. Figure 5.41 shows the difference in salinity between the four scenarios and the distance of salinity intrusion from the river mouth.

Here we discuss our results for salinization modelling in view of the relevant studies on this topic. Smajgl et al., 2015 studied the effects of a wide range of driving factors on salinization, including land use changes, sea level rise of 30 cm, development of all proposed upstream reservoir and irrigation, and an increasing number of dry years. The results stated that the isohaline of 4.0 PSU is relocated throughout the Hau River, with distance from the river mouth reaching approximately 70 km. Considerable differences in the 4.0 PSU isohaline between this study and Smajgl et al., 2015 can be attributed to differences between the scenario setups and boundary conditions in the two studies. Nguyen and Savenije, 2006 tested analytical solutions of salinity simulation in the Mekong estuaries based on observed data in 2005 for the Co Chien, Cung Hau and Hau estuaries. The results showed that salinity intrusion distances from the river mouth were 41 km and 23 km for spring tide and neap tide during the dry season in 2005, respectively. Furthermore, the finding by Trieu and Phong, 2015 concluded that the salinity intrusion of 1.0 PSU in Hau River was approximately 55–60 km for the dry season of 2010. This projection is higher than our results for all scenarios. All in all, results from this study show a strong dependency of salinization on upstream inflow and the changing tidal dynamics under sea level rise. Such a mechanism is also commonly reported in large river deltas of the world, including the Bangladesh Delta Bhuiyan and Dutta, 2012, Nobi and Gupta, 1997 and the Dutch Delta Oude Essink, Van Baaren, and De Louw, 2010.

Table 5.29 Max and min salinity at Dai Ngai and Tran De station

Stations	Max and min Salinity (PSU)							
	Scenario 1		Scenario 2		Scenario 3		Scenario 4	
	Max	Min	Max	Min	Max	Min	Max	Min
Dai Ngai (1st June)	5.44	0.076	5.74	0.071	5.83	0.066	5.91	0.054
Tran De (1st June)	29.41	25.02	30.39	25.31	30.27	25.20	30.31	25.44

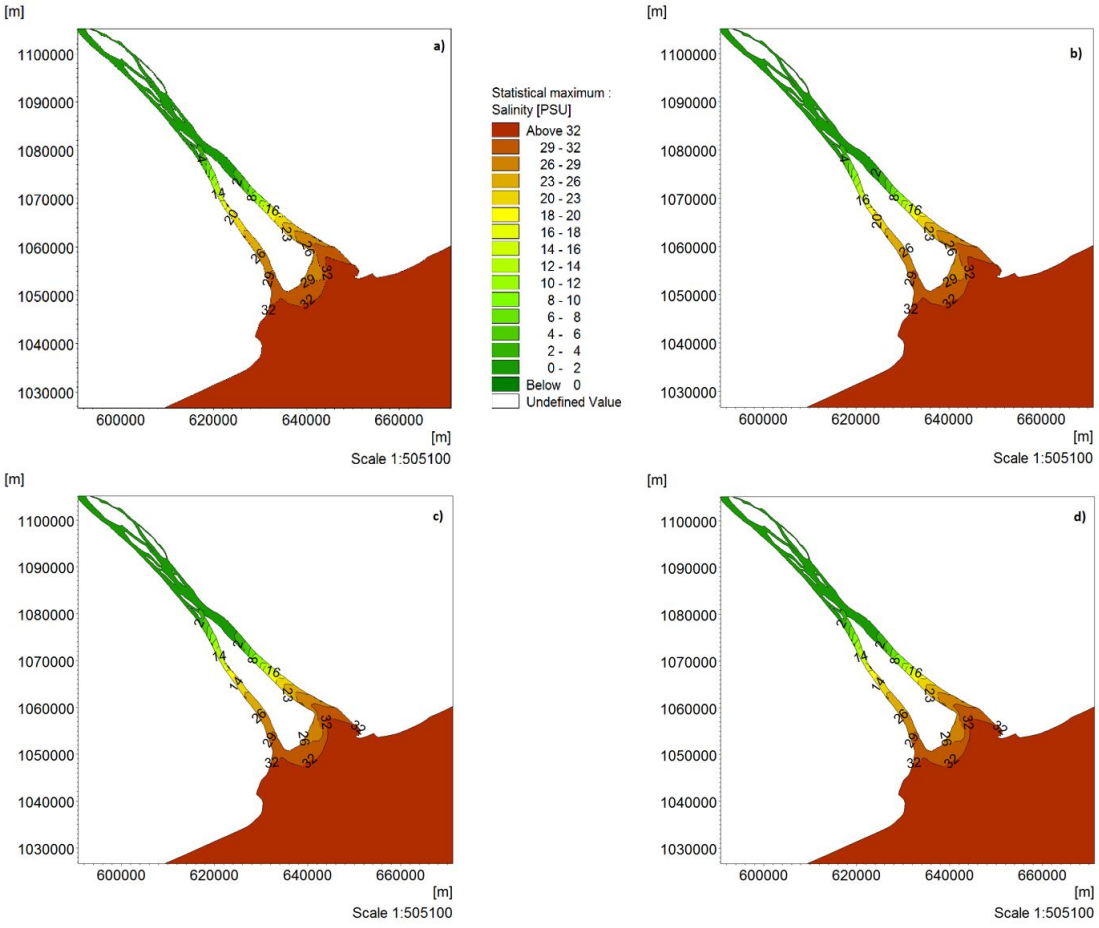

Fig. 5.40 Maximum salinity level across the modelling domain under for four scenarios

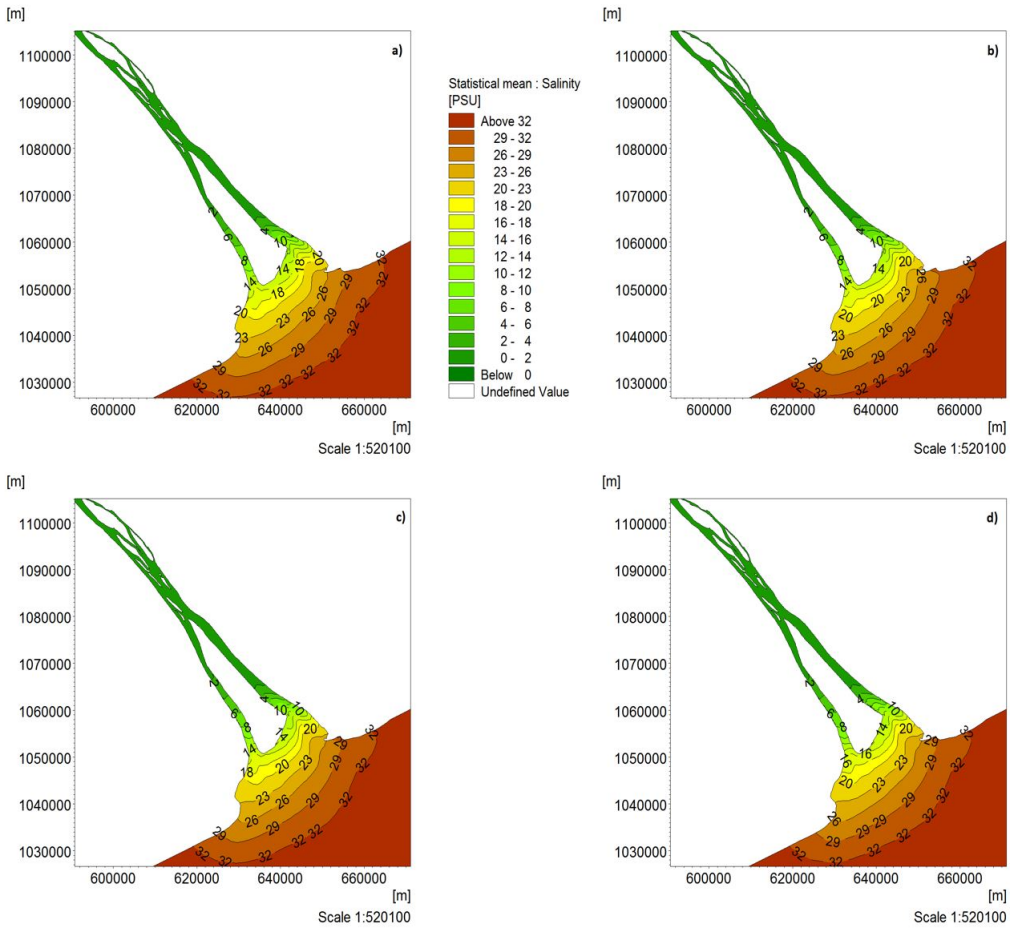

Fig. 5.41 Mean salinity distribution across the modelling domain under for four scenarios

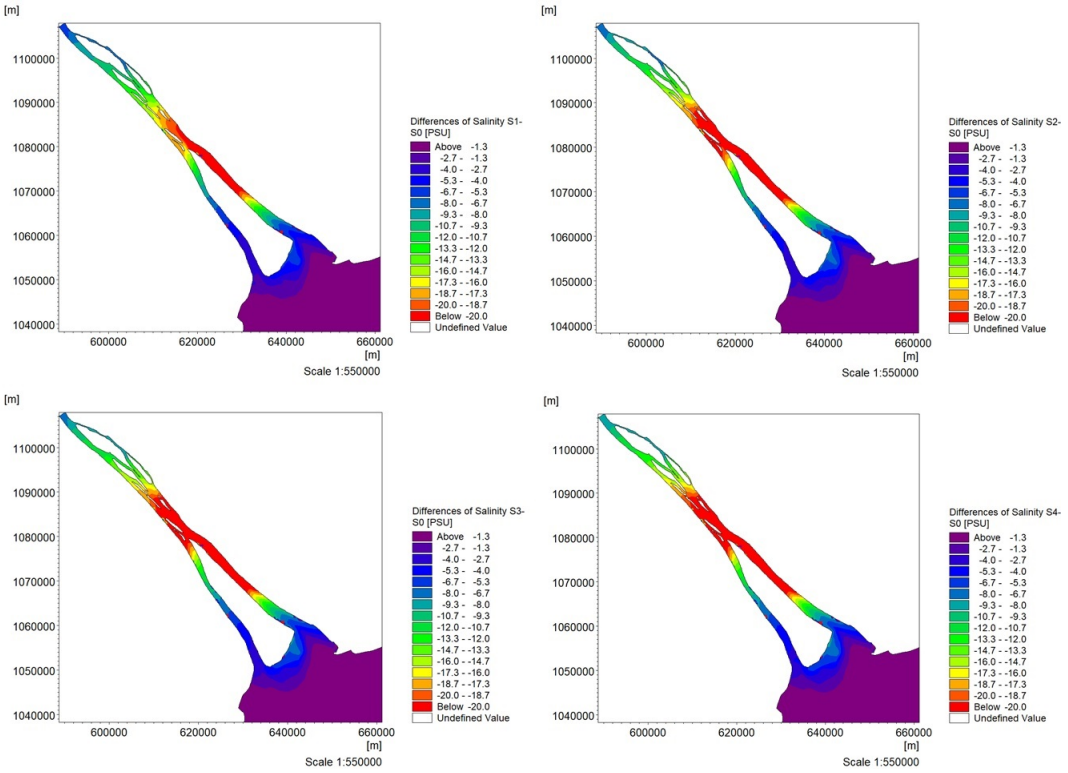

Fig. 5.42 The difference of max salinity distribution of four scenarios compared with baseline

5.5.4.2 Changes in salt intrusion length

We further assessed the changes in salinity intrusion length under the four future scenarios. The salinity intrusion length is defined as the distance from the estuary mouth to the location upstream with mean salinity at the cross section. There are three types of intrusion length: intrusion length at low water slack, intrusion length at high water slack, and tidal average intrusion length, which is considered to be an average of low and high (Vd Burgh, 1972; Savenije, 1993and Prandle, 2004). The salinity intrusion length is defined in this study as the distance from the Hau River mouth to the upstream limit location where the bottom salinity level drops down to a certain threshold, e.g., 1 PSU or 4 PSU. Figure 5.42 presents salinity distribution along the river for four scenarios, under spring tide and neap tide. Table 5.30 shows that the salinity intrusion lengths under spring tide are larger than those under neap tide. By comparing the baseline to the four scenarios, it can be seen that the intrusion lengths for all scenarios are consistently farther than that of the baseline. In Scenario 1, river discharge increases by 10% at Kratie, and therefore the inflow at Can Tho is also slightly higher than the other scenarios. This explains the difference in salinity intrusion length

between the baseline and Scenario 1. For Scenarios 2, 3 and 4, (with sea level rises of 23 cm, 35 cm and 35 cm, respectively) the differences in salinity intrusion lengths between the baseline and these three scenarios are relatively small. In essence, the results show that upstream discharge changes do not substantially affect salinity intrusion lengths, in contrast to the more dominant impacts of tidal regime.

Under sea level rise scenarios, salinity intrusion length in the Hau River would increase between 3.29 and 3.92 km (for 1.0 PSU salinity level) compared to the baseline in the spring tide condition. During neap tide, this length ranges between 4.36 and 4.65 km for the 1.0 PSU salinity level (Table 5.30). Scenario 4 shows the longest salinity intrusion length for spring and neap tide (Table 5.31) for both 1.0 PSU and 4.0 PSU isohaline. Such variation in the magnitude of salinity intrusion length is caused by changes in the stratification of the estuary. As the sea level rises, the river depth increases and the horizontal gradient of salinity changes, resulting in increased estuarine circulation. The model simulations indicate that the location of 4 PSU isohaline would migrate up from 43.58 to 44.27 km if sea level rises from 23 to 35 cm and the upstream discharges change from +10% to -20% at Kratie.

Our findings about increasing salinity intrusion length are in line with observed data, which confirms that when river discharge reduces in the Hau River, saline water moves upstream to Can Tho (Trieu and Phong, 2015, Williams, 1986). Any increase in the magnitude or duration of salinity intrusion at the location of the irrigation water intake would likely affect crop yield and aquaculture in Mekong Delta.

Table 5.30 The distance from the mouth river for different scenarios

Scenarios	Distance from the mouth (km)			
	Spring tide		Neap tide	
	1.0 PSU	4.0 PSU	1.0 PSU	4.0 PSU
Baseline	45.26	41.46	25.49	20.13
Scenario 1	48.55	43.58	29.85	22.03
Scenario 2	49.13	44.05	30.44	23.01
Scenario 3	49.16	44.17	30.07	22.48
Scenario 4	49.18	44.27	30.14	22.59

Table 5.31 The relative change of saline intrusion for four scenarios compared to baseline

Scenarios	Relative changes of saline intrusion (km)			
	Spring tide		Neap tide	
	1.0 PSU	4.0 PSU	1.0 PSU	4.0 PSU
Scenario 1	3.29	2.12	4.36	1.90
Scenario 2	3.87	2.59	4.95	2.88
Scenario 3	3.90	2.71	4.58	2.35
Scenario 4	3.92	2.81	4.65	2.46

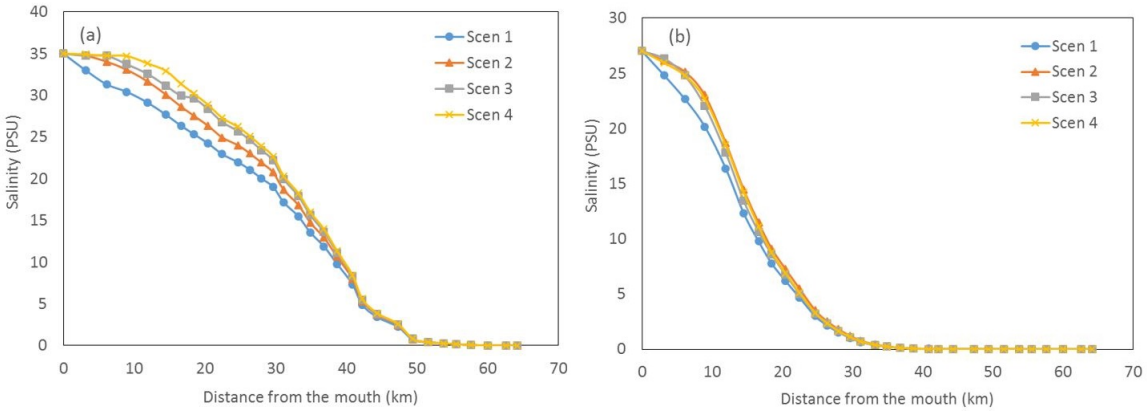

Fig. 5.43 Salinity distribution at center line of cross-section along river from the mouth to upstream (a) spring tide and (b) neap tide

5.5.4.3 Changes in flushing time

To examine the effect of river discharge changes on the temporal dynamics of salinity intrusion in the Hau River, we calculate flushing time with varying discharge conditions for baseline and four future scenarios. Flushing time is defined as the time required to replace the existing saltwater in the estuary using inflows at certain discharge levels (Dyer, 1973; Williams, 1986).To calculate the flushing time in the estuary, different freshwater discharges were selected based on maximum and minimum discharges from the dry season in 2011, with a range of 400 to 4500 m^3/s. The simulated flushing times for the baseline and the four scenarios were calculated and are presented for different discharge values in Figure 5.44.

The flushing time varies considerably under all considered scenarios, ranging between 10 h (at discharge 4500 m3/s) and 109 h (at discharge 400 m^3/s). For the most extreme scenario

(i.e., Scenario 4), flushing time varies within a range from 20.7 h to 182 h. The results also indicate that, for high flow, the flushing time under Scenario 1 is lower than under baseline conditions, while Scenarios 2, 3 and 4 consistently exhibit longer flushing time than the baseline. Longer flushing time caused by reducing discharges means that it would require a higher volume of freshwater to push saltwater back to the river mouth in the future.

Reductions in river discharge also cause the salinity boundary to move further upstream (Fig. 5.42). Salinity deceases substantially when river discharge increases, and as a result the salinity intrusion boundary migrates farther downstream. As freshwater discharge increases from 400 to 4500 m^3/s with different sea levels, the flushing time reduces significantly from 87.72 h to 10 h for Scenario 1, and 150 h to 20.7 h for Scenario 4.

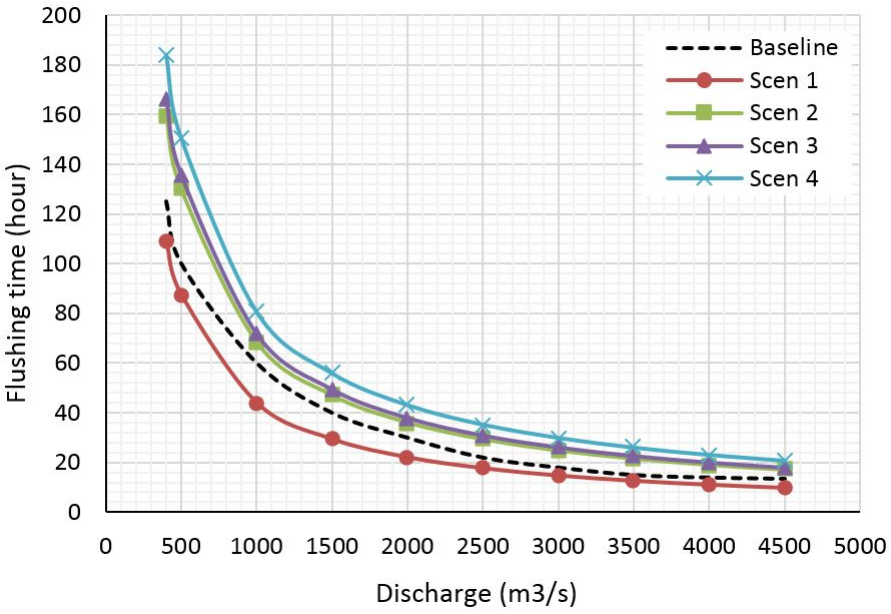

Fig. 5.44 Estimated flushing time and flow rate (Q, m^3/s) for four scenarios

5.5.4.4 Uncertainties, limitations and further research

The hydraulic models, including 1D-MIKE 11 and 2D-MIKE 21 HD and TR used in this study, entail limitations and assumptions. These limitations and assumptions exist in both the data and modelling approach. The major data used in this study were predicted river discharge, rainfall scenarios under climate change, and sea level rise. The climate change and sea level rise scenarios used in this study were obtained from different sources, such as GCMs outputs, SRHMC and SIWRR, and therefore our results might be subjected to errors caused by data inconsistencies. However, we implemented quality checks on our input data

and controlled for inconsistencies. Additionally, we acknowledge that climate change is a non-stationary and dynamic process; while the projected salinity intrusion from upstream discharge changes, rainfall and sea level rise alterations were treated in this study as part of a steady-state system. That means we assume that the relationship between these driving factors are also valid in the future and did not include their interrelations in the simulations. This assumption could lead to biases in future discharge and rainfall estimates, which in turn result in uncertainties in the simulated salinity intrusion. However, we think that the hydraulic and salinity dynamics in the Hau River of the Mekong Delta are primarily driven by changes in the considered driving factors and their interrelations play marginal roles. Therefore, the developed modelling approaches are useful and applicable for our modelling purposes.

Furthermore, we employed a two-step modelling procedure (see Section 3—Methodology and Model setup) for assessing changes in salinity intrusion in the Mekong Delta. A 1D model was applied to simulate delta-wide hydrodynamic conditions (i.e., discharge and water level), thereby providing boundary conditions for the more detailed hydrodynamic and salinity simulation with the 2D-MIKE 21 model. While the current data availability and computational capacity does not allow for detailed 2D simulation for the whole Mekong Delta domain, we suggest gradually increasing the domain size to cover larger areas in future studies. Last but not least, while our calibrated parameter set yields realistic simulation results for the current state of the delta system (i.e., 2010–2011), we did not consider changing delta settings and its hydraulic characteristics in the future. Therefore, we suggest focusing on this topic in future studies.

Chapter 6

Conclusions

6.1 Summary and results

The aim of this study was to expan on the knowledge of climate change impact on hydraulic regime and salinity intrusion on Hau River, Vietnamese Mekong delta. The objectives of this research were formulated as: (i) to forecast the amount of future rainfall in the study area under climate change conditions with different scenarios from 5 GCMs outputs; (ii) to develop a new model of Artificial Neural Network (ANN) and Recurrent neural network – Long short term memory (LSTM) for predicting rainfall and runoff; (iii) to apply 1D-MIKE 11 to simulate the total volume of rainfall at the VMD and the effect of discharge from Kratie station as the sources and sinks in MIKE 21 input; (iv) to apply 2D-MIKE 21 model to simulate hydraulic regime and salinity intrusion in the Hau river under different scenarios; and (v) to simulate fresh and salt water balance based on sea level rise and upstream water level scenarios. With the results presented in the previous chapters, these objectives have been met. As a result, a number of conclusions and recommendations have been formulated, which are presented below:

1) The Vietnamese Mekong River Basin is highly vulnerable to climate change, however its impacts together with the impacts of the upstream hydrological variabilities remains a challenge. In the present work, we attempted to deal with part of these challenges to provide more understanding the hydrological and hydraulic response of delta. This was done by conducting hydrodynamic modelling, using a combination of climate projection from five GCMs, two RCP scenarios, and four different discharge scenarios of upstream inflow variabilities. The possible alterations of future hydraulic regimes in the delta were predicted to show that negative consequences like shortage of water resources and salinity intrusion

are inevitable.

Our finding proved that climate change will most likely increase precipitation in the rainy season, for all GCM outputs within two time periods (1978–2001 vs. 2036–2065). Nevertheless, the ranges between GCMs are relatively large, depending not only on individual GCMs but also on RCP scenarios and considered locations. Moreover, among the two RCP scenarios applied, RCP4.5 and RCP8.5, there are significant variabilities in downscaled results and in bias correction of precipitation from five GCMs. In general, all precipitation projections of GCMs show similar trends of increasing precipitation in wet seasons and a decrease in dry seasons. To some extent, however, even the precipitation forecasting of a few GCMs remains uncertain. That means there is a certain degree of confidence in prediction that the VMD will suffer more droughts in dry seasons and higher floods in rainy seasons. Therefore, to reduce uncertainties, it is important to apply GCMs and RCP ensembles for assessing possible climate change impacts on the VMD hydraulic regime.

Our study also shows that the upstream flow condition in four considered scenarios is a driving force behind the changes in the hydraulic regime, whereas a sea level rise of 23 cm will have a smaller impact. Among the four considered scenarios of inflow, precipitation changes and sea level rise, we found that the simulated discharges at four main stations of the VMD change substantially, ranging from -2.45% to -100.21%. Furthermore, the predicted seasonal discharges show a remarkable reduction in the dry season in all scenarios. The calculated wet season discharges reduce significantly for scenarios 2, 3 and 4, but not for scenario 1.

This assessment of the impact of upstream flow alterations, climate change, and sea level rise on the VMD contribute a better understanding of the current and future hydraulic regime of the basin. Consequently, results from this study could be used as boundary conditions for further investigating the impact of climate change on salinity intrusion in Tien and Hau Rivers using a suitable 2D model. The results of such study could be useful to advance the currently limited body of knowledge about the saline distribution variation in the VMD.

2) The combination of 1D-MIKE 11 and 2D-MIKE 21 hydrodynamic (HD) and salt transport models (TR) was established to simulate the hydrodynamics and salinity distributions in the Hau (Bassac) River estuary of the Mekong delta in Southern Vietnam. The model was calibrated and verified using observational water level and salinity distribution

and tidal amplitudes from 2010 to 2011. The model simulation results agree well with the field observations during calibration and validation periods. The calibrated model was used to simulate future salinity intrusion to identify the potential impacts of upstream discharges, rainfall variabilities and sea level rise on salinity intrusion length and transport time scales including flushing time. The model results indicate that salinity intrusion moves farther upstream by 4855, 4913, 4916 and 4918 m from scenario one to four for the period of 2036 – 2065, respectively. The flushing time is between 125 hours and 13.5 hours under the baseline condition, and between about 180 hours and 10 hours under the four scenarios (equal to 7.5 days and half of day). We found that the flushing time for scenario 4 is higher in comparison to the other scenarios and the baseline, while the flushing time for scenario 1 is lowest under both low and high flow conditions. It will be more difficult to re-establish the freshwater condition in the estuary in the future due to salinity intrusion. Particularly for scenario 4, the flushing time required to replace saltwater with freshwater at the estuaries tend to increase between 7.27 hours for maximum discharge of 4500 m^3/s and 58.95 hours (more 2.5 days) for discharge of 400 m^3/s. We found that upstream discharge changes, rainfall alterations and sea level rise, not only affects salinity intrusion, but also induce changes in the upstream flows from Kratie and the required time to flush the saltwater out to the sea. Sea level rise would alter the location of the river estuary, thereby causing a change in marine diversity in the ecological system. Sea level rise would move the hydraulic regime backward, changing the habitats of fishing communities in the estuarine system, please add consequences for agriculture and freshwater supply. Increasing salinization along the Hau River will have detrimental consequences for crop production, freshwater supplies and freshwater ecosystems, requiring timely countermeasures. Moreover, Vietnamese Mekong delta in general and Hau River will be extremely vulnerable to climate change impacts and sea level rise because of low lying topography. It was found that the vulnerability of assets in the Mekong delta differ widely from economic sectors (agriculture sector to industry and service) and there is urgency to adapt with climate change and salinity intrusion.

2) An attempt was made in this thesis to investigate the use of the LSTM model for predicting the daily rainfall – runoff at the Chau Doc and Can Tho stations, Vietnamese Mekong River. To achieve this aim, the Python programming language was utilized to construct LSTM models using the Adam optimizer algorithm, and the MATLAB tool box was used to build ANN models based on the LM learning algorithms. Comparisons of the predicted results indicated that the models trained with the LSTM and ANN models were comparable in terms of accuracy and efficiency and they had great ability for predicting the daily rainfall

– runoff. To build the best possible ANN and LSTM models, six input combinations were tested for each model. The results show that the LSTM model performed better for discharge prediction than those predicted by the ANN model in the Can Tho station, especially on the peaks. For the high discharge values in this station, the results obtained by the LSTM model were closer to the 45°straight line in the scatter plots. The results for the Chau Doc stations were close to each other while the ANN model provided slightly better predictions. Moreover, the obtained results of MAPE indicated that for the most input combinations, ANN yielded lower values compared to LSTM, however the differences between the two models were small and both models had an acceptable performance index. Finally, it can be concluded that both models in this study showed good performance in rainfall – runoff prediction and can be used as alternatives to improve the prediction of hydrological data.

3) A new time-series prediction model has been proposed in this study that applies state of the art model – LSTM and compares the model efficiency with Seasonal Artificial Neural Network (SANN) and Artificial Neural Network (ANN). The new model has been validated with monthly rainfall data from Ca Mau rain gauges, located in the South of Vietnam. The model has been developed using MATLAB (Matrix Laboratory) based on its Levenberg-Marquardt algorithm. The LSTM model was implemented in Python. In comparison to ANN and SANN results, the validation results of LSTM indicated it has best performance in predicting monthly rainfall. Compared to other methods such as ANN and SANN, the LSTM show the ability to forecast sequential data per several statistical tests. It was also found that the LSTM model had very good accuracy in monthly rainfall data. Based on this combination, the estimated value of correlation coefficient (R), the root mean square error (RMSE), and the mean absolute error (MAE) were 0.989, 24.150 (mm) and 17.315 (mm), respectively, which is better than ANN and SANN in terms of statistical performance. Finally, LSTM is a promising model in hydro-meteorological and climatic applications for estimating more realistic precipitation forecasts.

6.2 Recommendation and further work

This research is to assess the response of hydraulics and salinity intrusion circumstance in Hau River estuary by the effect of the upstream discharge boundary, climate change related to changing precipitation, and sea level rise. It is suggested to take into account environmental, social and economic impact assessments, further study should be considered to assess all

relevant factors, including hydrology, ecosystems and anthropogenic activities.

The purpose of this study is to create different scenarios using the predicted discharge at Kratie given by Lauri et al., 2012 without new updated simulations of the upper hydrological regime for current and future conditions. It is recommended that the discharge scenarios at Kratie station should be calculated based on simulations for the upper Mekong delta with different updated climate change scenarios and future hydrology conditions.

There are several kinds of uncertainty in this study consisting of (i) insufficient meteorological and hydraulic data, (ii) coarse resolution in GCM models and drawback of statistical downscaling technique, (iii) the disadvantages of bias correction methods (iv) approximation of the hydrodynamic model and model structure, parametrization (v) future land cover and land use changes are not taken into account in this study. To solve five main problems as mentioned, extensive efforts in hydraulic study, climate change and hydrodynamic modelling should be developed in long term not only in water resources engineering but also in meteorological and climate change study.

Increasing the number of meteorological observation stations, continous measurements and smaller time steps significantly contribute to the accuracy of the modelling simulations. It is therefore recommended to extend data collection to include additional meteorological observation and stream flow data so the model can achieve better predictability. Improving the forecasted capacity of GCM model with higher horizontal resolution is a crucial task for the hydrological and meteorological community around the world.

The greatest obstacle in climate change study is the selection and combination of downscaling methods and RCP scenarios because this contributes largely uncertainty to model results. Therefore, it is recommended that the ensemble approach is a priority with a combination of different climate change scenarios, statistical downscaling methods and various bias correction techniques to account for all possible climate change effect on hydraulic and water resource assessments.

References

Abbott, Me B and F Ionescu (1967). "On the numerical computation of nearly horizontal flows". In: *Journal of Hydraulic Research* 5.2, pp. 97–117.

Abebe, AJ and RK Price (2003). "Managing uncertainty in hydrological models using complementary models". In: *Hydrological sciences journal* 48.5, pp. 679–692.

Abrahart, Robert J, Linda See, and Pauline E Kneale (2001). "Investigating the role of saliency analysis with a neural network rainfall-runoff model". In: *Computers & Geosciences* 27.8, pp. 921–928.

Ailliot, Pierre, Craig Thompson, and Peter Thomson (2009). "Space–time modelling of precipitation by using a hidden Markov model and censored Gaussian distributions". In: *Journal of the Royal Statistical Society: Series C (Applied Statistics)* 58.3, pp. 405–426.

Altun, H., A. Bilgil, and B.C. Fidan (2007). "Treatment of multi-dimensional data to enhance neural network estimators in regression problems". In: *Expert Systems with Applications* 32.2, pp. 599–605.

Anandhi, Aavudai, VV Srinivas, Ravi S Nanjundiah, and D Nagesh Kumar (2008). "Downscaling precipitation to river basin in India for IPCC SRES scenarios using support vector machine". In: *International Journal of Climatology* 28.3, pp. 401–420.

Anandhi, Aavudai, Allan Frei, Donald C Pierson, Elliot M Schneiderman, Mark S Zion, David Lounsbury, and Adao H Matonse (2011). "Examination of change factor methodologies for climate change impact assessment". In: *Water Resources Research* 47.3.

Anctil, François, Charles Perrin, and Vazken Andréassian (2004). "Impact of the length of observed records on the performance of ANN and of conceptual parsimonious rainfall-runoff forecasting models". In: *Environmental Modelling & Software* 19.4, pp. 357–368.

Andersen, Ole B and Per Knudsen (2009). "DNSC08 mean sea surface and mean dynamic topography models". In: *Journal of Geophysical Research: Oceans* 114.C11.

Araghinejad, Shahab (2013). *Data-driven modeling: using MATLAB® in water resources and environmental engineering*. Vol. 67. Springer Science & Business Media.

Arnell, Nigel W (1992). "Factors controlling the effects of climate change on river flow regimes in a humid temperate environment". In: *Journal of hydrology* 132.1-4, pp. 321–342.

Arnell, NW and NS Reynard (1996). "The effects of climate change due to global warming on river flows in Great Britain". In: *Journal of hydrology* 183.3-4, pp. 397–424.

Bardossy, A, I Bogardi, and I Matyasovszky (2005). "Fuzzy rule-based downscaling of precipitation". In: *Theoretical and Applied Climatology* 82.1-2, pp. 119–129.

Bardossy, A and HJ Caspary (1990). "Detection of climate change in Europe by analyzing European atmospheric circulation patterns from 1881 to 1989". In: *Theoretical and Applied Climatology* 42.3, pp. 155–167.

Bárdossy, András, Jiri Stehlík, and Hans-Joachim Caspary (2002). "Automated objective classification of daily circulation patterns for precipitation and temperature downscaling based on optimized fuzzy rules". In: *Climate Research* 23.1, pp. 11–22.

Bardossy, Andras and Jan MC Van Mierlo (2000). "Regional precipitation and temperature scenarios for climate change". In: *Hydrological Sciences Journal* 45.4, pp. 559–575.

Basheer, Amir K, Haishen Lu, Abubaker Omer, Abubaker B Ali, and Abdeldime MS Abdelgader (2016). "Impacts of climate change under CMIP5 RCP scenarios on the streamflow in the Dinder River and ecosystem habitats in Dinder National Park, Sudan". In: *Hydrology and Earth System Sciences* 20.4, p. 1331.

Beckmann, Björn-R and T Adri Buishand (2002). "Statistical downscaling relationships for precipitation in the Netherlands and North Germany". In: *International Journal of Climatology* 22.1, pp. 15–32.

Bergström, Sten, Bengt Carlsson, Marie Gardelin, Göran Lindström, Anna Pettersson, and Markku Rummukainen (2001). "Climate change impacts on runoff in Sweden—assessments by global climate models, dynamical downscaling and hydrological modelling". In: *Climate research* 16.2, pp. 101–112.

Bernstein, Lenny et al. (2007). "Climate change 2007: Synthesis report. Contribution of Working Groups I, II and III to the fourth assessment report of the Intergovernmental Panel on Climate Change". In: *IPCC: Geneva, Switzerland*.

Bhattacharya, B, RK Price, and DP Solomatine (2007). "Machine learning approach to modeling sediment transport". In: *Journal of Hydraulic Engineering* 133.4, pp. 440–450.

Bhuiyan, Md Jabed Abdul Naser and Dushmanta Dutta (2012). "Assessing impacts of sea level rise on river salinity in the Gorai river network, Bangladesh". In: *Estuarine, Coastal and Shelf Science* 96, pp. 219–227.

Block, Paul J, Francisco Assis Souza Filho, Liqiang Sun, and Hyun-Han Kwon (2009). "A streamflow forecasting framework using multiple climate and hydrological models". In: *JAWRA Journal of the American Water Resources Association* 45.4, pp. 828–843.

Boicourt, William C (1992). "Influences of circulation processes on dissolved oxygen in the Chesapeake Bay". In:

Bosshard, T, S Kotlarski, T Ewen, and C Schär (2011). "Spectral representation of the annual cycle in the climate change signal". In: *Hydrology and Earth System Sciences* 15.9, p. 2777.

Bui, Minh Duc, Keivan Kaveh, Petr Penz, and Peter Rutschmann (2015). "Contraction scour estimation using data-driven methods". In: *Journal of Applied Water Engineering and Research* 3.2, pp. 143–156.

Bürger, Gerd (1996). "Expanded downscaling for generating local weather scenarios". In: *Climate Research*, pp. 111–128.

Burton, A, CG Kilsby, HJ Fowler, PSP Cowpertwait, and PE O'Connell (2008). "RainSim: A spatial–temporal stochastic rainfall modelling system". In: *Environmental Modelling & Software* 23.12, pp. 1356–1369.

Busuioc, Aristita, Deliang Chen, and Cecilia Hellström (2001). "Performance of statistical downscaling models in GCM validation and regional climate change estimates: application for Swedish precipitation". In: *International Journal of Climatology* 21.5, pp. 557–578.

Cameron, WM and DW Pritchard (1963). "Estuaries (306–324)". In: *The Sea* 2.

Carew-Reid, Jeremy (2008). "Rapid assessment of the extent and impact of sea level rise in Viet Nam". In: *International Centre for Environment Management (ICEM), Brisbane* 82.

Cavazos, Tereza and Bruce C Hewitson (2005). "Performance of NCEP–NCAR reanalysis variables in statistical downscaling of daily precipitation". In: *Climate Research* 28.2, pp. 95–107.

CGIAR (2016). "Assessment Report: The drought and salinity intrusion in the Mekong River Delta of Vietnam". In: *Research Program on Climate Change, Agriculture and Food Security* 1.1, pp. 1–54.

Chiew, FHS, PH Whetton, TA McMahon, and AB Pittock (1995). "Simulation of the impacts of climate change on runoff and soil moisture in Australian catchments". In: *Journal of Hydrology* 167.1-4, pp. 121–147.

Christensen, J. H. et al. (2007). *Climate Change, 2007: The Physical Science Basis. Contribution of Working group I to the Fourth Assessment Report of the Intergovernmental Panel on Climate Change*, pp. 847–940.

Commission, Mekong River et al. (2010). "Assessment of basin-wide development scenarios–main report". In: *Mekong River Commission (MRC), Vientiane, Lao PDR*.

Costa-Cabral, Mariza C, Jeffrey E Richey, Gopi Goteti, Dennis P Lettenmaier, Christoph Feldkötter, and Anond Snidvongs (2008). "Landscape structure and use, climate, and water movement in the Mekong River basin". In: *Hydrological Processes* 22.12, pp. 1731–1746.

Coulibaly, P, F Anctil, and B Bobee (2000). "Daily reservoir inflow forecasting using artificial neural networks with stopped training approach". In: *Journal of Hydrology* 230.3-4, pp. 244–257.

Dang, Thanh Duc, Thomas A Cochrane, Mauricio E Arias, et al. (2018). "Future hydrological alterations in the Mekong Delta under the impact of water resources development, land subsidence and sea level rise". In: *Journal of Hydrology: Regional Studies* 15, pp. 119–133.

Dasgupta, Susmita, FARHANA AKHTER KAMAL, ZAHIRUL HUQUE KHAN, Sharifuzzaman Choudhury, and Ainun Nishat (2015). "River salinity and climate change: evidence from coastal Bangladesh". In: *WORLD SCIENTIFIC REFERENCE ON ASIA AND THE WORLD ECONOMY*. World Scientific, pp. 205–242.

Dasgupta, Susmita, Benoit Laplante, Craig Meisner, David Wheeler, and Jianping Yan (2009). "The impact of sea level rise on developing countries: a comparative analysis". In: *Climatic change* 93.3-4, pp. 379–388.

David, Lambkin (2010). "A Review of the Bed Roughness Variable in MIKE 21 FLOW MODEL FM, Hydrodynamic (HD) and Sediment Transport (ST) modules". In:

Dawson, CW and RL Wilby (2001). "Hydrological modelling using artificial neural networks". In: *Progress in physical Geography* 25.1, pp. 80–108.

De, N.N. (2006). "Farmers, agriculture and rural development in the Mekong Delta of Vietnam". In:

De Vos, NJ and THM Rientjes (2005). "Constraints of artificial neural networks for rainfall-runoff modelling: trade-offs in hydrological state representation and model evaluation". In: *Hydrology and Earth System Sciences Discussions* 2.1, pp. 365–415.

Delgado, J.M., B. Merz, and H. Apel (2012). "A climate-flood link for the lower Mekong River". In: *Hydrology and Earth System Sciences* 16.5, p. 1533.

Déqué, Michel et al. (2005). "Global high resolution versus Limited Area Model climate change projections over Europe: quantifying confidence level from PRUDENCE results". In: *Climate Dynamics* 25.6, pp. 653–670.

DHI, MIKE (2007). "A Modelling System for Rivers and Channels. Reference Manual". In: *DHI Water & Environment, Denmark*.

Diaz-Nieto, Jacqueline and Robert L Wilby (2005). "A comparison of statistical downscaling and climate change factor methods: impacts on low flows in the River Thames, United Kingdom". In: *Climatic Change* 69.2-3, pp. 245–268.

Dinh, Quang, S Balica, I Popescu, and A Jonoski (2012). "Climate change impact on flood hazard, vulnerability and risk of the Long Xuyen Quadrangle in the Mekong Delta". In: *International journal of river basin management* 10.1, pp. 103–120.

Doan, Quang Tri, Cao Don Nguyen, Yi Ching Chen, and Kumar Mishra Pawan (2014). "Modeling the influence of river flow and salinity intrusion in the Mekong river estuary, Vietnam". In: *Lowland Technology International* 16.1, pp. 14–25.

Donahue, Jeffrey, Lisa Anne Hendricks, Sergio Guadarrama, Marcus Rohrbach, Subhashini Venugopalan, Kate Saenko, and Trevor Darrell (2015). "Long-term recurrent convolutional networks for visual recognition and description". In: *Proceedings of the IEEE conference on computer vision and pattern recognition*, pp. 2625–2634.

Dung, Nguyen Viet, Bardossy Merz, András Bárdossy, Tang Duc Thang, and Heiko Apel (2011). "Multi-objective automatic calibration of hydrodynamic models utilizing inundation maps and gauge data". In: *Hydrology and Earth System Sciences* 15.4, pp. 1339–1354.

Duy Vinh, Vu, Sylvain Ouillon, Nguyen Van Thao, and Nguyen Ngoc Tien (2016). "Numerical simulations of suspended sediment dynamics due to seasonal forcing in the Mekong coastal area". In: *Water* 8.6, p. 255.

Dyer, Keith R (1973). *Estuaries: a physical introduction*.

Dyer, KR (1997). "Estuaries: A Physical Introduction, Wiley". In: *New York*.

Eastham, Judy, Freddie Mpelasoka, Mohammed Mainuddin, Catherine Ticehurst, Peter Dyce, Geoff Hodgson, Riasat Ali, and Mac Kirby (2008). *Mekong river basin water resources assessment: Impacts of climate change*.

Field, Christopher B et al. (2014). *IPCC, 2014: Climate Change 2014: Impacts, Adaptation, and Vulnerability. Part A: Global and Sectoral Aspects. Contribution of Working Group II to the Fifth Assessment Report of the Intergovernmental Panel on Climate Change*.

Flint, Lorraine E and Alan L Flint (2012). "Downscaling future climate scenarios to fine scales for hydrologic and ecological modeling and analysis". In: *Ecological Processes* 1.1, p. 2.

Fowler, HJ and CG Kilsby (2007). "Using regional climate model data to simulate historical and future river flows in northwest England". In: *Climatic Change* 80.3-4, pp. 337–367.

Fowler, HJ, M Ekström, S Blenkinsop, and AP Smith (2007). "Estimating change in extreme European precipitation using a multimodel ensemble". In: *Journal of Geophysical Research: Atmospheres* 112.D18.

Fowler, HJ, M Ekström, CG Kilsby, and PD Jones (2005). "New estimates of future changes in extreme rainfall across the UK using regional climate model integrations. 1. Assessment of control climate". In: *Journal of Hydrology* 300.1-4, pp. 212–233.

Frei, Christoph, Jens Hesselbjerg Christensen, Michel Déqué, Daniela Jacob, Richard G Jones, and Pier Luigi Vidale (2003). "Daily precipitation statistics in regional climate models: Evaluation and intercomparison for the European Alps". In: *Journal of Geophysical Research: Atmospheres* 108.D3.

Frei, Christoph, Regina Schöll, Sophie Fukutome, Jürg Schmidli, and Pier Luigi Vidale (2006). "Future change of precipitation extremes in Europe: Intercomparison of scenarios from regional climate models". In: *Journal of Geophysical Research: Atmospheres* 111.D6.

Frias, MD, E Zorita, J Fernández, and C Rodriguez-Puebla (2006). "Testing statistical downscaling methods in simulated climates". In: *Geophysical Research Letters* 33.19.

Frost, Andrew J et al. (2011). "A comparison of multi-site daily rainfall downscaling techniques under Australian conditions". In: *Journal of Hydrology* 408.1-2, pp. 1–18.

Gangopadhyay, Subhrendu, Martyn Clark, and Balaji Rajagopalan (2005). "Statistical downscaling using K-nearest neighbors". In: *Water Resources Research* 41.2.

Gates, WL et al. (1996). *Climate models–evaluation*. Cambridge University Press, Cambridge, United Kingdom and New York, NY, USA.

Graham, L Phil, Stefan Hagemann, Simon Jaun, and Martin Beniston (2007). "On interpreting hydrological change from regional climate models". In: *Climatic change* 81.1, pp. 97–122.

Graves, Alex and Navdeep Jaitly (2014). "Towards end-to-end speech recognition with recurrent neural networks". In: *International Conference on Machine Learning*, pp. 1764–1772.

Greene, Arthur M, Andrew W Robertson, and Sergey Kirshner (2008). "Analysis of Indian monsoon daily rainfall on subseasonal to multidecadal time-scales using a hidden Markov model". In: *Quarterly Journal of the Royal Meteorological Society* 134.633, pp. 875–887.

Gupta, Ashim Das (2005). *Challenges and opportunities for integrated water resources management in Mekong river basin*.

Hamzaçebi, Coşkun (2008). "Improving artificial neural networks' performance in seasonal time series forecasting". In: *Information Sciences* 178.23, pp. 4550–4559.

Hansen, Donald V (1965). "Gravitational circulation in straits and estuaries". In: *J. mar. Res.* 23, pp. 104–122.

Hanssen-Bauer, Inger, Eirik J Førland, JE Haugen, and OE Tveito (2003). "Temperature and precipitation scenarios for Norway: comparison of results from dynamical and empirical downscaling". In: *Climate Research* 25.1, pp. 15–27.

Hapuarachchi, Hapu Arachchige Prasantha, Kuniyoshi Takeuchi, Maichun Zhou, Anthony Stuart Kiem, Mikhail Georgievski, Jun Magome, and Hiroshi Ishidaira (2008). "Investigation of the Mekong River basin hydrology for 1980–2000 using the YHyM". In: *Hydrological processes* 22.9, pp. 1246–1256.

Hasson, Shabeh ul, Salvatore Pascale, Valerio Lucarini, and Jürgen Böhner (2016). "Seasonal cycle of precipitation over major river basins in South and Southeast Asia: A review of the CMIP5 climate models data for present climate and future climate projections". In: *Atmospheric Research* 180, pp. 42 –63. ISSN: 0169-8095.

Haykin, Simon (1994). *Neural networks, a comprehensive foundation*. Tech. rep. Macmilan.

Haylock, Malcolm R, Gavin C Cawley, Colin Harpham, Rob L Wilby, and Clare M Goodess (2006). "Downscaling heavy precipitation over the United Kingdom: a comparison of dynamical and statistical methods and their future scenarios". In: *International Journal of Climatology* 26.10, pp. 1397–1415.

Hellström, Cecilia and Deliang Chen (2003). "Statistical downscaling based on dynamically downscaled predictors: application to monthly precipitation in Sweden". In: *Advances in Atmospheric Sciences* 20.6, pp. 951–958.

Hewitson, BC and RG Crane (2002). "Self-organizing maps: applications to synoptic climatology". In: *Climate Research* 22.1, pp. 13–26.

Hewitson, Bruce C (1999). *Deriving regional precipitation scenarios from general circulation models*. Water Research Commission.

Hoang, L. P., H. Lauri, M. Kummu, J. Koponen, M. T. H. van Vliet, I. Supit, R. Leemans, P. Kabat, and F. Ludwig (2016). "Mekong River flow and hydrological extremes under

climate change". In: *Hydrology and Earth System Sciences* 20.7, pp. 3027–3041. DOI: 10.5194/hess-20-3027-2016. URL: https://www.hydrol-earth-syst-sci.net/20/3027/2016/.

Hoanh, Chu Thai, Kittipong Jirayoot, Guillaume Lacombe, Vithet Srinetr, et al. (2010). *Impacts of climate change and development on Mekong flow regimes. First assessment-2009*. Tech. rep. International Water Management Institute.

Hochreiter, Sepp and Jürgen Schmidhuber (1997). "Long short-term memory". In: *Neural computation* 9.8, pp. 1735–1780.

Hornik, Kurt, Maxwell Stinchcombe, and Halbert White (1989). "Multilayer feedforward networks are universal approximators". In: *Neural networks* 2.5, pp. 359–366.

Houghton, John Theodore, YDJG Ding, David J Griggs, Maria Noguer, Paul J van der Linden, Xiaosu Dai, Kathy Maskell, and CA Johnson (2001). *Climate change 2001: the scientific basis*. The Press Syndicate of the University of Cambridge.

Hu, Tiesong, Fengyan Wu, and Xiang Zhang (2007). "Rainfall–runoff modeling using principal component analysis and neural network". In: *Hydrology Research* 38.3, pp. 235–248.

Huang, Yong, Fengyou Wang, Yi Li, and Tijiu Cai (2014). "Multi-model ensemble simulation and projection in the climate change in the Mekong River Basin. Part I: temperature". In: *Environmental monitoring and assessment* 186.11, pp. 7513–7523.

Hughes, James P and Peter Guttorp (1994). "A class of stochastic models for relating synoptic atmospheric patterns to regional hydrologic phenomena". In: *Water resources research* 30.5, pp. 1535–1546.

Hughes, James P, Peter Guttorp, and Stephen P Charles (1999). "A non-homogeneous hidden Markov model for precipitation occurrence". In: *Journal of the Royal Statistical Society: Series C (Applied Statistics)* 48.1, pp. 15–30.

Huth, Radan (1999). "Statistical downscaling in central Europe: evaluation of methods and potential predictors". In: *Climate Research* 13.2, pp. 91–101.

Huu-Thoi, Nguyen and Ashim Das Gupta (2001). "Assessment of Water resources and salinity intrusion in the Mekong Delta". In: *Water international* 26.1, pp. 86–95.

Iizumi, Toshichika and Navin Ramankutty (2015). "How do weather and climate influence cropping area and intensity?" In: *Global Food Security* 4, pp. 46–50.

Jain, Ashu and Sanaga Srinivasulu (2006). "Integrated approach to model decomposed flow hydrograph using artificial neural network and conceptual techniques". In: *Journal of Hydrology* 317.3-4, pp. 291–306.

Jeong, Dae-Il and Young-Oh Kim (2005). "Rainfall-runoff models using artificial neural networks for ensemble streamflow prediction". In: *Hydrological processes* 19.19, pp. 3819–3835.

Jeong, Dae Il, André St-Hilaire, Taha BMJ Ouarda, and Philippe Gachon (2013). "A multi-site statistical downscaling model for daily precipitation using global scale GCM precipitation outputs". In: *International Journal of Climatology* 33.10, pp. 2431–2447.

Jeong, DI, A St-Hilaire, TBMJ Ouarda, and P Gachon (2012). "Multisite statistical downscaling model for daily precipitation combined by multivariate multiple linear regression and stochastic weather generator". In: *Climatic Change* 114.3-4, pp. 567–591.

Johnston, Robyn and Matti Kummu (2012). "Water resource models in the Mekong Basin: a review". In: *Water Resources Management* 26.2, pp. 429–455.

Jones, PD, M Hulme, and KR Briffa (1993). "A comparison of Lamb circulation types with an objective classification scheme". In: *International Journal of Climatology* 13.6, pp. 655–663.

Karl, Thomas R, Wei-Chyung Wang, Michael E Schlesinger, Richard W Knight, and David Portman (1990). "A method of relating general circulation model simulated climate to the observed local climate. Part I: Seasonal statistics". In: *Journal of Climate* 3.10, pp. 1053–1079.

Kaveh, Keivan, Minh Duc Bui, and Peter Rutschmann (2017). "A comparative study of three different learning algorithms applied to ANFIS for predicting daily suspended sediment concentration". In: *International Journal of Sediment Research* 32.3, pp. 340–350.

Keskinen, M, S Chinvanno, M Kummu, P Nuorteva, A Snidvongs, O Varis, and K Västilä (2010). "Climate change and water resources in the Lower Mekong River Basin: putting adaptation into the context". In: *Journal of Water and Climate Change* 1.2, pp. 103–117.

Kidson, John W (2000). "An analysis of New Zealand synoptic types and their use in defining weather regimes". In: *International journal of climatology* 20.3, pp. 299–316.

Kidson, John W and Craig S Thompson (1998). "A comparison of statistical and model-based downscaling techniques for estimating local climate variations". In: *Journal of Climate* 11.4, pp. 735–753.

Kilsby, CG, PD Jones, A Burton, AC Ford, HJ Fowler, C Harpham, P James, A Smith, and RL Wilby (2007). "A daily weather generator for use in climate change studies". In: *Environmental Modelling & Software* 22.12, pp. 1705–1719.

Kilsby, CG, PSP Cowpertwait, PE O'connell, and PD Jones (1998). "Predicting rainfall statistics in England and Wales using atmospheric circulation variables". In: *International Journal of Climatology: A Journal of the Royal Meteorological Society* 18.5, pp. 523–539.

Kingston, DG, Jonathan R Thompson, and Geoff Kite (2011). "Uncertainty in climate change projections of discharge for the Mekong River Basin". In: *Hydrology and Earth System Sciences* 15.5, pp. 1459–1471.

Kuo, Albert Y and Bruce J Neilson (1987). "Hypoxia and salinity in Virginia estuaries". In: *Estuaries* 10.4, pp. 277–283.

Kyselỳ, Jan (2002). "Comparison of extremes in GCM-simulated, downscaled and observed central-European temperature series". In: *Climate Research* 20.3, pp. 211–222.

Lamberts, Dirk and Jorma Koponen (2008). "Flood pulse alterations and productivity of the Tonle Sap ecosystem: a model for impact assessment". In: *AMBIO: A Journal of the Human Environment* 37.3, pp. 178–184.

Lauff, G. H. (1967). *Estuary*. Am. Assoc. Adv. Sci. Pub.88, 757p.

Lauri, H., H. de Moel, P. J. Ward, T. A. Räsänen, M. Keskinen, and M. Kummu (2012). "Future changes in Mekong River hydrology: impact of climate change and reservoir operation on discharge". In: *Hydrology and Earth System Sciences* 16.12, pp. 4603–4619. DOI: 10.5194/hess-16-4603-2012.

Leander, Robert and T Adri Buishand (2007). "Resampling of regional climate model output for the simulation of extreme river flows". In: *Journal of Hydrology* 332.3-4, pp. 487–496.

Lebel, Louis, Po Garden, and Masao Imamura (2005). "The politics of scale, position, and place in the governance of water resources in the Mekong region". In: *Ecology and society* 10.2, p. 18.

Legates, David R and Gregory J McCabe (1999). "Evaluating the use of "goodness-of-fit" measures in hydrologic and hydroclimatic model validation". In: *Water resources research* 35.1, pp. 233–241.

Lenderink, Geert, Adri Buishand, and W van Deursen (2007). "Estimates of future discharges of the river Rhine using two scenario methodologies: direct versus delta approach". In: *Hydrology and Earth System Sciences* 11.3, pp. 1145–1159.

Leung, L Ruby, Yun Qian, Xindi Bian, Warren M Washington, Jongil Han, and John O Roads (2004). "Mid-century ensemble regional climate change scenarios for the western United States". In: *Climatic Change* 62.1-3, pp. 75–113.

Luk, KC, James E Ball, and Ashish Sharma (2000). "A study of optimal model lag and spatial inputs to artificial neural network for rainfall forecasting". In: *Journal of Hydrology* 227.1-4, pp. 56–65.

Luu, Thi Nguyet Minh, Josette Garnier, Gilles Billen, Didier Orange, Julien Némery, Thi Phuong Quynh Le, Hong Thai Tran, and Lan Anh Le (2010). "Hydrological regime and water budget of the Red River Delta (Northern Vietnam)". In: *Journal of Asian Earth Sciences* 37.3, pp. 219–228.

Machado, Fernando, Miriam Mine, Eloy Kaviski, and Heinz Fill (2011). "Monthly rainfall–runoff modelling using artificial neural networks". In: *Hydrological Sciences Journal–Journal des Sciences Hydrologiques* 56.3, pp. 349–361.

Manh, Nguyen Van, Nguyen Viet Dung, Nguyen Nghia Hung, Bruno Merz, and Heiko Apel (2014). "Large-scale suspended sediment transport and sediment deposition in the Mekong Delta". In: *Hydrology and Earth System Sciences* 18.8, p. 3033.

Manson, GK (2012). *Configuration of Mike21 for the Simulation of Nearshore Storm Waves, Currents and Sediment Transport-Brackley Bight, Prince Edward Island*. Natural Resources Canada, Geological Survey of Canada.

Maraun, Douglas (2016). "Bias correcting climate change simulations-a critical review". In: *Current Climate Change Reports* 2.4, pp. 211–220.

Maraun, Douglas et al. (2017). "Towards process-informed bias correction of climate change simulations". In: *Nature Climate Change* 7.11, p. 764.

Marquez, M, A White, and R Gill (2001). "A hybrid neural network-feature-based manufacturability analysis of mould reinforced plastic parts". In: *Proceedings of the Institution of Mechanical Engineers, Part B: Journal of Engineering Manufacture* 215.8, pp. 1065–1079.

Mehrotra, R and Ashish Sharma (2005). "A nonparametric nonhomogeneous hidden Markov model for downscaling of multisite daily rainfall occurrences". In: *Journal of Geophysical Research: Atmospheres* 110.D16.

MIKE21, DHI and FM MIKE3 Flow Model (2009). "Hydrodynamic and Transport Module Scientific Documentation". In: *Denmark: DHl water & Environment*.

Mitchell, Timothy D and Mike Hulme (1999). "Predicting regional climate change: living with uncertainty". In: *Progress in Physical Geography* 23.1, pp. 57–78.

Modarres, R (2009). "Multi-criteria validation of artificial neural network rainfall-runoff modeling". In: *Hydrology and Earth System Sciences* 13.3, pp. 411–421.

MonRE (2009). "Climate Change, Sea Level Rise Scenarios for Vietnam". In: *Preventionweb*.

MRC (2007a). "Annual Mekong flood report 2006". In: *Mekong River Commission, Vientiane*.

— (2005). "Overview of the Hydrology of the Mekong Basin". In: *Mekong River Commission, Vientiane* 82.

— (2010). *State of the Basin Report 2010*. Mekong River Commission.

— (2007b). *The Flow of the Mekong*. Mekong River Commission.

Murphy, James (1999). "An evaluation of statistical and dynamical techniques for downscaling local climate". In: *Journal of Climate* 12.8, pp. 2256–2284.

Murphy, James et al. (2000). "Predictions of climate change over Europe using statistical and dynamical downscaling techniques". In: *International Journal of Climatology* 20.5, pp. 489–501.

Nash, J Eamonn and Jonh V Sutcliffe (1970). "River flow forecasting through conceptual models part I—A discussion of principles". In: *Journal of hydrology* 10.3, pp. 282–290.

Nguyen, AD and HH Savenije (2006). "Salt intrusion in multi-channel estuaries: a case study in the Mekong Delta, Vietnam". In: *Hydrology and Earth System Sciences Discussions* 10.5, pp. 743–754.

Nguyen, Cong Thanh (2013). "Processes and factors controlling and affecting the retreat of mangrove shorelines in South Vietnam". PhD thesis. Christian-Albrechts Universität Kiel.

Nobi, N and A Das Gupta (1997). "Simulation of regional flow and salinity intrusion in an integrated stream-aquifer system in coastal region: Southwest region of Bangladesh". In: *Groundwater* 35.5, pp. 786–796.

Osborn, Timothy J and Mike Hulme (1998). "Evaluation of the European daily precipitation characteristics from the atmospheric model intercomparison project". In: *International Journal of Climatology* 18.5, pp. 505–522.

Oude Essink, GHP, Esther S Van Baaren, and Perry GB De Louw (2010). "Effects of climate change on coastal groundwater systems: A modeling study in the Netherlands". In: *Water Resources Research* 46.10.

Palutikof, JP, CM Goodess, SJ Watkins, and T Holt (2002). "Generating rainfall and temperature scenarios at multiple sites: examples from the Mediterranean". In: *Journal of Climate* 15.24, pp. 3529–3548.

Pascanu, Razvan, Tomas Mikolov, and Yoshua Bengio (2013). "On the difficulty of training recurrent neural networks". In: *International Conference on Machine Learning*, pp. 1310–1318.

Pech, Sokhem and Kengo Sunada (2008). "Population growth and natural-resources pressures in the Mekong River Basin". In: *AMBIO: A Journal of the Human Environment* 37.3, pp. 219–224.

Piani, C, GP Weedon, M Best, SM Gomes, P Viterbo, S Hagemann, and JO Haerter (2010). "Statistical bias correction of global simulated daily precipitation and temperature for the application of hydrological models". In: *Journal of Hydrology* 395.3-4, pp. 199–215.

Piman, T, T Lennaerts, and P Southalack (2013). "Assessment of hydrological changes in the lower Mekong Basin from Basin-Wide development scenarios". In: *Hydrological Processes* 27.15, pp. 2115–2125.

Prandle, D (2004). "Saline intrusion in partially mixed estuaries". In: *Estuarine, Coastal and Shelf Science* 59.3, pp. 385–397.

Pritchar, D.W (1955). "Estuarine Circulation patterns". In: *the Proceedings of the American Society of Civil Engineers*.

Prudhomme, Christel, Nick Reynard, and Sue Crooks (2002). "Downscaling of global climate models for flood frequency analysis: where are we now?" In: *Hydrological processes* 16.6, pp. 1137–1150.

Rabiner, Lawrence and B.H. Juang (Feb. 1986). "An Introduction to Hidden Markov Models". In:

Rajaee, Taher (2011). "Wavelet and ANN combination model for prediction of daily suspended sediment load in rivers". In: *Science of the total environment* 409.15, pp. 2917–2928.

Raje, Deepashree and PP Mujumdar (2011). "A comparison of three methods for downscaling daily precipitation in the Punjab region". In: *Hydrological Processes* 25.23, pp. 3575–3589.

Raje, Deepashree and PP Mujumdar (2009). "A conditional random field–based downscaling method for assessment of climate change impact on multisite daily precipitation in the Mahanadi basin". In: *Water Resources Research* 45.10.

Riahi, Keywan, Shilpa Rao, Volker Krey, Cheolhung Cho, Vadim Chirkov, Guenther Fischer, Georg Kindermann, Nebojsa Nakicenovic, and Peter Rafaj (2011). "RCP 8.5—A scenario of comparatively high greenhouse gas emissions". In: *Climatic Change* 109.1-2, p. 33.

Salathé, Eric P (2005). "Downscaling simulations of future global climate with application to hydrologic modelling". In: *International Journal of Climatology* 25.4, pp. 419–436.

Savenije, Hubert HG (1993). "Predictive model for salt intrusion in estuaries". In: *Journal of Hydrology* 148.1-4, pp. 203–218.

Schmidli, Jürg, Christoph Frei, and Pier Luigi Vidale (2006). "Downscaling from GCM precipitation: a benchmark for dynamical and statistical downscaling methods". In: *International journal of climatology* 26.5, pp. 679–689.

Schmitz, Jones E, Roger J Zemp, and Mário J Mendes (2006). "Artificial neural networks for the solution of the phase stability problem". In: *Fluid Phase Equilibria* 245.1, pp. 83–87.

Schoof, Justin T, SC Pryor, and SM Robeson (2007). "Downscaling daily maximum and minimum temperatures in the midwestern USA: a hybrid empirical approach". In: *International Journal of Climatology* 27.4, pp. 439–454.

Seguí, P Quintana, Aurélien Ribes, Eric Martin, Florence Habets, and Julien Boé (2010). "Comparison of three downscaling methods in simulating the impact of climate change on the hydrology of Mediterranean basins". In: *Journal of Hydrology* 383.1-2, pp. 111–124.

Semenov, Mikhail A and Pierre Stratonovitch (2010). "Use of multi-model ensembles from global climate models for assessment of climate change impacts". In: *Climate research* 41.1, pp. 1–14.

Sennikovs, J and U Bethers (2009). "Statistical downscaling method of regional climate model results for hydrological modelling". In: *Proc. 18 th World IMACS/MODSIM Congress, Cairns, Australia*. Citeseer.

Senthil Kumar, AR, KP Sudheer, SK Jain, and PK Agarwal (2005). "Rainfall-runoff modelling using artificial neural networks: comparison of network types". In: *Hydrological processes* 19.6, pp. 1277–1291.

Shahin, Mohamed A, Mark B Jaksa, and Holger R Maier (2008). "State of the art of artificial neural networks in geotechnical engineering". In: *Electronic Journal of Geotechnical Engineering* 8, pp. 1–26.

Shooshtari, MM (2008). "Principles of flow in open channels". In: *Shahid Chamran University Press* 15.2, pp. 643–745.

Sillmann, J, VV Kharin, X Zhang, FW Zwiers, and D Bronaugh (2013). "Climate extremes indices in the CMIP5 multimodel ensemble: Part 1. Model evaluation in the present climate". In: *Journal of Geophysical Research: Atmospheres* 118.4, pp. 1716–1733.

Sivapragasam, C, Shie-Yui Liong, and MFK Pasha (2001). "Rainfall and runoff forecasting with SSA–SVM approach". In: *Journal of Hydroinformatics* 3.3, pp. 141–152.

Smajgl, Alexander, TQ Toan, DK Nhan, J Ward, NH Trung, LQ Tri, VPD Tri, and PT Vu (2015). "Responding to rising sea levels in the Mekong Delta". In: *Nature Climate Change* 5.2, p. 167.

Smola, Alex J and Bernhard Schölkopf (2004). "A tutorial on support vector regression". In: *Statistics and computing* 14.3, pp. 199–222.

Solomatine, Dimitri P and Khada N Dulal (2003). "Model trees as an alternative to neural networks in rainfall—runoff modelling". In: *Hydrological Sciences Journal* 48.3, pp. 399–411.

Solomatine, Dimitri P and Durga Lal Shrestha (2009). "A novel method to estimate model uncertainty using machine learning techniques". In: *Water Resources Research* 45.12.

Soulsby, Richard (1997). *Dynamics of marine sands: a manual for practical applications*. Thomas Telford.

Stocker, Thomas F et al. (2013). *Climate Change 2013: The Physical Science Basis. Contribution of Working Group I to the Fifth Assessment Report of the Intergovernmental Panel on Climate Change, 1535 pp*.

Storch, H. V. and F.W. Zwiers (1999). "Statistical analysis in climate research". In: *International Journal of Climatology* 20.7, pp. 811–812.

Storch, Hans von, Eduardo Zorita, and Ulrich Cubasch (1993). "Downscaling of global climate change estimates to regional scales: an application to Iberian rainfall in wintertime". In: *Journal of Climate* 6.6, pp. 1161–1171.

Sutskever, Ilya, Oriol Vinyals, and Quoc V Le (2014). "Sequence to sequence learning with neural networks". In: *Advances in neural information processing systems*, pp. 3104–3112.

Teutschbein, Claudia and Jan Seibert (2012). "Bias correction of regional climate model simulations for hydrological climate-change impact studies: Review and evaluation of different methods". In: *Journal of Hydrology* 456, pp. 12–29.

Thomson, Allison M et al. (2011). "RCP4. 5: a pathway for stabilization of radiative forcing by 2100". In: *Climatic change* 109.1-2, p. 77.

Todd, Martin C, RG Taylor, TJ Osborn, DG Kingston, NW Arnell, and SN Gosling (2011). "Uncertainty in climate change impacts on basin-scale freshwater resources–preface to the special issue: the QUEST-GSI methodology and synthesis of results". In: *Hydrology and Earth System Sciences* 15.3, pp. 1035–1046.

Toth, Elena and Armando Brath (2007). "Multistep ahead streamflow forecasting: Role of calibration data in conceptual and neural network modeling". In: *Water Resources Research* 43.11.

Trieu, Tran Thi Ngoc and Nguyen Thanh Phong (2015). "The impact of climate change on salinity intrusion and Pangasius (Pangasianodon Hypophthalmus) farming in the Mekong Delta, Vietnam". In: *Aquaculture International* 23.2, pp. 523–534.

Tripathi, Shivam, VV Srinivas, and Ravi S Nanjundiah (2006). "Downscaling of precipitation for climate change scenarios: a support vector machine approach". In: *Journal of hydrology* 330.3-4, pp. 621–640.

Trung, Nguyen Hieu, LA Tuan, TT Trieu, Ram C Bastakoti, and L Lebel (2013). "Multi-level governance and adaptation to floods in the Mekong delta". In: pp. 111–126.

Tuan, L.A., C.T Hoanh, F. Miller, and B.T. Sinh (2007). "Flood and salinity management in the Mekong Delta, Vietnam". In: *Bangkok/Sustainable Mekong Research Network* 61.

Turner, Barry (2013). "United Nations Framework Convention on Climate Change, UNFCCC". In: *The Statesman's Yearbook*. Springer, pp. 73–74.

Van, PDT, I Popescu, A Van Griensven, DP Solomatine, NH Trung, and A Green (2012). "A study of the climate change impacts on fluvial flood propagation in the Vietnamese Mekong Delta". In: *Hydrology and Earth System Sciences* 16.12, p. 4637.

Van Manh, Nguyen, Nguyen Viet Dung, Nguyen Nghia Hung, Matti Kummu, Bruno Merz, and Heiko Apel (2015). "Future sediment dynamics in the Mekong Delta floodplains: Impacts of hydropower development, climate change and sea level rise". In: *Global and Planetary Change* 127, pp. 22–33.

Varis, Olli, Matti Kummu, and Aura Salmivaara (2012). "Ten major rivers in monsoon Asia-Pacific: An assessment of vulnerability". In: *Applied Geography* 32.2, pp. 441–454.

Vastila, K, M Kummu, C Sangmanee, and S Chinvanno (2010). "Modelling climate change impacts on the flood pulse in the Lower Mekong floodplains". In: *Journal of Water and Climate Change* 1.1, pp. 67–86.

Vd Burgh, P (1972). "Ontwikkeling van een methode voor het voorspellen van zoutverdelingen in estuaria, kanalen en zeeen". In:

Vinyals, Oriol, Alexander Toshev, Samy Bengio, and Dumitru Erhan (2015). "Show and tell: A neural image caption generator". In: *Computer Vision and Pattern Recognition (CVPR), 2015 IEEE Conference on*. IEEE, pp. 3156–3164.

Vu, Minh Tue, Thannob Aribarg, Siriporn Supratid, Srivatsan V Raghavan, and Shie-Yui Liong (2016). "Statistical downscaling rainfall using artificial neural network: significantly wetter Bangkok?" In: *Theoretical and applied climatology* 126.3-4, pp. 453–467.

Wang, Yuqing, L Ruby Leung, John L McGREGOR, Dong-Kyou Lee, Wei-Chyung Wang, Yihui Ding, and Fujio Kimura (2004). "Regional climate modeling: progress, challenges, and prospects". In: *Journal of the Meteorological Society of Japan. Ser. II* 82.6, pp. 1599–1628.

Wassmann, Reiner, Nguyen Xuan Hien, Chu Thai Hoanh, and To Phuc Tuong (2004). "Sea level rise affecting the Vietnamese Mekong Delta: water elevation in the flood season and implications for rice production". In: *Climatic Change* 66.1-2, pp. 89–107.

Wetterhall, Fredrik, Sven Halldin, and Chong-yu Xu (2005). "Statistical precipitation downscaling in central Sweden with the analogue method". In: *Journal of Hydrology* 306.1-4, pp. 174–190.

Widmann, Martin and Christopher S Bretherton (2000). "Validation of mesoscale precipitation in the NCEP reanalysis using a new gridcell dataset for the northwestern United States". In: *Journal of Climate* 13.11, pp. 1936–1950.

Wigley, TML, PD Jones, KR Briffa, and G Smith (1990). "Obtaining sub-grid-scale information from coarse-resolution general circulation model output". In: *Journal of Geophysical Research: Atmospheres* 95.D2, pp. 1943–1953.

Wilby, RL, RJ Abrahart, and CW Dawson (2003). "Detection of conceptual model rainfall—runoff processes inside an artificial neural network". In: *Hydrological Sciences Journal* 48.2, pp. 163–181.

Wilby, Robert L (1994). "Stochastic weather type simulation for regional climate change impact assessment". In: *Water Resources Research* 30.12, pp. 3395–3403.

Wilby, Robert L, Christian W Dawson, and Elaine M Barrow (2002). "SDSM—a decision support tool for the assessment of regional climate change impacts". In: *Environmental Modelling & Software* 17.2, pp. 145–157.

Wilby, Robert L, Hany Hassan, and Keisuke Hanaki (1998). "Statistical downscaling of hydrometeorological variables using general circulation model output". In: *Journal of Hydrology* 205.1-2, pp. 1–19.

Wilby, Robert L, Cara S Wedgbrow, and Howard R Fox (2004). "Seasonal predictability of the summer hydrometeorology of the River Thames, UK". In: *Journal of Hydrology* 295.1-4, pp. 1–16.

Wilby, Robert L and TML Wigley (1997). "Downscaling general circulation model output: a review of methods and limitations". In: *Progress in physical geography* 21.4, pp. 530–548.

— (2000). "Precipitation predictors for downscaling: observed and general circulation model relationships". In: *International Journal of Climatology* 20.6, pp. 641–661.

Wilby, Robert L, SP Charles, E Zorita, B Timbal, P Whetton, and LO Mearns (2004). "Guidelines for use of climate scenarios developed from statistical downscaling methods".

In: *Supporting material of the Intergovernmental Panel on Climate Change, available from the DDC of IPCC TGCIA* 27.

Wilks, Daniel S (1992). "Adapting stochastic weather generation algorithms for climate change studies". In: *Climatic change* 22.1, pp. 67–84.

Wilks, Daniel S and Robert L Wilby (1999). "The weather generation game: a review of stochastic weather models". In: *Progress in physical geography* 23.3, pp. 329–357.

Williams, BL (1986). "Flushing time calculations for the upper Waitemata Harbour, New Zealand". In: *New Zealand journal of marine and freshwater research* 20.3, pp. 455–465.

Wood, Andrew W, Dennis P Lettenmaier, and Richard N Palmer (1997). "Assessing climate change implications for water resources planning". In: *Climate Change and Water Resources Planning Criteria*. Springer, pp. 203–228.

Wood, Andrew W, Lai R Leung, V Sridhar, and DP Lettenmaier (2004). "Hydrologic implications of dynamical and statistical approaches to downscaling climate model outputs". In: *Climatic change* 62.1-3, pp. 189–216.

Wu, CL and KW Chau (2011). "Rainfall–runoff modeling using artificial neural network coupled with singular spectrum analysis". In: *Journal of Hydrology* 399.3-4, pp. 394–409.

Wu, CL, KW Chau, and YS Li (2009). "Methods to improve neural network performance in daily flows prediction". In: *Journal of Hydrology* 372.1-4, pp. 80–93.

Xu, Chong-yu (1999). "From GCMs to river flow: a review of downscaling methods and hydrologic modelling approaches". In: *Progress in physical Geography* 23.2, pp. 229–249.

Xu, ZX and JY Li (2002). "Short-term inflow forecasting using an artificial neural network model". In: *Hydrological Processes* 16.12, pp. 2423–2439.

Zhang, Guoqiang, B Eddy Patuwo, and Michael Y Hu (1998). "Forecasting with artificial neural networks:: The state of the art". In: *International journal of forecasting* 14.1, pp. 35–62.

Zhu, Chunmei, David W Pierce, Tim P Barnett, Andrew W Wood, and Dennis P Lettenmaier (2004). "Evaluation of hydrologically relevant PCM climate variables and large-scale variability over the continental US". In: *Climatic Change* 62.1-3, pp. 45–74.

Zorita, Eduardo and Hvon Storch (1997). "A survey of statistical downscaling techniques". In: *NASA* 19980211102.

About the author

Duong Tran Anh was born in Thanh Hoa, Vietnam. He obtained his outstanding academic performance on Bachelor degree at the Water Resources University, Hanoi during 2000-2005. Subsequently he completed his MSc at Asian Institute of Technology (AIT), Thailand with full scholarship from Swedish International Development cooperation Agency (SIDA) in the period 2010-2012. During his MSc he specialized in climate change, hydrodynamic modelling and water resources engineering within the Water Engineering Management Department at AIT. During his MSc study, Duong successfully received full scholarship from German academic Exchange Service (DAAD) for the exchange program at Leichtweiß-Institute for Hydraulic Engineering and Water Resources, TU Braunschweig, Germany. Thereafter, he commenced his PhD research at the Chair of Hydraulic and Water Resources Engineering, Technical University of Munich, Germany with full two rounds scholarship from IPCC scholarship program funded by Cuomo Foundation and Prince Albert II of Monaco covering a duration of 2013-2016. During his entire PhD candidature, Duong had chance to conduct his exchange program at Department of Civil and Environmental Engineering, Colorado State University, USA. His major research interest is hydrodynamic modelling, climate change and downscaling and artificial neural network for rainfall, runoff prediction. He has published several journal and conference articles to date.

Publications:

1. **Duong, T.A.**, Long, P.H, Bui, M.D, Rutschmann, P. (2018). Modelling seasonal flows in the Vietnamese Mekong due to upstream discharge variation, climate change and sea level rise. *Journal of River Basin Management.* https://doi.org/10.1080/15715124.2018.1505735
2. **Duong, T.A.**, Long, P.H, Bui, M.D, Rutschmann, P. (2018). Simulating future flows and salinity intrusion using combined one- and two-dimensional hydrodynamic modelling–The case of the Hau river, Vietnamese Mekong Delta. *Journal of Water* 2018, *10*(7), 897; https://doi.org/10.3390/w10070897.
3. **Duong, T.A**., Bui, M.D, Rutschmann, P. (2018). Application of Long Short Term memory in statistical downscaling in rainfall forecasting by climate change. *Hydrological Sciences Journal* - Manuscript ID HSJ-2018-0329 (under review).
4. **Duong, T.A**., Bui, M.D, Rutschmann, P. (2018). Data pre-processing combined with Artificial Neural Network to improve the performance of time series modelling. 5th IAHR Europe Congress, Trento University, Italy.
5. **Duong, T.A**., Bui, M.D, Rutschmann, P. (2018). A comparative study of three different models to predict monthly rainfall in Ca Mau; Vietnam. *Proceeding of Wasserbau-Symposium 2018, TU Gräz, 18-20 Sept. 2018, Austria.*
6. **Duong, T.A.**, Bui, M.D, Rutschmann, P. (2016). Effect of Upstream Discharge and Climate Change on the Hydraulic Regime in Vietnamese Mekong Delta. *Proceeding of Wasserbau-Symposium 2016, Wallgau, Oberbayern, Germany.*
7. **Duong, T.A**., Bui, M.D, Rutschmann, P. (2015). Impact of climate change on salinity intrusion in Mekong delta. *Proceeding of 14th International conference on Environmental Science and Technology, Rhodes, Greece*.